

**Investigation, Modelling and Control of the  
1.9 K Cooling Loop for Superconducting Magnets  
for the Large Hadron Collider**

by

Bjørn Flemsæter

A Thesis Submitted for the Degree of Doktor Ingeniør

Norwegian University of Science and Technology  
Department of Refrigeration and Air Conditioning

January 2000



## Abstract

The temperature of the superconducting magnets for the 27 km LHC particle accelerator under construction at CERN is a control parameter with strict operating constraints imposed by (a) the maximum temperature at which the magnets can operate, (b) the cooling capacity of the cryogenic system, (c) the variability of applied heat loads and (d) the accuracy of the instrumentation. A pilot plant for studying aspects beyond single magnet testing has been constructed. This magnet test string is a 35-m full-scale model of the LHC and consists of four superconducting cryomagnets operating in a static bath of He II at 1.9 K.

An experimental investigation of the properties dynamic characteristics of the 1.9 K cooling loop of the magnet test string has been carried out. A first principle model of the system has been created. A series of experiments designed for system identification purposes have been carried out, and black box models of the system have been created on the basis on the recorded data. A Model Predictive Controller has been implemented for controlling the temperature of the 1.9 K level, using models obtained in the system identification. A temperature control with a narrower control band can in principle be achieved with an MPC-type controller than when using a PID controller. Experiments show that the controller has promising properties for tackling the dynamic challenges posed by the design of the 1.9 K cooling loop.

Through the experimental investigation it has been found that:

- the amount of pressurised He II in the cold mass is 180 kg
- the thermal conductance of the heat exchanger tube is 74 W/Km
- the velocity of the advancing liquid in the heat exchanger is in the order of 10 cm/s.
- The interaction between the gas and liquid phase is weak
- longitudinal and transverse heat transfer capability is very high

The system is found to be:

- strongly non-linear primarily through He II and the density of the helium gas
- non-minimum phase and exhibiting inverse response
- open loop unstable, also denoted non self-regulating
- containing variable transport delay

The first principle model is capable of reproducing steady state and transient characteristics of the system. Of particular importance the pressure drop calculation in the heat exchanger is verified to be in good agreement with observed behaviour. Linear black box models are verified to satisfactory represent the system around the working point. Using linear models the performance of the MPC controller was found to be as good as or better than the classical PID control structure used up to date. Results indicate that improved performance will offset the increased initial cost and technical complexity of the control system and add to a robust and fault tolerant operation of the system.

## Acknowledgements

More than four years of work is drawing towards a conclusion. The work started late in the autumn of 1995 in Trondheim. From the winter of 96 through to spring of 99 most of the time was spent at CERN at the Franco-Swiss border near Geneva. This was possible through the Doctoral Student Programme at CERN supplying most of the financial support. The write-up of the report was done in Trondheim at the Department of Refrigeration and Air Conditioning. This period was supported by the department in Trondheim.

During such a period one get to meet and cooperate with a lot of people both professionally and socially. All have made a contribution in some way for this period to have turned out as it has. Without the ambition of giving a complete autobiography I would like to take this opportunity and distribute thanks at least where it is most deserved. Without ranking the recipients I do this in a chronological order.

First I would like to thank Geir Owren for being the main responsible for initiating this work through his interest in the field and his contacts at CERN. Gratitude also for filling the role of main supervisor and staying with it throughout.

Gratitude to Steinar Sælid for finding the time on a hectic agenda to meet and exchange ideas and give guidelines and inspiration.

The first autumn in Trondheim would not have been the same without the social focal point that the very special orchestra Strindens constituted. As a retired member of the orchestra that was a rich source of energy and diversion for going through with the required courses of the thesis work. A most memorable visit by the orchestra when I lived in Geneva puts an extra touch to that period as well.

When at CERN, work revolved around the Instrumentation and Process Control Section of the Accelerator Cryogenic Group of the Large Hadron Collider division. My knowledgeable section leader and supervisor Juan Casas Cubillos was the man in charge. Thank you Juan for help, support, encouragement and for believing when progress was slow and obstacles many. Enrique Blanco Viñuela, my office mate and fellow doctoral student: thank you for sharing many a long evening and weeks and in the lab, for fruitful discussions and your effort of getting the MPC controller up and running. Invaluable in retrospect. To all off the section: thanks for memorable coffee breaks and interesting discussions about the similarities and differences of people and culture around Europe and Colombia. 14 people from 9 countries is a rich environment. And with good coffee!! (Italian, not Colombian. No offense.) Also skiing outings, barbecue evenings and dinners in Geneva will not be easily forgotten.

But life was not all work. Luckily. Memories for life can be attributed to Kate & Gunnar, Karin & Wolfgang, Gunilla & Eirik, Nils & Marianne, Anders, Rob, Dieter, Philippe, Serge, Marianne, Henning, Øyvind, Jens & Yvonne. Places like Chamonix, Val d'Isere,

Trois Valleees, Corsica, Cote d'Azur, Paris, Bern, Bordeaux, Valle de Rhone, Beaujolais and Pyrinees have their names connected with yours. And Eva...

Back here in Trondheim work has been mostly a solo enterprise. Nobody wanted to write this report for me... However the important part of social life at work has been supplied by Bent, Sivert, Jan, Cato, Hanne, Kjetil, Even, Bjørn A., Henning (the same), Geir, Bengt and Ole Jørgen . Football is a topic without end. The frequent questions about a date of dissertation I could have done without though.

Lastly I want to thank my family for their support, encouragement and visits when home was far away. Being away for so long has been a sacrifice. Not without dividend, but a sacrifice nonetheless.

## Table of content

<b>1</b>	<b>INTRODUCTION.....</b>	<b>13</b>
1.1	MOTIVATION FOR THE THESIS .....	13
1.2	PREVIOUS WORK.....	14
1.3	PRESENT CONTRIBUTION .....	15
1.4	SURVEY OF THE THESIS .....	16
<b>2</b>	<b>SUPERCONDUCTIVITY .....</b>	<b>17</b>
2.1	THEORY OF SUPERCONDUCTIVITY .....	17
2.2	SUPERCONDUCTING MAGNETS.....	18
2.3	RESISTIVE TRANSITION, QUENCHING .....	19
2.4	SUPERCONDUCTING MAGNETS FOR THE LHC .....	20
<b>3</b>	<b>HELIUM AND LOW TEMPERATURE HEAT TRANSFER .....</b>	<b>21</b>
3.1	ISOTOPES OF HELIUM .....	21
3.2	LIQUID AND GASEOUS HELIUM.....	21
3.3	THE TWO-FLUID MODEL OF He II .....	22
3.4	TRANSPORT PROPERTIES OF He II.....	24
3.5	STEADY STATE HEAT TRANSPORT .....	26
3.6	KAPITZA CONDUCTANCE.....	27
<b>4</b>	<b>THE LHC LAYOUT AND CRYOGENIC SYSTEM .....</b>	<b>30</b>
4.1	PLANT LAYOUT.....	30
4.1.1	<i>The arc cells.....</i>	30
4.1.2	<i>Dipole bending magnets and quadrupole focusing magnets.....</i>	31
4.2	THE LHC CRYOGENIC SYSTEM.....	33
4.2.1	<i>The General Layout .....</i>	33
4.2.2	<i>Magnet Cooling Scheme .....</i>	34
4.3	HEAT LOADS .....	35
4.3.1	<i>Steady state heat loads.....</i>	35
4.3.2	<i>Transient Heat Loads.....</i>	36
4.4	MAGNET TEST STRING .....	36
4.4.1	<i>Liquid Supply and Flow Measurement.....</i>	38
4.4.2	<i>Very-Low-Pressure Heat Exchanger .....</i>	39
4.4.3	<i>Joule-Thomson Valve.....</i>	39
4.4.4	<i>The Bayonet Heat exchanger .....</i>	39
4.4.5	<i>Electrical Heaters .....</i>	41
4.4.6	<i>Temperature sensors .....</i>	41
4.4.7	<i>Disturbances .....</i>	42
<b>5</b>	<b>CONTROL ASPECTS FOR THE 1.8 K COOLING LOOP.....</b>	<b>43</b>
5.1	PRESENT CONTROL STRATEGY FOR THE 1.8 K COOLING LOOP .....	43
5.2	PROCESS CHARACTERISTICS .....	44
5.3	TEMPERATURE MARGINS AND CONTROL BAND .....	45
5.4	CLASSICAL VERSUS ADVANCED CONTROL .....	46
5.4.1	<i>PID control .....</i>	47
5.4.2	<i>MPC control.....</i>	47
<b>6</b>	<b>EXPERIMENTAL INVESTIGATION.....</b>	<b>51</b>
6.1	LIQUID VELOCITY IN THE HEAT EXCHANGER TUBE .....	51
6.2	AMOUNT OF PRESSURIZED He II IN THE MAGNETS/COLD-MASS .....	53
6.3	THERMAL CONDUCTIVITY OF THE 1.9 K HEAT EXCHANGER TUBE .....	55
6.4	HEAT TRANSFER IN THE INTERCONNECTIONS .....	58

6.5	INVERSE RESPONSE.....	59
<b>7</b>	<b>FIRST PRINCIPLE MODELLING THE LHC TEST STRING.....</b>	<b>62</b>
7.1	.....	63
7.2	ASSUMPTIONS AND SIMPLIFICATIONS .....	64
7.3	THE SUB-MODELS .....	66
7.3.1	<i>The Joule-Thomson Valve.....</i>	66
7.3.2	<i>Liquid flow in the Heat Exchanger .....</i>	67
7.3.3	<i>Gas flow in the Heat Exchanger, Pressure Drop.....</i>	69
7.3.4	<i>Cooling by the Heat Exchanger.....</i>	71
7.3.5	<i>Magnet Temperatures .....</i>	71
7.4	IMPLEMENTATION OF THE MODEL .....	72
7.4.1	<i>Length increments of the heat exchanger tube.....</i>	73
7.5	SENSITIVITY STUDY OF DESIGN PARAMETERS.....	73
7.5.1	<i>Heat Transfer Coefficient.....</i>	75
7.5.2	<i>Amount of helium in the cold mass .....</i>	76
7.5.3	<i>Liquid velocity in heat exchanger. ....</i>	76
7.5.4	<i>Amount of flash over JT-valve.....</i>	77
7.5.5	<i>Friction factor.....</i>	77
7.5.6	<i>Threshold of mass in corrugation .....</i>	78
7.6	VALIDATION OF FIRST PRINCIPLE MODEL.....	78
7.6.1	<i>Varying the heat load.....</i>	78
7.6.2	<i>Manipulating the Joule-Thomson valve .....</i>	80
<b>8</b>	<b>BLACK BOX MODELING OF THE LHC TEST STRING.....</b>	<b>83</b>
8.1	THE PROCEDURE OF SYSTEM IDENTIFICATION.....	83
8.2	DESIGN OF EXPERIMENTS FOR SYSTEM IDENTIFICATION.....	84
8.3	SELECTION OF MODEL STRUCTURE AND ORDER .....	86
8.3.1	<i>Models of Linear Time Invariant (LTI) Systems .....</i>	86
8.3.2	<i>LTI Models for the String.....</i>	88
8.4	LTI MODELS AND VALIDATION .....	89
8.4.1	<i>Parameter estimation.....</i>	91
8.4.2	<i>ARX and IV models .....</i>	92
8.4.3	<i>Output error (OE) models.....</i>	94
8.4.4	<i>ARMAX models .....</i>	95
8.4.5	<i>Box-Jenkins (BJ) models.....</i>	96
8.4.6	<i>Verification of the models .....</i>	97
<b>9</b>	<b>MPC CONTROL OF THE 1.8 K COOLING LOOP .....</b>	<b>100</b>
9.1	REFERENCE TRAJECTORY.....	102
9.2	CRITERION FUNCTION .....	102
9.3	THE PREDICTIVE CONTROL LAW.....	104
9.4	CONSTRAINTS .....	104
9.5	SYSTEM MODEL FOR THE MPC .....	105
9.6	DESIGN PARAMETERS .....	105
9.6.1	<i>Controller output weighting.....</i>	106
9.6.2	<i>Prediction, minimum cost and control horizon.....</i>	107
9.6.3	<i>The disturbance model.....</i>	110
9.7	PERFORMANCE OF THE MPC CONTROLLER .....	111
<b>10</b>	<b>DISCUSSION AND CONCLUSION.....</b>	<b>117</b>
10.1	INVESTIGATION OF THE 1.9 K LEVEL .....	117
10.2	FIRST PRINCIPLE MODELLING.....	118
10.3	BLACK BOX MODELLING .....	121
10.4	MODEL PREDICTIVE CONTROL OF THE SYSTEM .....	122

<b>11</b>	<b>REFERENCES .....</b>	<b>124</b>
<b>12</b>	<b>A-1 DATA AND MEASUREMENT FOR CALCULATING LIQUID VELOCITY .....</b>	<b>127</b>
<b>13</b>	<b>A-2 AMOUNT OF HELIUM IN THE COLD MASS .....</b>	<b>128</b>
<b>14</b>	<b>A-3 DATA FOR THE THERMAL CONDUCTIVITY OF THE HEAT EXCHANGER.....</b>	<b>129</b>
<b>15</b>	<b>A-4 HEAT TRANSFER IN THE INTERCONNECTIONS .....</b>	<b>130</b>
<b>16</b>	<b>B-1 FIT FUNCTION FOR DENSITY OF HELIUM GAS.....</b>	<b>131</b>
<b>17</b>	<b>B-2 FIT FUNCTION FOR SPECIFIC HEAT OF HE II.....</b>	<b>132</b>
<b>18</b>	<b>C-1 MANUAL FOR SIMULATION PROGRAM .....</b>	<b>133</b>
18.1	C-1.1 OPENING AND UNDERSTANDING THE PROGRAM.....	133
18.1.1	<i>The Main Window .....</i>	<i>133</i>
18.1.2	<i>Pumping Pressure .....</i>	<i>134</i>
18.1.3	<i>Heat Inleak.....</i>	<i>134</i>
18.1.4	<i>JT Valve .....</i>	<i>134</i>
18.1.5	.....	136
18.1.6	<i>Magnet (Pressure Vessel) .....</i>	<i>136</i>
18.1.7	<i>Heat Exchanger .....</i>	<i>136</i>
18.1.8	<i>Output File and Clock.....</i>	<i>140</i>
18.2	C-1.2 EDITING THE PROGRAM .....	140
18.3	C-1.3 RUNNING THE PROGRAM .....	141
18.4	C-1.4 VIEWING THE SIMULATION RESULT .....	142
18.5	D-1 PAPER SUBMITTED TO ICEC 17 .....	143
18.6	APPLYING ADVANCED CONTROL TECHNIQUES FOR .....	144
18.7	TEMPERATURE REGULATION OF THE LHC SUPERCONDUCTING MAGNETS .....	144



## List of symbols

### Latin Letters

a	width perpendicular to b
A	Gorter-Mellink parameter [ms/kg]
	ampere
	area [m <sup>2</sup> ]
b	width perpendicular to a
B	measured output of controlled variable
B <sub>c</sub> , B <sub>c1</sub> , B <sub>c2</sub>	critical magnetic field
cm	centimeter
cp	specific heat [J/kg-K]
d	delay in discrete time, dead time
D	diameter
e	deviation variable, error signal
E <sub>0</sub>	zero point energy
f	friction factor [-]
h	Planck's constant
	enthalpy
	height
H <sub>c</sub>	control horizon
h <sub>global</sub>	heat transfer coefficient for heat exchanger [W/Km]
h <sub>k</sub>	Kapitza conductance [W/m <sup>2</sup> K]
He	helium
h <sub>fg</sub>	latent heat of vaporization [J/g]
Hg	mercury
H <sub>m</sub>	minimum cost horizon
H <sub>p</sub>	prediction horizon
Hz	hertz [1/s]
I	nuclear spin
	current
J	criterion function
J <sub>c</sub>	critical current density
k	thermal conductance
	discrete time
K	Kelvin
K <sub>c</sub>	controller gain
kg	kilogram
L	length
m	meter
	mass
M	magnetization
N	number of samples in a data series
NbTi	Niobium-Titanium alloy
Δp	uncertainty in momentum

p	controller output
p,P	pressure
q	heat flux
	shift operator in discrete time
Q	power [W]
$Q_d$	filter polynomial
$Q_n$	filter polynomial
$q^*$	maximum heat flux
R	radius
	resistance to heat transfer
	set point
Re	Reynolds number [-]
s	second
Sp	set point
T	polynomial for disturbance model
$T_c$	critical temperature
Tev	terra electron volt
$T_p$	transition temperature from He I to He II
$T_s$	sampling time
u	manipulated variable
$u_m$	mean velocity
v	velocity
	disturbance signal
$v\%$	valve opening in percent
V	volume
$v_{liq}$	velocity of liquid
w	reference trajectory
W	watt
x	vapor fraction
y	controlled variable

### Greek Letters

$\rho$	gradient of reference trajectory w
$\rho$	roughness
$\rho$	constant Kapitza conductance
$\rho$	viscosity
$\rho$	lambda point, transition to He II
$\rho$	viscosity [ $m^2/s$ ]
	tuning factor for polynomial filter
$\rho_0$	permeability of free space, $4\pi 10^{-7}$ [Tm/A]
$\rho$	density
	weighting factor
$\rho$	time constant
$\rho$	regressor vector

$\rho$	parameter vector
$\rho_s$	sampling frequency
$\rho_b$	band width

## Abbreviations

ALICE	LHC experiments
ATLAS	LHC experiments
ARMAX	Auto Regressive Moving Average eXogenous
ARX	Auto Regressive eXogenous
BCS	Bardeen, Cooper, Schrieffer
BJ	Box-Jenkins
CERN	European Center for Particle Physics
CCU	Cold Compressor Unit
CMS	LHC experiments
HTS	High Temperature Superconductor
HX	Heat exchanger
IV	Industrial Variable
JT	Joule-Thomson
LEP	Large Electron Positron collider
LHC	Large Hadron Collider
LHC-B	LHC experiments
LTI	Linear Time Invariant
MB	bending dipole
MIMO	Multiple Input Multiple Output
MPC	Model Predictive Control
OE	Output Error
PID	Proportional, Integral, Derivative
PLC	Programmable Logic Controller
PRBS	Pseudo Random Binary Signal
QBF	Quench Buffer Vessel
QP	Quadratic Programming
R&D	Research and Development
ROC	Region of Convergence
RST	pole placement control
SC	superconducting
SFB	String Feed Box
SRB	String Return Box
SISO	Single Input Single Output
TC	Temperature Controller
TCV	Temperature Controlled Valve
TT	Temperature Transmitter
SSS	Short Straight Section, housing the quadrupole focusing magnet



# 1 Introduction

## 1.1 Motivation for the Thesis

[1] [2] In high-energy physics the particle accelerator is the most important tool for performing experiments. The size and power of these accelerators have been steadily growing over the years in search of new physics at ever-higher energy levels. Key components of a particle accelerator are the magnets used for guiding and focusing the particle beam. The present demand for high magnetic field can only be met by superconducting magnet technology operating at liquid helium temperature. This has led to the introduction of cryogenic systems as an integrated and vital part of accelerator design, and is one of the limiting factors both from a performance and economical point of view.

The next accelerator planned at the European Laboratory for Particle Physics (CERN) is the Large Hadron Collider (LHC). It is planned to be operational in 2005 and will then be the largest scientific instrument in the world. The LHC will bring protons and later heavy ions into head-on collisions at higher energies than ever achieved before ( $2 \times 7$  TeV for the proton beams). This will allow scientists to penetrate further into the structure of matter and recreate the conditions prevailing in the early universe  $10^{-12}$  seconds after the Big Bang when the temperature was  $10^{16}$  K. The LHC will make use of superconducting magnets operating at 1.9 K along the whole circumference of 27 kilometres. The refrigeration system will have a capacity equivalent of 144 kW @ 4.5 K, the largest part of which is consumed at the 1.9 K level. With an effect factor (COP) of about 1:250 at 4.5 K the required energy input to the cooling system of 36 MW.

The temperature of the superconducting magnets is a control parameter with strict operating constraints imposed by (a) the maximum temperature at which the magnets can operate, (b) the cooling capacity of the cryogenic system, (c) the variability of applied heat loads and (d) the accuracy of the instrumentation.

Good control and smooth operation of the LHC machine will limit the cost of running the cryogenic system. It will ease demand on accuracy and calibration of the several thousand temperature sensors. Operating the magnets at higher field closer to their transition limit ultimately lead to better physics.

A thorough understanding of the characteristics and processes involved at the 1.9 K level of the LHC cooling system is necessary for addressing the constraints and obtain the benefits. When understanding the challenges of 1.9 K cooling loop, a control strategy can be sought.

The aim of the work presented in this thesis is to investigate the 1.9 K cooling loop as a basis for developing a control structure capable of handling the challenges imposed by the process characteristics.

## 1.2 Previous work

Superfluid helium cryogenic has been subject to a decade of dedicated R&D program at CERN. It has resulted in development in fields such as thermo-hydraulics, two-phase saturated superfluid helium, large capacity refrigeration at 1.9 K and industrial precision thermometry below 4 K.

In the superfluid helium test rigs the flow of liquid helium into the 1.9 K level has been regulated by a standard industrial PID controller. The performance of this controller has itself been subject to dedicated study [my thesis]. A need has been recognized in more detail to study the possibility of improving the control of liquid flow into the 1.9 K level. This flow governs the temperature of the superconducting magnets in presence of variations of the heat load. A possible improvement in controlling the magnet temperature can be gained by using a controller better adapted for handling the challenges posed by the dynamic characteristics of the 1.9 K cooling loop. In particular the class of Model Predictive Control (MPC), a so-called modern control technique, offers prospects of improved control compared with standard PID controllers.

The MPC technology is today a mature field and there are several commercial products. From industry there are more than two thousand reported applications as well several made in-house but not well known due to proprietary reasons. The majority of applications are reported in refining and petrochemical industry [44]. Apart from five applications in air separation industry no report has been found where MPC technology has been implemented on a cryogenic process and in particular not for a process involving He II as a coolant, which inherently makes the process highly non-linear.

The MPC technique involves developing a model to be used as an integral part of the control structure for predicting future plant behaviour. By far the majority of reported applications are using linear models. The field of non-linear MPC control has not yet reached the stage of a mature technique with a solid theoretical foundation. Several aspects concerning both local and global stability become much more complex when using non-linear models. As a result linear approximations of more or less non-linear processes are being used.

System Identification is the most widely employed method for creating a model intended to be used in an MPC control structure. System identification and parameter estimation has for more than 30 years been one of the most active fields of control engineering [R. Henriksen.].

### 1.3 Present Contribution

Steady state properties of the cooling loop have been verified to be satisfactory. However subject to a decade of research, the aspect of the dynamic properties of the 1.9 K cooling loop has not been properly addressed. Plant design determines the dynamic characteristics of the process as well as the operability of the plant. In extreme situations the plant may be uncontrollable even though the process design appears satisfactory from a steady-state point of view. In recent years there has been a growing recognition of the importance of considering dynamics and control issues early in the plant design.

The presented work is addressing this concern. A study is undertaken to understand the dynamic characteristics of the cooling loop. The main tool for investigating the 1.9 K cooling loop is a 35-meter full-scale prototype of the future accelerator. The Magnet Test String consists of three ten-meter dipole bending magnets and one short straight section housing a quadrupole focusing magnet.

A first principle model of the system has been developed. This model is useful for investigating and understanding the cooling loop. First principle models can also be used to study control aspects.

An MPC controller on the 1.9 K cooling loop has been implemented. This regulator shows promising properties for tackling the challenges posed by the dynamic properties identified in the study of the system.

Benefits of using MPC technology instead of a standard PID controller have been verified. The implemented software is a prototype developed at the University in Valladolid, Spain, intended for use in the sugar industry. It is not a commercially available product in its present form. A future implementation on the LHC will demand a product that also addresses needs not related to the mathematics of the algorithms; including software and hardware compatibility, user interface requirements, personnel training and configuration and maintenance issues. These aspects are not treated in this study.

Following a recent simplification of the cryogenic system, executed after this work was performed, the local cooling loops are now fixed to be 107-meter, twice that of the previous configuration and three times that of the Magnet Test String used for this study. This further increases the requirement of a controller capable of handling the dynamic challenges of the system. It has been shown that using a linear identified model the MPC controller shows characteristics superior to that of a PID controller. A study to investigate the possibility of using a non-linear model in the MPC implementation is being carried out.

The changing slope with a maximum gradient of 1.4 % of the tunnel of the future machine imply that the model to be used in an MPC controller for each local cooling loop

should be custom made for that specific location. A satisfactory first principle model can be used to generate data for identifying black box model for the various locations. This would facilitate the implementation of MPC control loops for the future machine, as it would by-pass the general procedure where recorded plant data is used for generating such models.

## 1.4 Survey of the Thesis

The work presented in this thesis is based on technology and equipment employing superconductivity and He II as a technical coolant. Chapter 2 and Chapter 3 give an introduction to these aspects.

In particular the work is based on the Magnet Test String, normally referred to as the String, which is a prototype half-cell of the LHC layout before the simplification of the cryogenic system. Chapter 4 gives an overview of the layout of the LHC machine, and describes in more detail the cryogenic aspects of the 1.9 K level of the Magnet Test String.

One of motivations for the work is to investigate control aspects of the 1.9 K cooling loop. Chapter 5 describes the present layout of the control scheme and treats the advantages and disadvantages of the employed strategy. It then treats the possible benefits, advantages and disadvantages of using a Model Predictive Control for the regulation of the cooling loop.

Chapter 6 treats the experimental investigation of the 1.9 K cooling loop that has been carried out. It describes a series of experiments that were performed in order to gain knowledge about the characteristics and dominant features of the system.

Chapter 7 deals with first principle modelling of the cooling loop. The chapter is concluded by a sensitivity study of the parameters and validation of the model against String behaviour.

Chapter 8 deals with system identification and the construction of black box models of the system. Several structures of models are investigated and the structure best describing the system is identified.

Black box models are an integrated part of the MPC control structure presented in Chapter 9. The MPC technology and a description of the design parameter are presented. The chapter is concluded by the MPC controlled implemented on the 1.9 K cooling loop of the Magnet Test String.

Chapter 10 contains discussion and conclusion of experimental investigation described in chapter 6, the first principle developed in chapter 7, the black box modelling in treated in chapter 8 and the MPC control structure presented in Chapter 9.



## 2 Superconductivity

First an introduction to superconductivity is presented. This leads to relevant aspects of superconducting magnets for the LHC. [3] and [4] are the main sources cited.

Superconductivity is the ability to transfer electricity without loss of energy. A superconductor is material that exhibits two unusual properties when cooled down to low temperature:

- it has no resistance to electrical current
- it expels magnetic fields

When the Dutch physicist H. K. Onnes in 1911 cooled down a sample of Hg to 4.2 K he observed that the resistivity went to zero. He was the first to discover the effect of superconductivity. In 1933 the German physicists Meissner and Osenfeld found that superconductors repulse magnetic fields. This effect was explained in 1957 when J. Bardeen, L. N. Cooper and J. R Schrieffer produced the BCS theory of superconductivity. This theory is based on quantum mechanical effects acting to completely eliminate electrical resistance.

In 1987 for the first time a compound was found that became superconducting at 94 K. Then standard liquid nitrogen technology could be used instead of expensive liquid helium technology in superconducting applications. It spurred a surge of research into so-called High Temperature Superconductors (HTS) and has resulted in increasing number of commercial applications involving superconductivity.

### 2.1 Theory of superconductivity

In a normal conductor the electrons are bumping into impurities and imperfections in the vibrating lattice and fly off in all directions losing energy in the form of heat; resistance. In the superconducting state the conduction electrons are ordered and do not experience this resistance.

Cooper argued that in a superconductor the electrons form pairs, now called Cooper pairs that are able to move unimpeded through the material. As one negatively charged electron passes by positively charged ions, the lattice of the superconductor becomes distorted, which causes packets of sound waves (phonons) to be emitted. This forms a positive charge around the electron and before the lattice springs back into place, a second electron is drawn towards it. The force exerted by the phonons overcomes the electrons natural repulsion, and they move along separated by some distance and screened by the phonons. When one of the electrons forming the pair passes a positively charged ion a vibration starts which passes from ion to ion until the second electron comes along and absorbs the vibration. The net effect is that one electron has emitted a phonon and the other one has absorbed it. It is this exchange that keeps the Cooper pairs

together. This electron pairing is favorable because it puts the material into a lower energy state, the electrons are condensed into a macroscopic quantum ground state. When a superconductor is heated up the vibrations of the lattice become more violent and start breaking up the Cooper pairs and destroy the superconducting capability.

## 2.2 Superconducting magnets

The electromagnetic field theory described by Maxwell's equations relates the electric field density and intensity to the magnetic field density and intensity. It states that an electrical current in a conductor produces a magnet field. The capability of superconducting materials to carry large currents enables them to form powerful magnets, and to do so without the electrical losses associated with ordinary resistive electromagnets.

The superconducting state exists below a phase surface that is delimited by the three critical parameters of temperature  $T_c$ , magnetic field  $B_c$  and current density  $J_c$ . Figure 2.1 [5] shows the phase diagram for niobium-titanium (NbTi) alloy which is used in the LHC magnets.

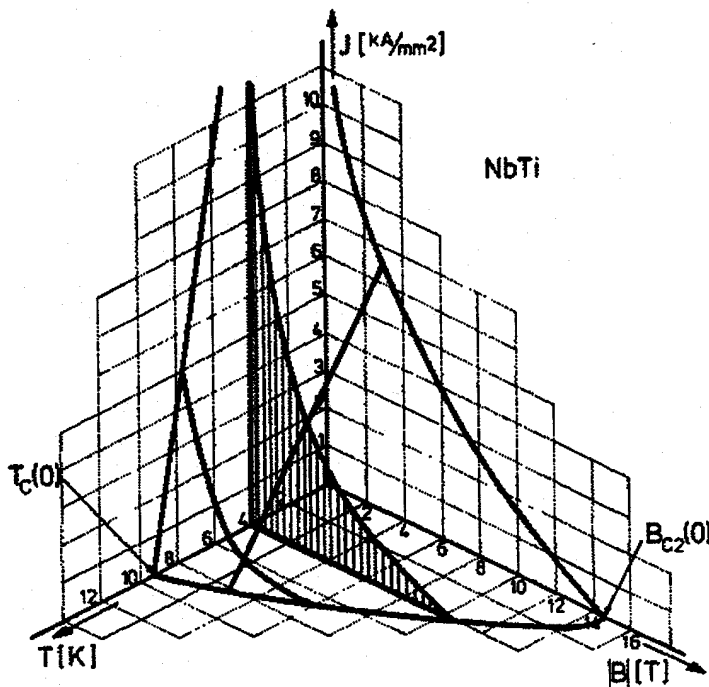


Figure 2.1 The phase diagram of the NbTi superconductor.

For a given temperature a phase plane and critical magnetic field and current density is defined as illustrated by the hatched surface in the figure.

When a superconductor is placed in a magnetic field it will ‘push’ the field out of itself. It does this by creating a current in a very thin outer shell of the body that exactly counters the external field, canceling magnetic flux in its interior. This flux exclusion is what is referred to as the Meissner effect, and can be demonstrated by placing a magnet over it. This magnet will then hover over the superconductor. It is this effect that is utilized in e.g. magnetically levitated trains.

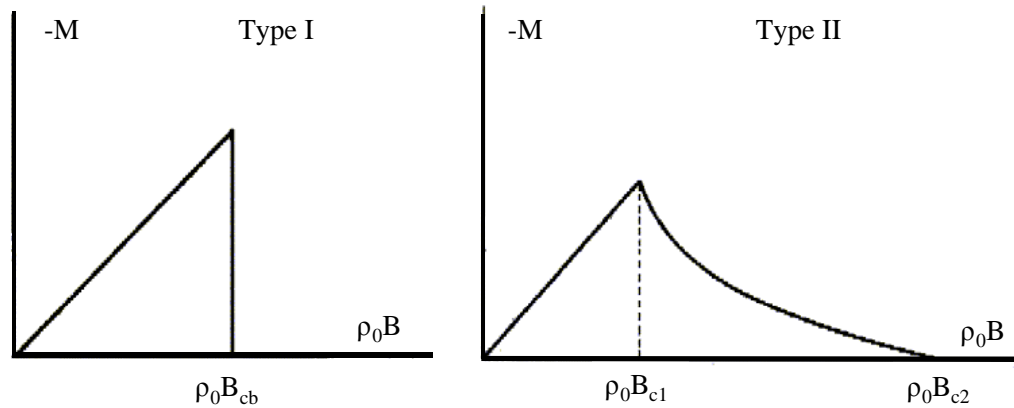


Figure 2.2 Magnetization curves for Type I and Type II superconductor.

Superconductors are of type I or type II, illustrated in Figure 2.2 [6]. The type I superconductors are perfect diamagnets and have no magnetization at all below the transition field  $B_c$ . They show a complete Meissner Effect until the superconducting property disappears, but have very low values of  $B_c$  and are not applicable as magnets for high field applications. Type II superconductors have two critical fields,  $B_{c1}$  and  $B_{c2}$  and a vortex state between them. They behave as type I until  $B_{c1}$  is reached. Then the field starts to penetrate, part of the Meissner Effect is lost, and the superconducting property decreases gradually and is disappeared when  $B_{c2}$  is reached. Type II conductors can reach much higher magnetic fields than type I conductors, and are ones used for most applications.

### 2.3 Resistive transition, quenching

If any of the three critical values are exceeded anywhere within a superconductor the material loses its superconducting property and goes into the normal conducting phase with its associated resistance. The high current that goes through the normal conduction area of the material produces a high voltage and power release in form of heat. This

resistive transition is commonly known as quenching, and is an important source of concern in magnet design.

A quench in a magnet is initiated because of a local energy release. This might be due to movements of magnet coils under electromagnetic forces. It spreads along the magnet wire with velocities of typically 20-100 m/s. The energy that is stored in the magnet is released during a quench and must be absorbed by the magnet in the form of heat. If all the energy is deposited in a small volume the magnet might melt or be mechanically deformed due to the expansion of the coil.

To avoid local peak temperatures the whole volume of the magnet can be made resistive when a quench is detected. Some of the energy might also be extracted by a discharge resistance. A quench detection system involving detecting and triggering devices is very important in the design of devices involving superconducting magnets with high fields.

## 2.4 Superconducting magnets for the LHC

The LHC will reuse the existing 27-km circular tunnel existing at CERN, and make use of the well-proven fabrication method of cables and coils made of NbTi superconductor, a type II superconductor. In order to obtain the desired field of 8.7 T with sufficient margin the magnets will have to be operated below 2 K. Specific heat of metallic parts at this temperature is very low (an order of magnitude lower than at 4.2 K), with a consequent faster temperature rise for a given deposit of energy. Special care must be taken to limit temperature excursions and the motion of the superconductor to avoid quenching the magnets. Temperature stability is obtained by immersing the superconducting magnets in a static bath of pressurized He II.

The design of the collider require two separate beam tubes with field of equal strength but in opposite direction. To reduce cost and total complexity of the machine these two sets of coils have been put into the same structure. This two-in-one configuration has demanded special care in magnet design since the two fields operate close to each other.

Producing the dipole magnets for the LHC will require 1200 tons of NbTi superconducting cable. This equals more than six years production with today's available production capacity. In total the LHC will require more than 8000 superconducting magnets for bending, focusing and correcting the particle beams [7].

### 3 Helium and Low Temperature Heat Transfer

Helium is the only cryogenic fluid that can be used for cooling strings of superconducting magnets at 1.9 K. The theory presented in this chapter is unless otherwise noted compiled from [8] and [9]. [8] gives a broad overview of the present state of helium cryogenic and contains extensive references to more detailed work.

#### 3.1 Isotopes of helium

Two stable isotopes of helium exist:  $\text{He}^4$  with boiling point 4.21 K, and the much rarer ( $1:10^{-6}$  in atmospheric helium)  $\text{He}^3$  boiling at 3.19 K. In addition two unstable isotopes  $\text{He}^6$  and  $\text{He}^8$  have lifetimes just under one second.

$\text{He}^3$  has one less neutron in the nucleus and thus an odd number of hadrons with a resulting nuclear spin  $I=1/2$ , and is therefore a fermion.  $\text{He}^4$  with an even number of hadrons resulting in zero nuclear spin, is a boson. The two isotopes therefore obey different kind of statistics causing substantial differences in their low temperature behavior. Only the  $\text{He}^4$  isotope is relevant for this work and will in the continuation be termed simply helium and He.

#### 3.2 Liquid and gaseous helium

When liquid helium at atmospheric pressure is cooled below its boiling point it remains liquid, and will do so down to absolute zero. It takes a pressure of more than 25 bars to make it solidify as can be seen from the phase diagram, Figure 3.1. This behavior arises from the low mass of the helium atom and weak interatomic forces.

The interatomic (van der Waals) binding forces are weak due to the simplicity of the atom and closed electronic s-shell, giving no static dipole moment. The quantum-mechanical uncertainty relation states that a particle has an uncertainty in the momentum:

$$\Delta p \sim \frac{h}{R} \quad (3.1)$$

which results in a kinetic energy of localization (zero-point energy):

$$E_0 \sim \frac{(\Delta p)^2}{m} \quad (3.2)$$

where  $m$  is the mass of the atom,  $h$  is Planck's constant and  $R$  is the radius of the volume within which the atom is contained. From the relation we see that the low mass of the helium atom gives a high zero-point energy.

For the formation of solid helium, the zero-point energy is so large that the lattice is unstable unless large external pressure is applied, and helium remains liquid below this pressure. In hydrogen the polarized molecules yield van der Waals force that outweighs the zero-point energy, and the solid state is the stable one. Since all other substances are heavier than hydrogen and have stronger van der Waals forces, helium is unique in remaining liquid at indefinitely low temperatures.

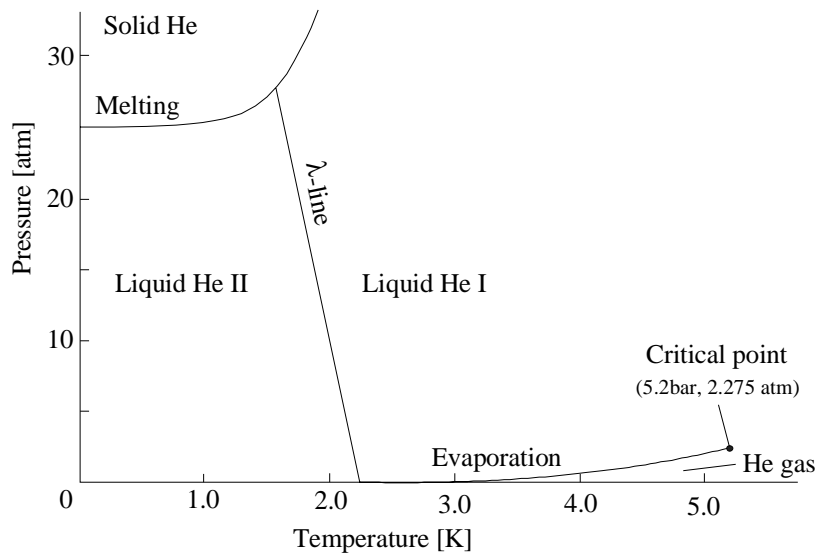


Figure 3.1 Phase diagram of helium [10].

Gaseous helium behaves more like an ideal gas than any other commonly known substance. This is brought on by the weak inter-atomic potential and the spherically symmetric molecular configuration. It is often most beneficial to consider properties of gaseous helium in terms of extensions from the ideal gas mode.

### 3.3 The two-fluid model of He II

Immediately below the boiling point helium essentially behaves like a classical fluid with small viscosity and low density. When the temperature is decreased by lowering the vapor pressure above the bath, the liquid boils and bubbles of vapor form within the bulk. At  $T=2.17\text{ K}$  a transition occurs and the liquid becomes quite still and no more bubbles

are formed when the liquid is cooled further. This transition is signaled by a specific heat anomaly whose shape has given the name  $\rho$ -point (lambda) to the temperature  $T_\lambda$  where it occurs, Figure 3.2. The  $\rho$ -transition is a second-order phase transition and the two phases cannot coexist in equilibrium. Specific heat of liquid helium is very large compared to other materials at low temperatures e.g.  $10^5$  larger than that of copper at 1.5 K. Further it is highly non-linear with temperature.

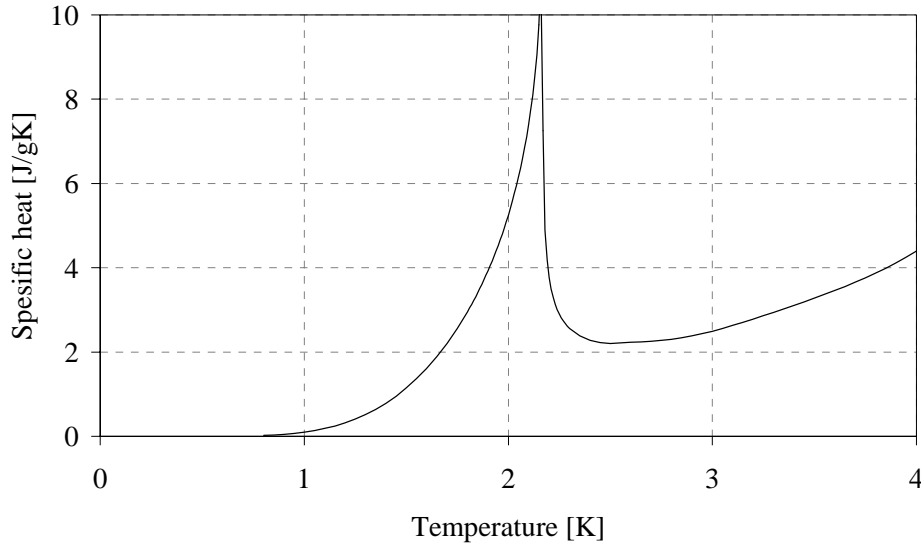


Figure 3.2 Specific heat of helium at 1 bar. Figure based on data from Hepak [11]

Above  $T_\lambda$  helium is termed He I, whereas below it is termed He II. Below the  $\lambda$ -temperature the state and transport properties of helium can only be explained using a quantum mechanical description. The Landua theory (1940) of excitations in He II, although semiempirical has considerable physical basis and is successful in describing state properties such as specific heat and entropy. However the transport properties such as heat and mass transport cannot be interpreted easily in terms of this theory. The transport of the properties of He II are better understood through the *two-fluid model* suggested by Tsiza (1938). This theory takes the state properties of He II as empirically determined quantities.

According to this model, He II is thought to consist of a mixture of two interpenetrating liquids; the normal fluid and the superfluid. This picture is not to be taken too literally. It is only a model and the existence of superfluid and normal fluid is a hypothesis. The normal fluid is assumed to behave as an ordinary fluid possessing viscosity  $\rho_n$ , entropy  $s_n$  and density  $\rho_n$ . The superfluid has density  $\rho_s$ , no entropy  $s_s=0$  and no viscosity  $\mu_s=0$ . The properties of the liquid are a linear combination of the properties of the two components. Hence the density is given as:

$$\mu = \mu_n + \mu_{sl} \quad (3.3)$$

Since the superfluid has no entropy, the He II entropy becomes:

$$\mu S = \mu_n S_n \quad (3.4)$$

It is assumed that  $s_n = s_\lambda$  the entropy at the lambda point, and that the strong temperature dependence of the entropy,  $\sim T^{5.6}$ , enters through the variation of the normal fluid density. It follows that:

$$\frac{\rho_n}{\rho} = \frac{\sum T}{\sum T_\lambda} \quad \text{for } T \leq T_\lambda \quad (3.5)$$

$$\frac{\rho_n}{\rho} = 1 \quad \text{for } T \geq T_\lambda$$

Because of this strong temperature dependence He II is 99 % superfluid at 1 K.

Two points are worth noting concerning terminology:

- The two fluids cannot be separated, and it is not permissible to regard atoms as belonging to either normal or superfluid, as all helium atoms are identical.
- He II might sometimes be termed *superfluid*, as it was before the introduction of the two-fluid model. It is now more correct to refer to helium below  $T_\lambda$  as He II, and the component in the model as superfluid.

### 3.4 Transport properties of He II

Heat- and mass-transport properties of He II can be understood through the two-fluid model.

Experiments to determine viscosity might be divided in two classes: (1) measuring viscous resistance to flow, (2) detecting viscous drag on a body moving in the liquid. Normally these two methods yield essentially the same result for liquids, whereas for He II the two methods give very different values. A virtually zero value for the viscosity is measured using a capillary channel flow experiment. Experiments using a rotating-disc record 'normal' values of viscous drag, and He II seems to be capable being both viscous and non-viscous at the same time.

This apparent contradiction might be explained through the two-fluid model. For the capillary type experiments the normal component is clamped in the tube but the superfluid component may flow without friction. In the rotating-disc experiments the normal component is forced to flow against its own viscous drag and a value for the



viscosity is recorded. Such a setup is used to measure the variation of  $\mu_s/\mu$  as a function of temperature.

This explains the property of film-flow observed in He II, where an empty container partially submerged in He II is seen to fill until the level in the container equals that of the surrounding bath. There exists a film of He II ( $\sim 100$  atomic layers) on the surface exposed to the saturated helium vapor. This film acts as a siphon and the superfluid component flows under the force of gravity into the container.

Thermal conductivity of He II is found to be very high, tending to infinity for small heat currents, and it is impossible to establish a temperature gradient in the bulk liquid. This accounts for why boiling suddenly stops when passing through the  $\rho$ -line: vaporization only occurs at the free surface since the absence of a temperature within the bulk fluid prohibits the formation of bubbles.

A temperature gradient can be set up between two vessels of He II connected by a superleak. A superleak is a channel which clamps the normal component but allows the superfluid component to flow e.g. a porous plug of fine powder. If heat is supplied to one side of the superleak, a temperature gradient is set up along with a pressure head giving a higher level in the vessel on the side where heat is supplied. Since  $\mu_s/\mu$  increase with decreasing temperature it can be inferred that the superfluid flows to the region of higher temperature in order to reduce the temperature gradient and conserve the overall density of the liquid.

In He II heat is not transferred by the normal processes of conduction and convection. Instead heat is transferred by an internal convection where the normal fluid flows from the heat source and the superfluid in the opposite direction, while preserving constant density everywhere in the fluid. This is illustrated in figure Figure 3.3.

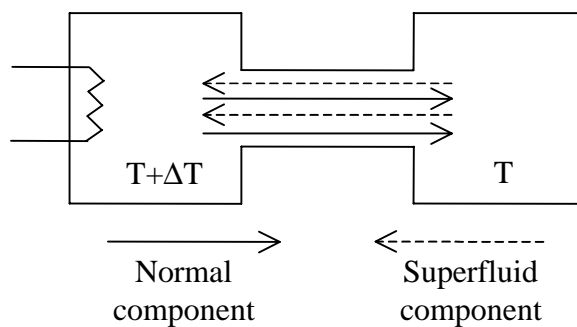


*Figure 3.3 Internal convection of superfluid and normal fluid in a channel of He II [12].*

The maximum heat flux  $q^*$  is that can be carried through the channel is characterized by the point where the helium adjacent to the interface of the heat source exceeds the local boiling point.  $q^*$  is strongly geometry and helium state dependent.

### 3.5 Steady state heat transport

The temperature difference  $\Delta T$  in He II occurs because of two mechanisms: normal fluid viscous interaction with the boundaries and mutual friction between the two turbulent fluid components. Normal fluid viscous interaction is dominant for small diameters, but for most practical applications the mutual friction is the limiting factor.

The turbulent heat transport equation in one dimension is written in the form:

$$\frac{dT}{dx} = f(T)q^m \quad (3.6)$$

Where  $f(T) = A\rho_n/(\rho_s^3 s^4 T^3)$  and  $m$  is a numerical coefficient which theory indicates should be equal to 3 but which experimentally has been shown to vary from below 3 to nearly 4 as temperature approaches  $T_\lambda$ .  $A$  is the Gorter-Mellink mutual friction parameter and  $\rho_n$  and  $\rho_s$  are the normal and superfluid densities respectively. The quantity  $f^{-1}(T)$  behaves much like a thermal conductivity, determining the temperature gradient in the presence of a heat flux. Figure 3.4 illustrates this quantity as a function of temperature and pressure. It shows strong temperature dependence with a maximum at about 1.9 K at 1 bar.

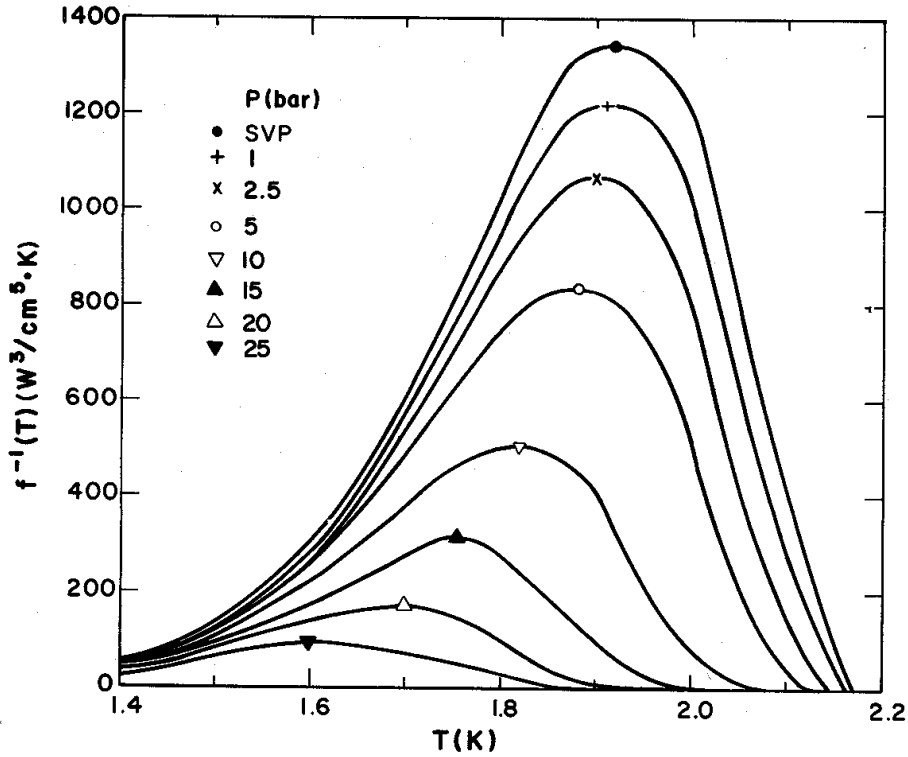


Figure 3.4 Heat conductivity function for turbulent He II. Symbols indicate the location of the peak value [13].

Heat transport in a channel of finite length  $L$  can be determined by integration of equation 3.6. The maximum heat flux along a channel is found by integrating from the bath temperature  $T_b$  to  $T_\lambda$ , the maximum allowable temperature difference:

$$q^* = \frac{\sum 1}{\sum L} \frac{\sum_{T_b}^{T_\lambda} dT}{\sum f(T)} \quad (3.7)$$

### 3.6 Kapitza Conductance

At low  $\Delta T$  no boiling occurs and the heat transfer is controlled by a phenomenon called Kapitza conductance. This thermal boundary conductance was first discovered by Kapitza in 1941 [14] when he observed a sizable temperature difference between the surface of a copper block and the bath of He II in which it was He II. In contrast the temperature in the bulk liquid was almost homogenous.

Kapitza conductance now refers to the interfacial thermal boundary conductance that occurs between any two dissimilar materials where electronic transport does not contribute. Since the effect is strongly temperature dependent it makes a negligible contribution to heat transfer except at low temperature. However, it is of great interest since at low temperature it can cause the largest temperature difference. To illustrate, a  $0.1 \text{ W/cm}^2$  heat flux can lead to a temperature difference of 100 mK across a surface due to the Kapitza resistance. To achieve the same temperature difference in heat transfer in a channel of He II would require the channel to 1000 meters long.

Ideally Kapitza conductance is defined as

$$h_{k_o} = \lim_{\Delta T \rightarrow 0} \frac{q}{\Delta T_s} \quad (3.8)$$

where the subscript 0 refers to the limit as  $\Delta T_s \rightarrow 0$ . A more general and practical definition relates the finite values of  $q$  and  $\Delta T$

$$h_k = \frac{q}{\Delta T_s} \quad (3.9)$$

Theories trying to explain this phenomenon are rather complex. Their basis is that the difference in the wavelength of the quantized lattice vibrations, phonons, between the helium and the solid constitutes a resistance to conduction. On the interface a large part of the phonons are reflected, and only a few with the right angle of attack might pass energy across.

Predictions made by the different models may vary by more than two orders of magnitude, and furthermore it is clear that Kapitza conductance is strongly affected by the nature of the surface, whether it is dirty, clean or treated in some way. For practical applications it is therefore important to obtain the Kapitza conductance of the surfaces involved preferably by measurement. Theories predict the conductance to be proportional to  $T^3$ , while experimental data show values of  $h_k \sim T^n$  where  $n$  is varying from 2 to 4. It is generally agreed to be 3 and  $h_k$  is then given as:

$$h_k = \beta \cdot T^3 \quad [W/m^2 K] \quad (3.10)$$

where  $\beta$  is constant which literature gives as 900 for clean surface and 400 for dirty surface.

Heat that is transferred between two baths of He II separated by a wall, will encounter the Kapitza resistance on warm side, the solid resistance in the wall and at last the Kapitza resistance on the cold side. The resulting temperature profile will qualitatively be as in

Figure 3.5.

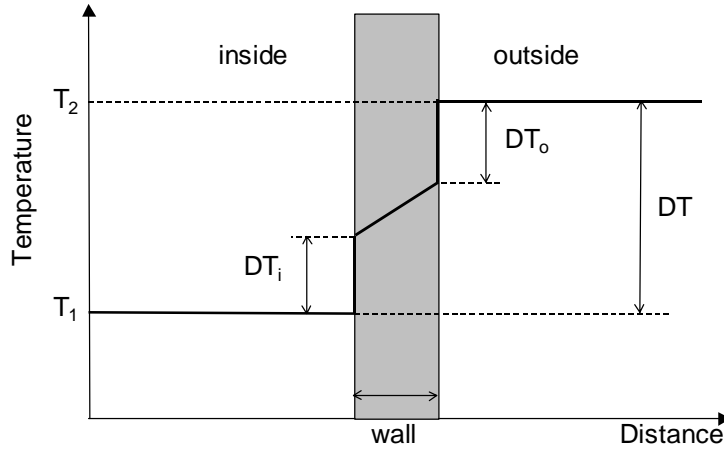


Figure 3.5 Temperature profile (bold line) over a wall separating two bodies of He II.

Heat flux is given by:

$$q'' = \frac{T_{\infty o} - T_{\infty i}}{R_{tot}} \quad (3.11)$$

$T_{\mu o}$  and  $T_{\mu i}$  are the temperatures of the two baths as there is no temperature gradient within bulk He II. The total resistance,  $R_{tot}$ , is

$$R_{tot} = \frac{\sum 1}{\sum h_{ki}} + \frac{1}{k_{wall}} + \frac{1}{h_{ko}} \sum \quad (3.12)$$

where  $k_{wall}$  is the thermal conductance of the wall material.

For the heat exchanger at the 1.8 K level of the String the following has been found [15]:

$$\begin{aligned} d &= 0.9 \text{ mm} \\ k_{wall} &= 5 \text{ W/Km} \\ \beta &= 860 \pm 30 \text{ W/m}^2\text{K} \end{aligned}$$

Using the same temperature of 1.8 K to calculate the Kapiza conductance on the inner and outer wall, the Kapiza resistance stand for 70 % of the total resistance to heat transfer.

## 4 The LHC Layout and Cryogenic System

The CERN Council approved the Large Hadron Collider (LHC) project in December 1994. Upon its completion in 2005 it will be the largest scientific instrument in the world. Recreating the conditions prevailing in the early universe  $10^{-12}$  seconds after the Big Bang when the temperature was  $10^{16}$  degrees, it will be used to study the structure of matter and basic forces of nature.

This circular particle accelerator will be built in a 27-km tunnel presently occupied by the Large Electron Positron (LEP) Collider. It will accelerate and bring into collision two counter rotating beams of protons and later also ions. In order to focus and bend these two beams into a circular path at a sufficiently high energy level of 7 TeV per proton beam, it will make use high-field superconducting magnets. The magnets will be constructed using NbTi conductor and operate in a static bath of pressurized superfluid helium at 1.9 K throughout the circumference. The presented description of the LHC is based on the conceptual design study of the LHC Study Group [16].

### 4.1 Plant layout

The LHC will mirror the layout of the existing LEP with its eight identical sectors of 2.9 km separated by straight sections used for the four experiments and utilities, Figure 4.1. Due to geological constraints the tunnel is constructed at an angle of 1.4 % and at a depth ranging from 60 to 140 meters.

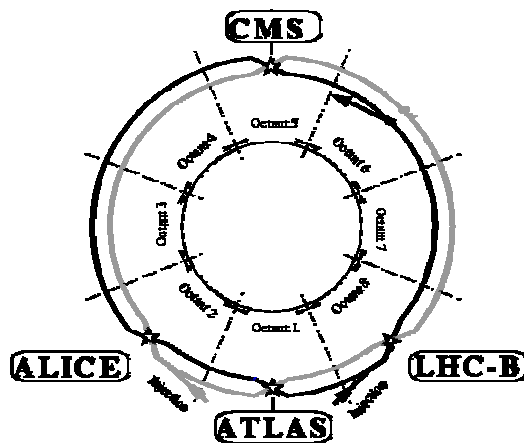
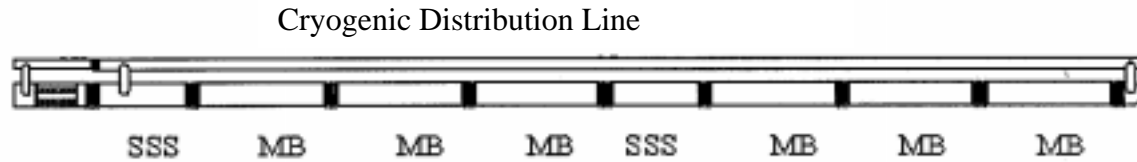


Figure 4.1 The layout of the Large Hadron Collider with experiments [17].

#### 4.1.1 The arc cells

The building block of the arcs are the 106.9 meter long independent cells each consisting of two times three bending dipoles (MB) and a focusing quadrupole (SSS), Figure 4.2. In

addition there are several types of smaller higher order magnets for various kinds of correction of the circulation particle beams. The cells are fed with cryogenic liquid by the cryogenic distribution line.



*Figure 4.2 The layout of the 106.9 meter full cells of the LHC consisting of two times three dipoles and a short straight section housing the quadrupole bending magnet [18].*

#### 4.1.2 Dipole bending magnets and quadrupole focusing magnets

The particle beams are kept in a circular path by the dipole bending magnets. There will be 1232 twin-aperture dipoles, with a magnetic length of 14.2 meters. Figure 4.3 shows the cross section of the bending dipoles.

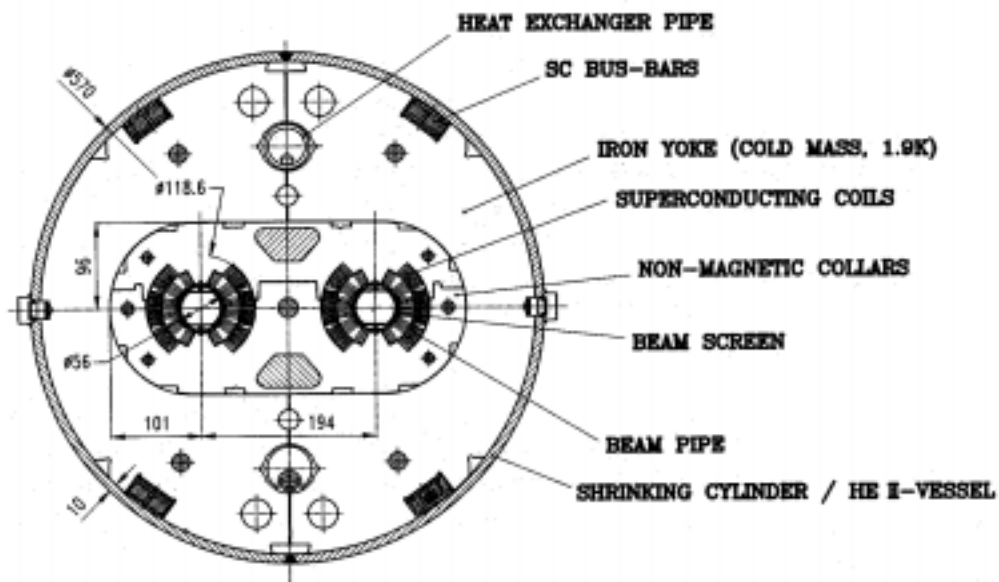


*Figure 4.3 The cross section of the cold mass containing the dipole bending magnets. The outer diameter of the cold mass is 57 cm [19].*

The two beam pipes are surrounded by two sets of superconducting dipole magnets. They are held in place by aluminum non-magnetic collars, which in turn are encapsulated by an iron yoke with the purpose of stabilizing the magnetic fields. The heat exchanger pipe is threading its way through all the six magnets of the cell. The iron yoke has holes for providing a longitudinal thermal bridge within the cold mass. A beam screen is located inside the beam tube. It is cooled to 5-20 K and will intercept stray particles from the beam to reduce the heat load on the 1.9 K level. The cold mass at 1.9 K is placed inside a closed shrinking cylinder/He II-vessel with a diameter of 58 cm. The iron yoke and non-magnetic collars consist of longitudinally stacked elements, illustrated in Figure 4.4.

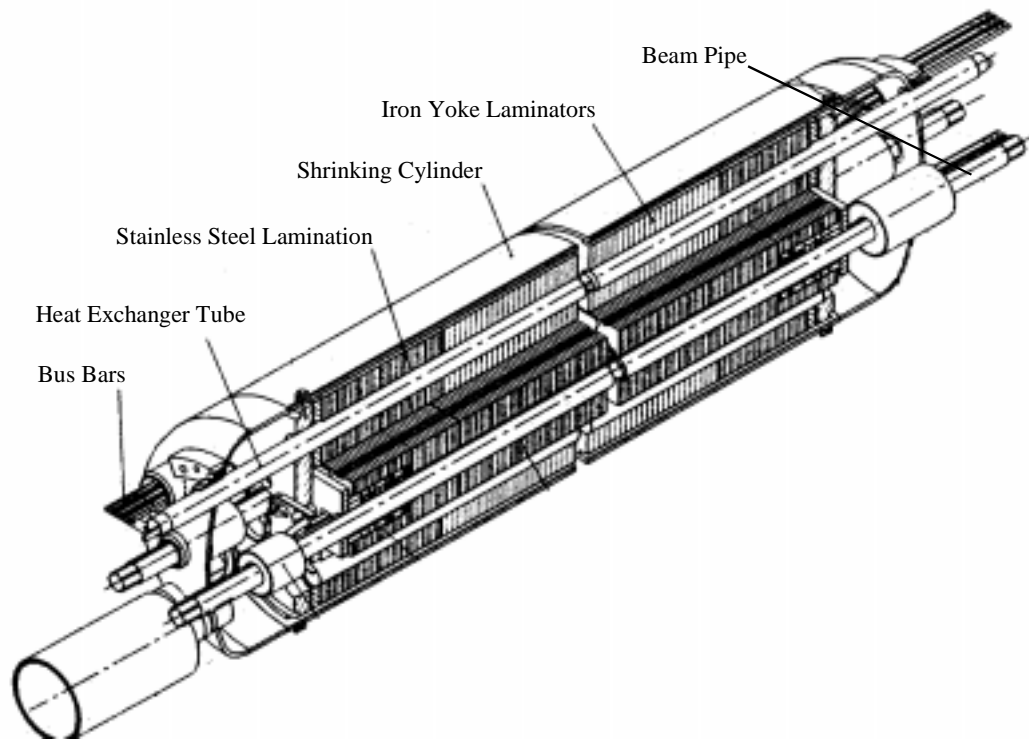


*Figure 4.4 Assembly of the dipole cold mass showing the longitudinally stacked elements [20].*

Static pressurized superfluid helium is filling the longitudinal holes and also penetrates into the transverse minute spacing between the yoke and collar elements, ensuring good transversal heat transfer and making the cold mass into a continuous body of He II.

To minimize heat inleak the cold mass is covered with layers of radiative insulation outside the shrinking cylinder. In the vacuum outside the shrinking cylinder there is an actively cooled thermal shield at 55-75 K and the whole assembly is sitting inside a vacuum vessel with an outer diameter of just under one meter.



Two support post made of composite per magnet are designed to minimize heat inleak and have a heat intercept connected to the thermal shield.

The cross section and design of the 3.1-meter focusing quadrupoles is essentially the same as for the dipoles except for the layout of the superconducting coils. The quadrupole is mounted in a short straight section that also can house smaller correction magnets.

## **4.2 The LHC Cryogenic System**

The superconducting magnets to be used throughout the circumference of the LHC will require very stable operating conditions around 1.9 K. The cryogenic system must be able to transfer cooling power over long distance (3.3 km) and small temperature difference ( $\sim 100\text{mK}$ ). As a basis the cryogenic system will reuse the present infrastructure and cryoplants in operation at the present LEP accelerator. The cryogenic system must also handle the static head in the cryogenic transfer lines resulting from the 1.4% slope of the tunnel and the 100 height difference from the lowest to the highest point of the ring.

In view of the high thermodynamic cost of refrigeration at low temperature, actively cooled thermal shields will intercept most of the system heat loads at higher temperature than 1.9 K. As a result the LHC requires a mix of refrigeration duties at different levels of temperature.

### **4.2.1 The General Layout**

Refrigeration will be produced by eight cryogenic helium plants evenly distributed around the ring. Each cryopant will have an equivalent capacity of 18 kW at 4.5 K and a total capacity of 144 kW at 4.5 K. The major part of the cryoplants will be located on the surface in order to reduce the requirement for underground space. Pressurized liquid at 20 K is led down through a vertical transfer line to the underground area where the rest of the cryopant is located. Each cryopant will supply two adjacent sectors of 3.3 kilometers with cryogenic liquid at different required temperatures through a cryogenic distribution line.

The large requirement, low saturation pressure of helium at 1.9 K and the limited space in the underground areas imposes the use of cold hydrodynamic compressors. The heat of compression deposited at low temperature demands high efficiency in these cold compressors for the technological and economical aspects of the project to be feasible. This technology was not available from industry when the LHC was approved constructed. Efficient and reliable solution has been developed by CERN in close collaboration with industry. The cold compressor units (CCU) will provide a pumping capacity of eight times 120 g/s at 16 mbar.

A major component of the cryogenic system is the cryogenic distribution line running alongside the magnets. The 106.9 meter long cells are fed cryogenic helium at several temperature levels through jumper connections from this line. The cells have individual cooling loops.

In case of a resistive transition (quench) in one or more of the superconducting magnets the pressurized liquid He II in the cold mass will be ejected from the magnets and into the distribution line. The ejected liquid and gas will be led to surface storage tanks and reintroduced into the system from there.

#### 4.2.2 Magnet Cooling Scheme

The thermal conductivity of static pressurized superfluid is large but not infinite, and cannot be used to transfer the heat loads involved over the distance required for the LHC. Cooling schemes based on forced flow of pressurized He II are hampered by pressure drop and Joule-Thomson heating and are also not applicable for the LHC.

The LHC cooling scheme is based on a quasi-isothermal heat sink running through the magnets in a bayonet heat exchanger [ref], the location of which can be seen in Figure 4.3. A flow of stratified two-phase saturated He II advances in the heat exchanger absorbs the heat loads as it evaporates. This scheme will be implemented as individual cooling loops for each cell as shown in Figure 4.5.

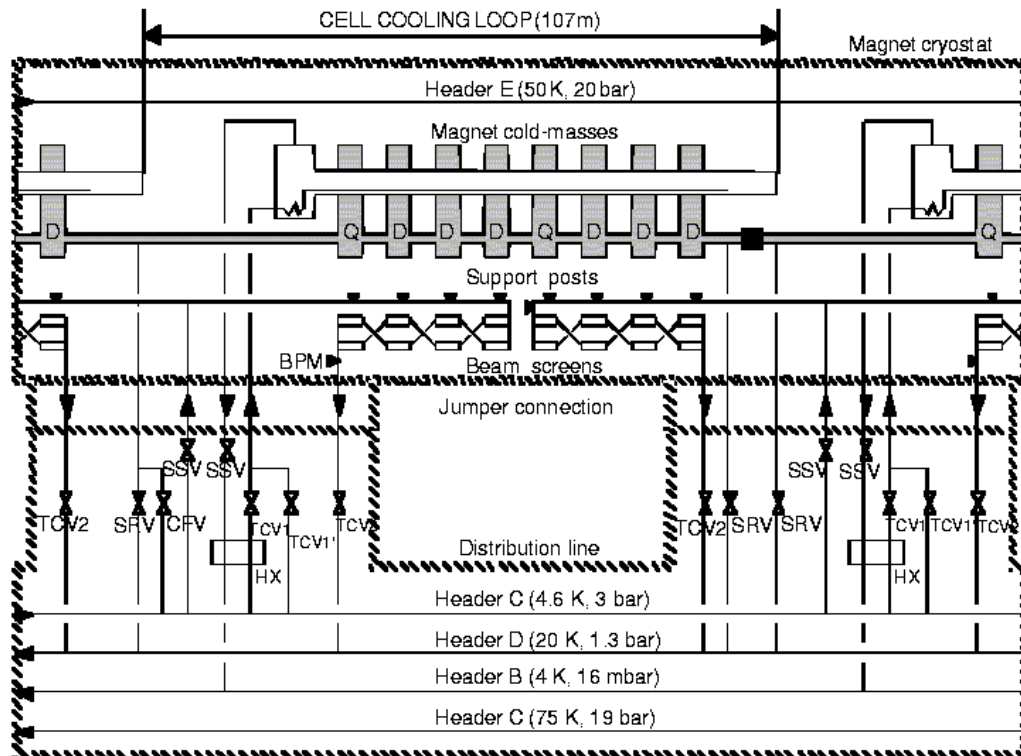


Figure 4.5 LHC full cell cooling scheme [21].

Pressurized helium at 4.6 K and 3 bar is taken from header C, and cooled against the out-flowing low-pressure helium vapor to 2.2 K in a heat exchanger (HX). It is then expanded to 1.9 K and 18 mbar by Joule Thompson throttling (TCV1) and fed into the bayonet heat exchanger. The liquid and flash gas from the throttling flow in co-current along the heat exchanger and the liquid is completely vaporized before it can reach the far end of the heat exchanger. In normal operation the liquid is vaporized after advancing about 1/3 of the length. The slightly superheated 1.9 K gas is then returned through the sub-cooling heat exchanger (HX) into header B which runs back to the helium plant.

The cooling loop for the thermal shield and support posts is fed from header E. The cooling loop for the beam screen is fed from line C.

## 4.3 Heat Loads

In normal operation of the machine there will be steady state heat load on the system as well some heat load that will occur as transients.

### 4.3.1 Steady state heat loads

The steady state heat load in normal operating conditions are grouped in three categories according to their origin:

- Natural heat inleak from ambient temperature.

This is heat conducted through the support posts, radiative insulation, quench valves and instrumentation feed-throughs, as well as radiation through the insulation vacuum. The natural heat inleak is foreseen to be about 0.5 W/m for the LHC machine. The natural heat inleak is larger for the Magnet Test String and measured to be about 1 W/m.

- Resistive heating.

This heat comes from the non-superconducting sections, like current feed-throughs and splices in the superconducting magnet.

- Beam induced heating.

This is heat load brought on by the circulating proton beams and arising from synchrotron radiation, image currents, longitudinal impedance and beam gas scattering.

Heat will be intercepted at 50-75 K, at 4.5-20 K and at 1.9 K as described in the previous section.

### 4.3.2 Transient Heat Loads

The transient heat loads during the operation of the machine come from:

-Losses during ramping and de-ramping of the magnet current.

These losses are due to hysteresis in the filaments, interfilament coupling, interstrand coupling- and eddy currents. The loss has two components. The hysteresis loss which is proportional with the current, and the coupling loss which is proportional to the ramping rate ( $dI/dt$ ). For nominal magnet current and ramping rate of 12.4 kA and 10 A/s respectively, this produces a heat load in the order of 0.2 W/m.

-Halo loss.

The halo is the outermost part of the circulating beam. At all times this part of the beam hits the wall and produces heat. The location in the machine where this happens is changing with the tuning of the machine. Although a continuous process it must be regarded as a transient heat load since its location changes arbitrary. The halo loss is estimated to be about 1 W/m over a section of 30 meters. It is the largest of the transient heat load and is the greatest cause of concern from a temperature-control point of view.

-Introduction of the proton beam.

The beam induced heating described under steady state heat loads will appear as a transient when the proton beams are fed into the beam pipes.

## 4.4 Magnet Test String

[22] The accelerator magnet test string is a 35-meter working model of a LHC half-cell such as it was before the simplification of the cryogenic scheme. It is assembled from three prototype dipole cryomagnets of 10 meters and one quadrupole cryomagnet housed in a short straight section of 5 meters according to the foreseen layout for the LHC at the time of its construction. In the present layout the LHC a half-cell is 53.45 meters.

Figure 4.6 shows the String viewed from on top of the String Feed Box (SFB) with the short straight section as the closest part. Among others the pneumatic motor of the Joule-Thomson valve can be seen in front. It is mounted with a 1.4 % gradient sloping towards the camera. This corresponds to the maximum slope of the LHC.

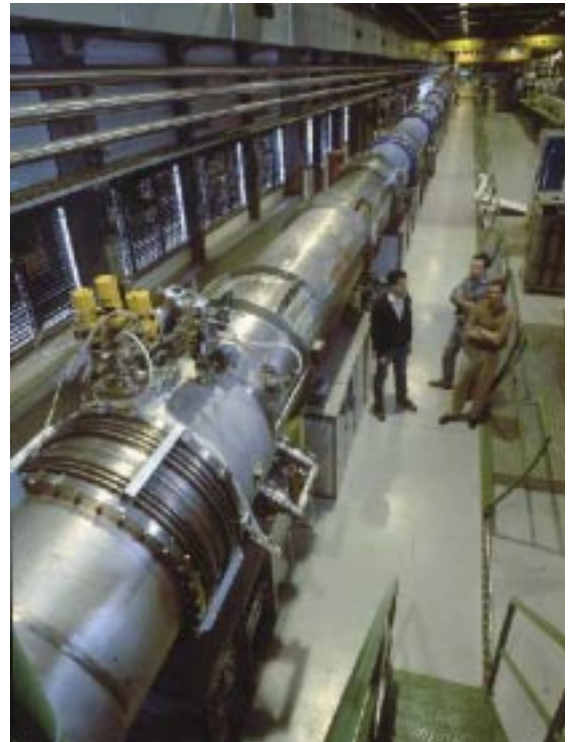


*Figure 4.6 The Magnet Test String viewed from on top of the String Feed Box. The short straight section housing the quadrupole is the first section of the String in this picture.*

The String was constructed to investigate aspects beyond single-magnet tests such as cryogenic transients, control aspects, electrical and thermohydraulic quench propagation effects, beam and insulation vacuum performances as well as installation and quality assurance procedures. In its five years of operation until its decommissioning in December 1998 it has operated 12 600 hours below 2 K for studying these aspects.

Apart from the apparent difference in length between the LHC and this String layout, a major difference is that the String has incorporated all of the cryogenic piping into the main cryostat and consequently does not have a separate cryogenic distribution line. Figure 4.7 shows the cryogenic flow scheme for the LHC Test String.

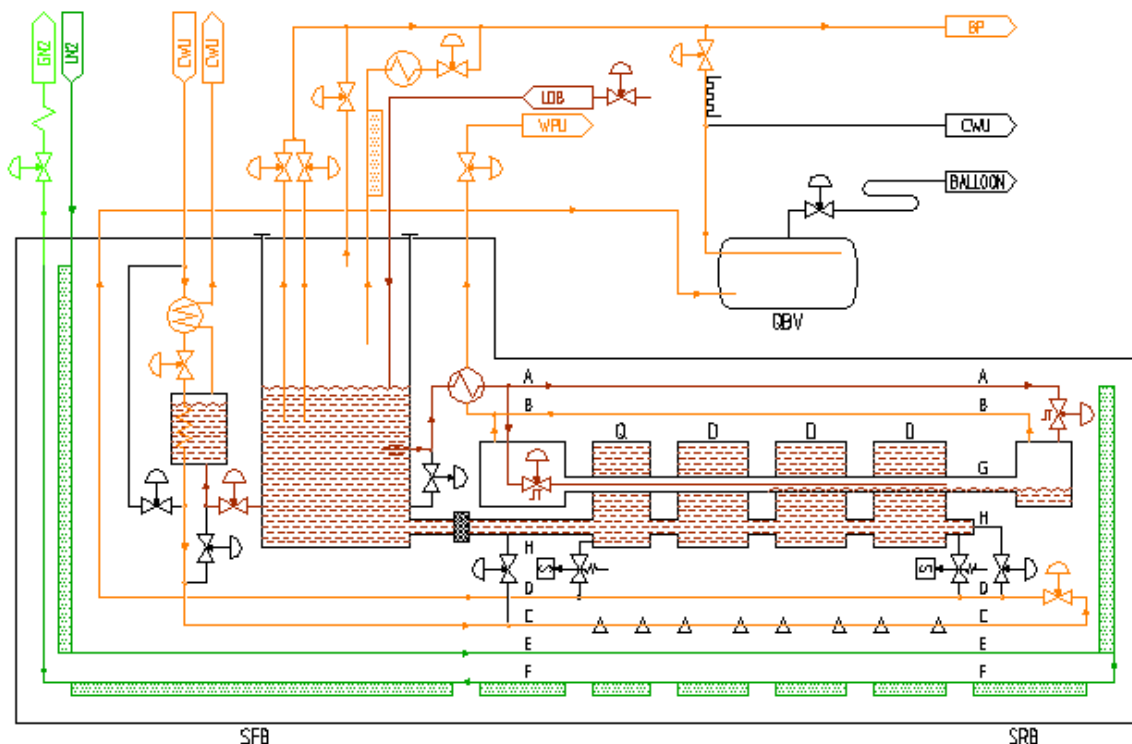


*Figure 4.7 Cryogenic flow-scheme for the LHC Test String. The String Feed Box (SFB) is on the left and the String Return Box (SRB) is on the right hand side [23].*

Liquid He I is taken from the main cryostat and subcooled in a very-low-pressure-heat-exchanger against the outflowing gas. It is then distributed through line A and expanded to saturation through a Joule-Thomson valve and fed to the far end of the heat exchanger tube. Saturation pressure is maintained by pumping the vapour through line B and the very-low-pressure-heat-exchanger. Line C supplies supercritical helium for cooling the magnet support post at 4.5 K. Line E and F are supplying liquid nitrogen to the thermal shield and magnet support to intercept heat at the 90 K level. After a magnet resistive transition the resulting pressure rise is kept below the 2 MPa maximum design pressure of the cold mass by opening the quench relief valve on the quench trigger and discharging helium in line D which leads to the Quench Buffer Vessel (QBF).

#### 4.4.1 Liquid Supply and Flow Measurement

The normal liquid He at 4.2 K in the main cryostat is separated from the superfluid helium in the cold mass by the lambda-plate, indicating the point where the temperature drops below the lambda point.

Liquid from the main cryostat goes into line A through a flow valve. This flow valve is fitted with a venturi flow meter. In line A additionally a thermal mass flow measurement can be done by means of two temperature sensors mounted on either side of an electrical heater. Measured temperature increase for the applied heat load and conservation of energy gives the mass flow. Conservation of energy gives:

$$\dot{m}T_1Cp(T_1) + \dot{q} = \dot{m}T_2Cp(T_2) \Leftrightarrow \dot{m} = \frac{\dot{q}}{T_2Cp(T_2) - T_1Cp(T_1)} \quad (4.1)$$

This type of mass flow measurement has the disadvantage of adding to the heat load on the system. It is therefore not continuously in use.

The thermal mass flow measurement gives relatively better results at lower mass flow rate since the observed temperature rise increases. Contrary the venturi flow meter performs better at high flow rates. Below 0.5 g/s it is not considered to give a reliable reading and the value is set to zero. Consequently attempting to measure liquid consumption integrated over a period of time will yield a result with a degree of uncertainty.

#### 4.4.2 Very-Low-Pressure Heat Exchanger

This is a vital part of the cryogenic system where the helium is cooled to a temperature inside the inversion curve where it can undergo Joule-Thomson expansion into the liquid phase.

The pressure drop for the gas directly affects suction pressure hence the work required from the pumping system. The efficiency of the heat exchange affects the overall mass-flow requirement since liquid fraction after expansion depends on the temperature of liquid upstream.

Knowing the pressures and having no vapor before the valve, conservation of enthalpy gives vapor fraction,  $x$ , after expansion as:

$$h_{1liq} = (1-x)h_{2liq} + xh_{2gas} \Leftrightarrow x = \frac{h_{1liq} - h_{2liq}}{h_{2gas} - h_{2liq}} \quad (4.2)$$

where 1 and 2 indicates before and after expansion. At design-pressures 1.15 bar and 18 mbar the vapor fraction will be  $x=0.12$  with 2.2 K before the valve. A temperature of 3 K before expansions increases the flash to  $x=0.21$ .

#### 4.4.3 Joule-Thomson Valve

The Joule-Thompson (JT) valve supplies saturated liquid and flash gas to the heat exchanger through a small supply line resting at the bottom inside the heat exchanger. According to the characteristic from the supplier it is linear up to 80 % opening where it supplies 6 g/s, and logarithmic thereafter supplying 12 g/s at 100 % opening. It is operated by a pneumatic motor.

#### 4.4.4 The Bayonet Heat exchanger

The liquid that has been expanded through the JT valve is fed to the far end of the bayonet heat exchanger [24] by a small tube resting on the bottom of the HX tube. The HX threads its way through all the magnets, and the liquid flows back by the force of gravity as it vaporizes. The helium gas is pumped out of the system at the far end. The heat exchanger is a corrugated copper tube with dimensions as shown in

Table 4.1



Table 4.1 Dimensions of the 1.9 K heat exchanger.

Wall thickness (e)	0.9	mm
Outer radius ( $r_{out}$ )	2.53	cm
Inner radius ( $r_{in}$ )	2.10	cm
Length of pattern ( $l_d$ )	1.50	cm
Pitch	1.22	cm

Figure 4.8 show a schematic view of the 1.9 K heat exchanger tube.

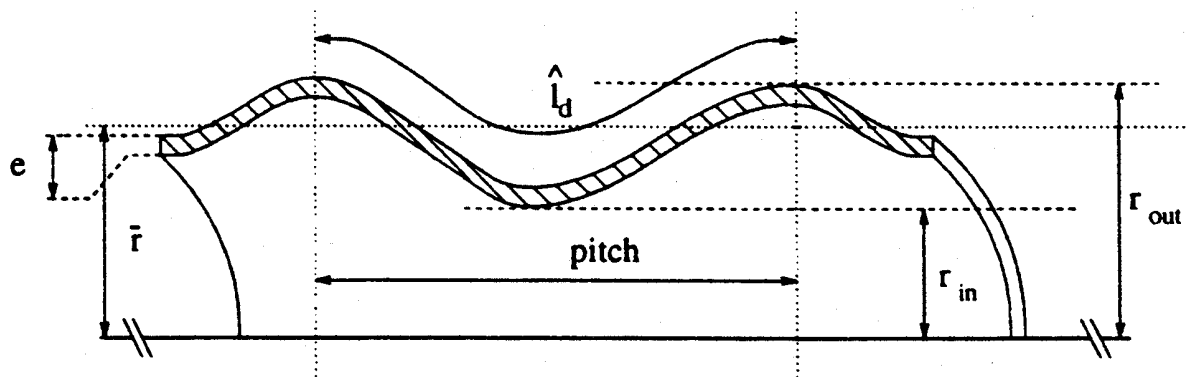


Figure 4.8 Schematic view of a section of the 1.9 K heat exchanger tube.

#### 4.4.5 Electrical Heaters

The magnets are equipped with electrical heaters for simulating heat loads. They are capable of producing heat-loads up to 40 W per magnet, well above any foreseen heat-loads for the LHC.

#### 4.4.6 Temperature sensors

The most important part of the instrumentation are the eight temperature sensors, one on each end of the four magnets, mounted at the vacuum side at the end plate of the pressure vessel.

They are CERNOX Model CX-1050-SD resistive temperature sensors with negative temperature coefficient (high resistance at low temperature and vice versa) manufactured by the LAKE SHORE company.

They are calibrated in-situ using the saturation pressure in the heat exchanger pipe as the temperature reference. This pressure measurement is the most accurate means of providing a reference.

The calibration is inserted into the PLC as a table deduced from the calibration function which is corrected according to the in-situ measurements.

The resulting accuracy is  $\pm 10$  mK below 4.2 K for the sensor. The electronic components have an accuracy of  $\pm 10$  mK below 4.2 K. The resulting accuracy for the temperature reading is  $\pm 20$  mK. The relative accuracy of the temperature sensors is an order of magnitude better and estimated to  $\pm 1$  mK [25].

#### **4.4.7 Disturbances**

The LHC Test String is subject to disturbances that will not be present in the future LHC.

The gas out of the heat exchanger tube is let into a central suction line leading to the pumping group of the facility. The central cryogenic system has several users injecting helium gas into this pumping line according to their need of refrigeration. Consequently the pressure in this line is not stable. A stable pumping pressure in the String system is maintained by a pressure controlled valve regulating on the pressure in the overflowing pot and with the back pressure in the central line as a disturbance. This control loop is always active and has a sampling time of one second, and the pumping pressure constantly exhibits  $\pm 1$ -2 mK oscillations. The pressure in the return line of the Cryogenic Distribution Line of the LHC is foreseen to be more stable than what is the case for the String, and the control of the 1.9 K cooling loop will not be subject to this disturbance.

Nitrogen cooling loop for the thermal shield and magnet support posts exhibits oscillations with a time constant in the order of several hours. The heat inleak to the 1.9 K level varies accordingly. This can be observed as a increase in liquid consumption in steady state condition where the JT valve opening will oscillate with  $\pm 2$  % opening and the same time constant as the nitrogen loop to match the variation in heat inleak. The corresponding variation in heat inleak is about  $\pm 2.5$  W, which is non-neglectable compared with the overall heat inleak of about  $1 \text{ W/m} = 35 \text{ W}$ . This disturbance is also not foreseen to be present in the LHC machine.

## 5 Control Aspects for the 1.8 K Cooling Loop

[26] [27] A *process* might be described as an object where variables interact to produce observable signals. Observable signals are called *outputs* also denoted controlled variables of the system. External signals that can be manipulated by the observer are called *inputs* also denoted manipulated variables of the system. External signals that cannot be manipulated by the observer are called *disturbances*. Disturbances are distinguished according to whether they might be measured directly or if their influence only can be observed on the output. Systems having a single input and single output are called a SISO system. Systems with multiple inputs and outputs are denoted MIMO system.

There is a fundamental difference between *feedback* and *feedforward* control of a process.

Feedback controller takes corrective action when the controlled variable deviates from the set point, regardless of the source and type of disturbance. An implicit disadvantage is that no control action can be taken until after a deviation is observed. The concept of feedforward control is to measure the disturbance and take corrective action before it upsets the system. Achieving this presumes the disturbance can be measure online, also a relationship between control action and effect must be established. The accuracy of the relationship impacts on the performance of the feedforward action.

Selection of the controlled, manipulated and measured variables represents a major decision in control system design. Relevant guidelines for this selection include:

- Controlled variable: select variables that are not self-regulating. Variable that may exceed equipment and operating constraints, and variables that seriously interact with other controlled variables (MIMO system).
- Manipulated variables: select inputs that have large effect on the controlled variables, and inputs that rapidly affect the controlled variables.
- Measured variables: reliable, accurate measurements are essential for good control. Measurement points should be selected to minimize time delays and time constants.

### 5.1 Present control strategy for the 1.8 K cooling loop

The control strategy for the 1.8 K cooling loop of the LHC Test String has evolved through an R&D program over many years involving several test benches. The process and control strategy for the accelerator itself will be a further refinement or alteration based on the experience gained through the String and the ongoing R&D program.

The present control strategy is an industrial PID feedback control applied on a SISO system. The manipulated variable is the Joule Thomson valve and the controlled and measured variable is the magnet temperatures as illustrated in Figure 5.1. None of the imaginable disturbances in steady state operation are measurable. Disturbances during

ramping, de-ramping of magnet current and introduction of the particle beams can be anticipated and their magnitude estimated. They can be regarded as measurable disturbances.

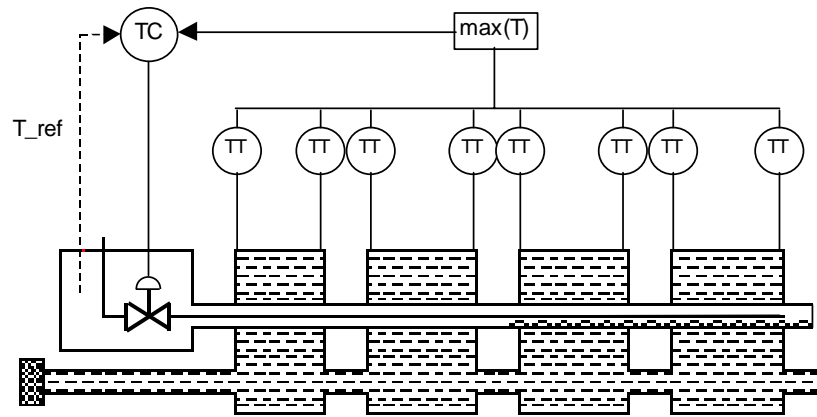


Figure 5.1 Control scheme for the 1.8 K Cooling Loop showing the eight temperature sensors (TT), the temperature controller (TC) and the Joule-Thomson valve.

The highest of the measurements from the eight temperature transmitters (TT) is at every sampling interval chosen and fed to the temperature controller (TC). The reference temperature ( $T_{ref}$ ) given to the controller is the saturation temperature measured in the volume of the overflow pot at the end of the heat exchanger. The set point temperature, which is the temperature the controller seeks to keep the magnets on, is a fixed offset from  $T_{ref}$  to allow a temperature margin for heat transfer in the system. The set point is an adjustable parameter of the controller along with the proportional, derivative and integral action.

## 5.2 Process Characteristics

From a control point of view there are several features that are important to identify since they affect the dynamic behaviour of the cooling loop of the system and impact on the control system design. For the 1.8 K cooling loop of the Magnet Test String the following has been identified.

### -Integrating process

also denoted non-self regulating or open loop unstable process in literature. For an integrating process in steady state submitted to a step in the manipulated variable, the controlled variable will either increase or decrease with time, and no new steady state will be attained. The temperature control of the cooling loop is an integrating process as a

change in either the manipulated variable (JT-valve) or the heat inleak (unmeasurable disturbance) will not lead to a new steady state of the system.

- Non linear

The process contains several non-linear physical parameters. Most importantly the specific heat of He II more than doubles its value between 1.8 to 2.2 K. In addition heat transfer in superfluid helium is a strongly non-linear process. The gas density varies noticeably in the temperature region. This change impacts on the pressure drop hence the saturation temperature in the heat exchanger and consequently the temperature margin for heat transfer.

- Variable dead time

**The heat exchanger is operated with a partial wetting of the length of the tube. The degree of wetting varies according to the heat load, the temperature difference between the saturation temperature along the tube and the magnet temperature and the history of the liquid flow from the JT-valve still stored in the wetted profile. This constitutes a variable time delay in the process.**

- Non minimum phase

**A process is non-minimum phase when competing dynamic effects operate on two different time scales. When increasing the JT valve opening to increase the cooling power, also the amount of flash gas and consequently the pressure drop along the Hx-tube increases. This leads to a higher saturation pressure profile along the tube consequently decreasing the actual cooling power provided by the wetted length and the temperature will increase during a transient period. This inverse response makes the system non-minimum phase.**

### 5.3 Temperature Margins and Control Band

The temperature of the superconducting magnets is a control parameter with strict operating constraints imposed by (a) the maximum temperature at which the magnets can operate, (b) the cooling capacity of the cryogenic system, (c) the variability of applied heat loads and d) the accuracy of the instrumentation.

A temperature regulation with a narrow control band will ease the demands on these constraints as illustrated in Figure 5.2. Less frequent recalibration of the temperature sensors and less accurate sensors and electronic equipment can be tolerated. Higher suction temperature at the compressors will ease the required work of compression. The magnets can be operated at a lower temperature and higher magnetic fields.

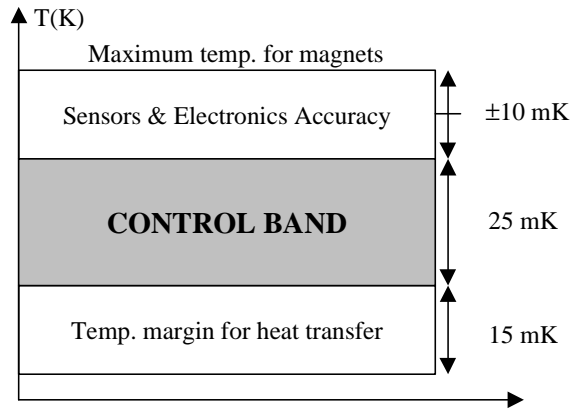


Figure 5.2 Temperature margins for the process (indicative numbers).

## 5.4 Classical versus advanced control

Possible choices for control structure for the 1.8 K cooling loop can be categorized in two broad classes: (a) conventional or classical control, normally a PID type controller, (b) advanced also denoted modern control.

A narrower control band can in principle be achieved by implementing a modern control. [28]. The class of modern control now hosts a variety of different approaches such as pole placement (RST), adaptive control, fuzzy logic,  $H_p$  control, Linear Quadratic control, and an array of predictive controllers.

A unified approach to Model Predictive Control (MPC) has been developed [29]. This approach unifies a number of well known predictive controllers and is also set in reference to approaches such as pole placement and. Adaptive control can be an extension to MPC control. MPC is the most frequently applied advanced control methodology and works satisfactory in the majority of the applications. This is the class of advanced control that is investigated for implementation on the 1.9 K cooling loop.

### 5.4.1 PID control

Standard PID controllers are of the form [31]:

$$p(t) = p_0 + K_c \frac{\sum}{\sum} e(t) + \frac{1}{\tau_I} \sum_0^t e(t) dt + \tau_D \frac{de}{dt} \frac{\sum}{\sum} \quad (5.1)$$

$p(t)$  is the controller output,  $p_0$  is the nominal action,  $K_c$  [-] is the controller gain,  $e(t)$  is the error signal,  $\tau_I$  [s] is the integral time and  $\tau_D$  [s] is the derivative time. The error signal  $e(t)$  is given by:

$$e(t) = R(t) - B(t) \quad (5.2)$$

where  $R(t)$  is the set point and  $B(t)$  is the measured value of the controlled variable.

Advantages of the PID controller are that they are simple, cheap and readily available off the shelf. They do not require a model of the process, and can be tuned with only a very limited knowledge about the process that they shall regulate. It is the most well known, widely applied and recognized control structure.

PID regulators are not optimal when one or more of the following characteristics are present: non-linearities, long time delay, or non-minimum phase. Feed forward action from measurable disturbances is not a structured part of the controller, but can be incorporated if required. Handling constraints in the process is also not incorporated in the structure. A drawback compared to MPC controllers is that there is not a clear connection between the tuning parameters and the response of the controller; the tuning is not performance oriented.

### 5.4.2 MPC control

[30] Predictive control belongs to the class of model-based controller design concepts. The success of MPC technology as a process control paradigm can be attributed to three important factors. Firstly the incorporation of an explicit process model into the control calculation. This allows the controller, in principle, to deal directly with all significant features of the process dynamics. Secondly the MPC algorithm considers plant behaviour over a future horizon in time. This means that the effects of feedforward and feedback disturbances can be anticipated and removed, allowing the controller to drive the plant more closely along a desired future trajectory. Finally the MPC controller considers process input, state and output constraints directly in the control calculation. This means that constraint violations are far less likely, resulting in tighter control at the optimal constrained steady state for the process.

### 5.4.2.1 The predictive control concept

The way predictive controller operates for a SISO system is illustrated in Figure 5.3. The time scale is discrete and relative to the sample  $k$ , which denotes the present.  $u$  is the controller output,  $y$  is the process output,  $w$  is the desired output called reference trajectory.  $H_p$  is the prediction horizon and the symbol  $\hat{\cdot}$  denotes estimation.

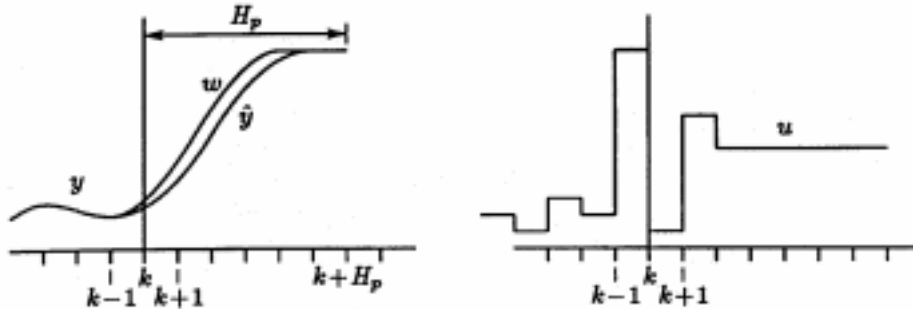


Figure 5.3 The concept of receding horizon predictive control. At the next sampling interval updated values for the used [32].

A predictive controller calculates a future controller output sequence  $u$  such that the predicted output of the process is 'close' to the desired output  $w$  which can be an arbitrary sequence. Only the first element of the controller output sequence is used to control the process. At the next sample time  $k+1$  the whole procedure is repeated using the latest measured information. This is what is referred to as the receding horizon principle. Receding horizon approach allows compensating for future disturbances or modelling errors. The process output is predicted by a model of the process to be controlled. In order to define how well the predicted process output tracks the reference trajectory, a criterion function is used. A more detailed description of the predictive control concept is given in chapter 7.

### 5.4.2.2 Advantages and drawbacks of MPC

Three factors were mentioned as the basis for the success of the MPC technology: (1) incorporation of an explicit process model, (2) considering plant behaviour over a future horizon in time and (3) considering input, state and output constraints directly in the control algorithm. These factors give rise to several attractive features.

MPC can be used to control a wide variety of processes without the designer having to take special precautions. It can be used to control 'simple' processes as well as 'difficult'



processes containing time delay, being non-minimum phase and processes that are open loop unstable.

MPC has automatic dead time compensation and it makes a clear distinction between reference tracking (feedforward) and noise rejection (feedback). In a natural way feed-forward action can be introduced, and pre-scheduled reference trajectories or set point can be dealt with.

The methodology is the only that can handle process constraints in a systematic way during the design of the controller. This is what most clearly distinguishes MPC from other process control paradigms.

It is not restricted to SISO processes, and extending the predictive controller to a MIMO process is straightforward. Non-linear models can also be introduced, with potential improved performance over linear MPC controllers for highly non-linear processes. However there still remains significant work before the field of non-linear MPC control can be considered a mature technology.

MPC controllers are relatively easy to tune, making them attractive to a wider class of control engineers and even people that are not control engineers. The tuning parameters are closely linked to the performance of the process. The tuning parameters are more decoupled than what is the case for the PID tuning parameters.

Finally as an advantage MPC is an open methodology, meaning that within the framework of predictive control there are many ways to design the controller.

This point is also a drawback of the MPC. Since it is an open methodology many different controllers can be derived having different properties, differences that can yield very different behaviour of the closed loop system. As a result it can be quite difficult to select which predictive controller that should be used to solve a particular control problem.

Perhaps the biggest drawback compared with PID control is that a model of the process must be available. In developing a controller two phases can be distinguished: modelling and controller design. Predictive control methodology provides only a solution for the controller design part. The process of deriving an appropriate model for an MPC controller has not been addressed in the same structured manner as has the control design. This obstacle has been recognized and more effort is now being put into the field of modelling for MPC controllers. However it still is a major drawback, and it has been reported that as much as 90 % of the effort of designing an MPC controller goes into creating the process model.

The disadvantage of predictive control being much more demanding from a computational point of view is becoming less important as computers steadily become less expensive and more powerful. Nonetheless the cost of developing a predictive controller is significantly higher than using a classical controller. The benefits in process

control must be offset by the increased cost of development and hardware for a predictive controller to be attractive.

In view of the advantages and drawbacks of MPC and PID control and the challenges posed by the dynamic properties of the system there is a strong motivation to investigate the use of a predictive controller for the 1.8 K cooling loop of the Magnet Test String and the future LHC.

## 6 Experimental Investigation

For properly being able to model and control a system a thorough understanding of the characteristic features and dominant parameters of that system is required. In this chapter a series of experiments are described. They were performed prior to and during the course of the modelling of the system and design of the MPC controller described in chapter 8. They identify and demonstrate fundamental features and have been an essential part of the development of the model and the MPC controller.

The experiments have two purposes: obtaining data required for building the first principle described in chapter 7, and experiments performed in order to identify and understand fundamental features of the system.

### 6.1 Liquid velocity in the heat exchanger tube

The velocity of the advancing saturated He II liquid from the Joule Thomson valve in the heat exchanger tube was realized to be an important feature. This velocity governs how fast liquid can be transported to the dry area of the heat exchanger and increase the cooling of the system. A set of measurements to determine the characteristic of this flow were performed as follows:

The temperature of the system was lowered to the temperature where the whole length of the heat exchanger is needed to extract the heat leak. This is the lowest achievable temperature for a given saturation pressure. This was achieved by opening the valve in manual slightly more than the steady state opening observed with the regulator in automatic mode and the system in steady state conditions. Eventually the heat exchanger is totally wetted and slightly overflowing which was detected by observing a continuously increasing level in the overflowing pot located at the outlet of the heat exchanger tube.

The valve was then in manual mode set to a higher opening, thereby increasing the liquid flow and creating a wave of liquid travelling along the already totally wetted heat exchanger tube.

The arrival of this wave in the overflowing pot was detected by a sharp increase in the rate of filling of the pot. The flow velocity is calculated as the ratio of the length of the tube over the recorded time for the wave front to arrive. The frequency of the logging system and uncertainty in detecting the transition in rate of filling makes the timing measurement accurate to within 10 seconds. In addition there might be an uncertainty in whether the tube and the corrugations at the end of the tube are completely wetted continuously. This because the flow of liquid in the supply line to the JT valve as observed by reading the FT 9202 (located before the Very Low Pressure Heat Exchanger)

is sometimes observed to fluctuate. These factors give an uncertainty in the results of 10 %.

With a steady state opening of 25 % this procedure was carried out for valve opening between 40 to 80 %, and at two different pressures, 10 and 21 mbar. 21 mbar is around nominal operating conditions while 10 mbar was the lowest pressure allowed by the cryogenic system. The results with 10 % error bars are shown in the left graph of Figure 6.1. On the right side in the figure is shown the same data with valve opening converted to liquid flow according to the valve characteristic described in section 4.4.4. At 10 mbar the flash over the expansion is  $x=0.1441$ , and at 21 mbar  $x=0.1182$ , an 18 % increase. Data from these experiments are found in Section A-1.

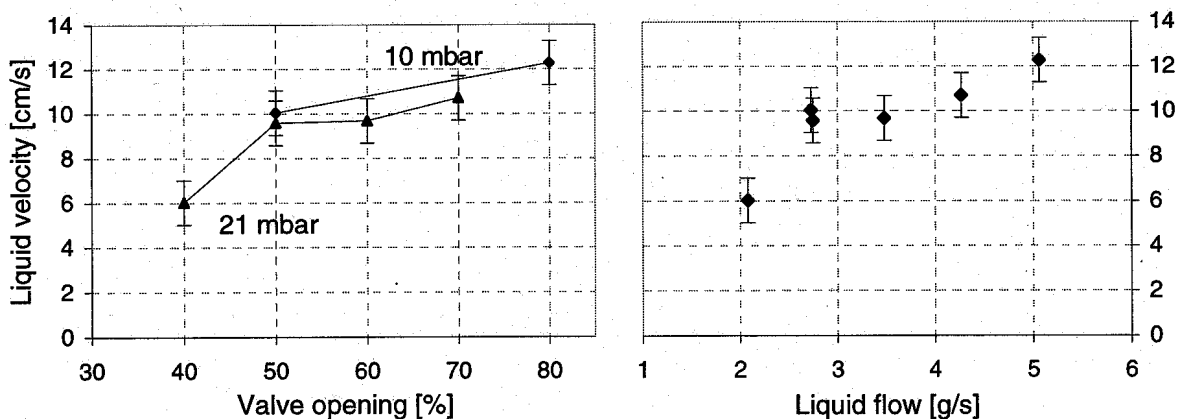


Figure 6.1 Liquid velocity in the heat exchanger tube. On the left hand figure shown as a function of valve opening, and on the right hand figure as a function of liquid flow.

The velocity of the advancing liquid is in the order of 10 cm/s. It is showing a fairly linear dependence of the valve opening with a minimum of about 6 cm/s. The lower flow velocity at low opening of the valve is thought to arise because some of the liquid of the advancing wave-front is retained in the tube. At high opening relatively less of the wave front is retained.

Within the error of measurement the velocity of the advancing liquid is independent of the pressure in the tube as can be seen on the left-hand side of Figure 6.1. There is a doubling of the density of the gas from 10 to 21 mbar, furthermore the increase in flash over the valve results in more than twice the velocity of the gas for the same valve opening. This leads to the conclusion that there is only a feeble interaction between the liquid and the gas states.

## 6.2 Amount of pressurized He II in the magnets/cold-mass

The pressurized He II present in the cold mass dominates the heat capacity of the system at 1.9 K in spite of constituting less than one percent of the total weight at this temperature level. This is due to the extreme specific heat of He II at this temperature and the decrease of specific heat of metals at low temperature. Clearly a good estimate of the amount of He II in the pressure vessel is important.

Various estimates of the He II content of the cold mass exist. These estimates are based on geometrical considerations, measurement of the He II expelled from the following a quench and measurement of the helium inserted during filling of the cold mass. However the values from these vary with more than a factor of two, and moreover it is difficult to assess the nature and magnitude of the factors giving rise to these diverging figures. Consequently a reliable estimate of the amount of He II in the cold mass can not be derived from these results.

This was the motivation for devising an experiment intended to estimate the amount of He II by observing the rate of temperature increase of the system when no cooling was provided.

Starting in normal operating conditions, the supply of cooling liquid was stopped and the system was allowed to warm up by the steady state natural heat inleak. When the temperature had risen half the way up to a maximum temperature imposed by security considerations, an additional 34.75 W was added evenly along the length by the heaters in the magnets thereby increasing the rate of warming up. The outcome of the experiment is shown in Figure 6.2.

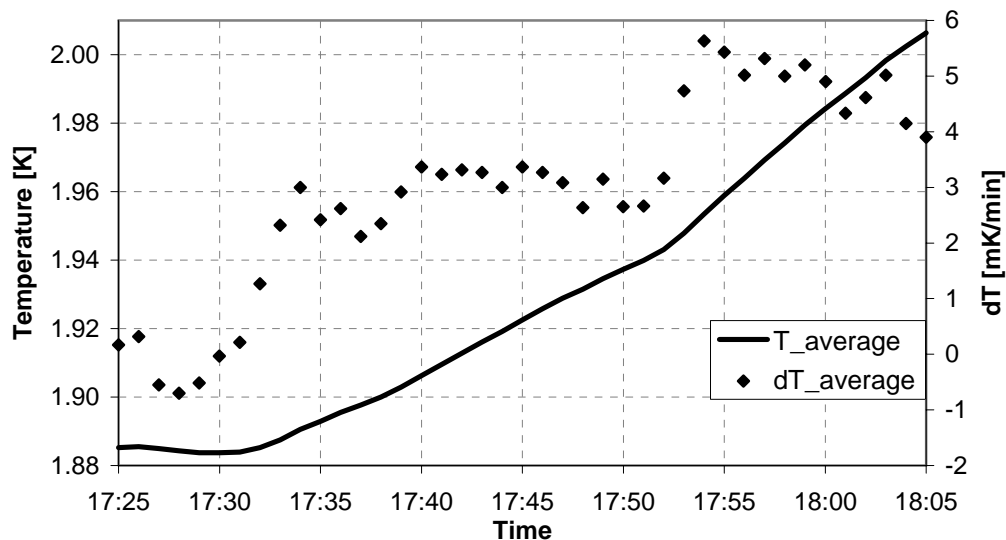


Figure 6.2 Thermal measurement of the He II content of the String, derived from the observed change in rate of warming when extra heat load is applied.

The specific heat of the system and the magnitude of the natural heat inleak can be deducted from this data by the following reasoning:

The rate of temperature increase is described by:

$$\frac{dT}{dt} = \frac{q(t)}{Cp(T)} dt \quad (6.1)$$

Assuming that the specific heat of the system arises solely from the He II and that the heat inleak is time independent the equation becomes

$$\Delta T_{1 \rightarrow 2} = \frac{q_{ss}}{m_{HeII} \bar{c}p_{HeII}(T_{1 \rightarrow 2})} \quad (6.2)$$

where

$$\bar{c}p_{HeII}(T_{1 \rightarrow 2}) = \frac{1}{\Delta T_{1 \rightarrow 2}} \sum_{T_1}^{T_2} cp(T) dT \quad (6.3)$$

denotes the average specific heat between temperatures  $T_1$  and  $T_2$ .

Knowing the temperature dependence of  $cp$  for He II allows finding the values for  $m_{HeII}$  and  $q_{natural}$  by solving the matrix:

$$\frac{1}{m_{HeII}} \cdot \frac{\sum q_{natural}}{\sum \bar{c}p(T_{1 \rightarrow 2})} = \frac{\sum \Delta T_{1 \rightarrow 2}}{\sum \Delta T_{3 \rightarrow 4}} \quad (6.4)$$

where  $q_2 = q_{natural} + q_{input}$ ,  $\mu T_{1 \mu 2}$  and  $\mu T_{3 \mu 4}$  indicate that the temperature increase is evaluated during the two steady ramp rates observed in Figure 6.2

The apparent content of He II was found to be 180.6 kg. The natural steady state heat inleak was found to be  $q_{natural} = 38.6 \text{ W} = 1.10 \text{ W/m}$ . Data underlying these figures is found in Section A-2.

Some aspects concerning the uncertainty of these results should be addressed. Firstly it is apparent to question the temperature measurements, as cryogenic temperatures are reputedly difficult to measure. The temperature used in the calculations is taken as the

average of the reading of the eight temperature sensors. The sensors have a relative accuracy of  $\pm 1$  mK and the measured temperature increases during the two ramps similarly accurate. The sensors have an absolute accuracy of  $\pm 20$  mK which must be taken into account when evaluating the specific heat used in the calculations. The value of  $c_p$  changes 6 % per 20 mK in the temperature range.

Secondly is the question of uncertainty of the pressure at which specific heat is evaluated. At 1.9 K the change in  $c_p$  from 1 to 2 bar is about one percent. The pressure is measured to be 1.2 bar well within that interval, hence the uncertainty related to the pressure is of second order compared to that of the temperature sensors.

Thirdly it is natural to ask whether the heat exchanger is completely free of liquid and the temperature allowed to rise freely. Examining the derivative of the average temperature it is observed to exhibit the same behaviour as the inverse of the derivative of the  $c_p$  over the corresponding temperature intervals. A 10 % and 15 % increase of the  $c_p$  is observed as comparatively similar decreases in ramp rate during the two ramps respectively. This is also a verification of the procedure.

### 6.3 Thermal conductivity of the 1.9 K heat exchanger tube

The heat load at the 1.9 K level is transferred from the static He II, through the copper wall of the heat exchanger tube and to the saturated He II in the 1.9 K. An experiment was carried out to measure the thermal conductance of the 1.9 K heat exchanger.

Starting in steady state at normal operating temperature and pumping pressure, the valve was opened in manual mode 10 % above the steady state opening previously observed in automatic mode. The temperature decreased and eventually reached a new steady state with the heat exchanger tube wetted along all the length. This was verified by observing a continuously slowly rising level in the overflowing pot.

An additional heat load of 0.2 W/m was then added by the electrical heaters, and the system was allowed to warm up and reach a new steady state temperature. The heat load was increased in steps of 0.2 W/m up to a maximum of 2 W/m, at each step allowing the system to reach steady state. Heat load was then decreased to 1.3, 0.9 and 0.5 W/m, at each level reaching steady state, to test against hysteresis effects. Valve opening was for each step adjusted to ensure fully wetted conditions. Data from this experiment is found in Section A-3.

The temperature increases observed by all the sensors have been averaged and least square estimate method applied to the trend of the data. The result of the experiment is shown in Figure 6.3.

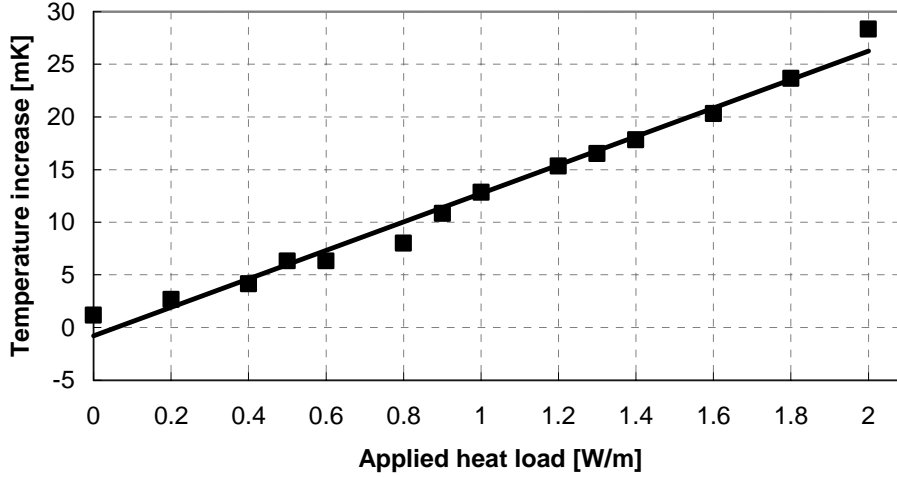


Figure 6.3 Thermal conductivity measurement of the 1.9 K heat exchanger.

No hysteresis effects are observed. The data recorded while decreasing the heat load falls in line with the data recorded while increasing the heat load.

The global heat transfer coefficient for the tube can be calculated from the observed temperature increase as a function of applied heat load according to the relation:

$$h_{global} = \frac{dq}{dT} \quad [\text{W/Km}] \quad (6.5)$$

where the values for  $dq$  and  $dT$  come from the trend line of the averaged data. Global heat transfer coefficient calculates to be:

$$h_{global} = 73.9 \text{ W/Km} \quad (6.6)$$

Note that the coefficient is given per unit length and not as the normal convention in literature per unit area. This is based on the assumption that the part of the circumference of the tube that is wetted is constant during the measurement.

This is partly justified by the corrugated geometry of the tube, which provides good wetting with little liquid. Literature suggests, without giving correlations, that liquid might creep up the wall, also that entrapment of liquid droplets in the gas enhance heat transfer of a partly wetted geometry.

Separate experiment [15] has found the thermal conductance of this tube to be 304 W/mK when totally wetted. This indicates a wetted perimeter of 25 % during normal operating conditions of the tube.



To assess the effect of the liquid flow on the wetting of the tube, the following reasoning can apply. An overflowing corrugated tube has all the corrugations filled. Liquid in the corrugations does not contribute to advance liquid other than providing a base over which additional liquid can flow. A straight tube would not have this static liquid present. It would require a higher overall liquid flow for the tube to contain the same amount of liquid as its corrugated equivalent as illustrated in Figure 6.4.

With static amount of liquid 10.6 g/m and flow velocity 10 cm/s this higher liquid flow equals 1.06 g/s.

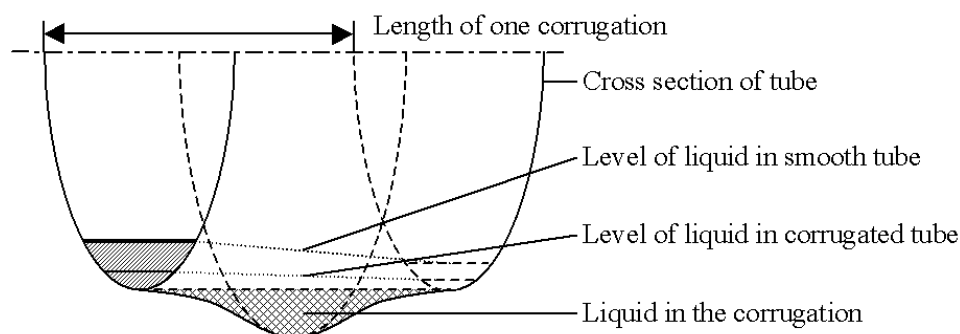


*Figure 6.4 The liquid in the corrugated tube is shown together with the amount needed in a straight tube to obtain the same amount of wetted surface.*

Assuming the liquid vaporizes evenly along the straight tube the average amount of liquid corresponds to half of that coming from the valve. Adding the amount arising from the corrugated equivalent gives an apparent average liquid flow in a straight tube. In Table 6.1 the resulting wetted circumference for liquid flows encompassing 10 % - 65 % valve opening is calculated.

*Table 6.1 Wetted circumference for a straight tube equivalent*

Liquid flow [g/s]	Apparent average liquid flow [g/s]	Apparent average wetting of circumference [%]
0.5	1.31	20.5
1	1.56	21.9
2	2.01	24.2
4	3.06	28.0

Note that there is only a 35 % increase in apparent wetted circumference following an eight-time increase in liquid supply. This supports giving the thermal conductivity with

dimension  $W/Km$ . The numbers are in good agreement with the 25 % proportion calculated from the thermal conductance.

Sources of uncertainty relating to the calculated thermal conductivity stem from the relative accuracy of the temperature sensors and whether the heat exchanger is fully wetted throughout the experiment. There are also uncertainties related to the effect of the pressure on the saturation temperature along the heat exchanger and to the fact that the wetted circumference is not constant for different mass flows.

## 6.4 Heat Transfer in the Interconnections

An experiment was devised to gain knowledge about the longitudinal heat transfer taking place in the pressure vessels and over the interconnections. The object of the experiment was to observe the longitudinal temperature profile when heat was added to only one part of the heat exchanger.

The experiment was set up with a large  $\Delta T$  for heat transfer to operate with a short wetted length, hence a large part of the heat exchanger providing no cooling. The maximum heat load allowed by the resistive heater was then added to the quadrupole, the magnet furthest away from the wetted part of the heat exchanger. This ensured that all of the added heat plus the static heat on the quadrupole load had to be transferred through the interconnection between the quadrupole and the first dipole, to be extracted higher up in the heat exchanger.

The experiment proved very difficult to perform. As the applied heat load more than five times exceeded the maximum foreseen heat load on the system, it turned out impossible to tune the automatic controller to operate the system in steady state. The valve exhibited persistent and large oscillations in opening with a corresponding oscillating behaviour in magnet temperature. Consequently the controller had to be operated in manual mode, a procedure which is delicate when a constant temperature is sought. It required adjusting both valve opening and applied heat load for a prolonged period to obtain steady state temperature at an absolute temperature correspondence to the temperature before extra heat was applied.

Data was recorded at two heat loads, and can be found in Section A-4. In Table 6.2 is shown the increase, from the state of no extra heat applied, in temperature splits that was observed.

*Table 6.2 Increase in temperature splits from zero applied heat.*

Applied heat [W]	$\Delta T$ quadrupole [mK]	$\Delta T$ interconnection [mK]	$\Delta T$ first dipole [mK]
20	0.34	0.78	2.65
28.5	1.46	1.38	3.70

Recorded temperature increases are surprisingly small and in order of magnitude in the same range as the relative accuracy of the temperature sensors. A quantitative analysis of the results is therefore pointless. However a qualitative considerations still yield valuable insight.

The increased temperature split over the interconnection is smaller than over the first dipole. Hence the interconnection does not constitute a considerable thermal resistance compared the to the cold masses. This also applies for the transient period of the experiment where the largest temperature split was observed over the length of the first magnet and not over the interconnection.

An order of magnitude analysis of the heat transfer over the interconnection is based on the theory of superfluid heat transfer:

$$\dot{q} = A \frac{\sum \Delta T}{\sum L} F(T) \sum \frac{1}{L} \quad (6.7)$$

where  $A$  [ $cm^2$ ] and  $L$  [ $cm$ ] are the cross section and length of the interconnection respectively.  $F(T)$  [ $W^3/cm^5K$ ] is the conductivity function for He II. Calculated from designer drawings the efficient cross section for heat transfer is about  $30\text{ cm}^2$  and the length is  $52\text{ cm}$ . The interconnection has a cross section of  $66\text{ cm}^2$  when unobstructed. At the relevant temperature the conductivity function is  $F(T)=1500\text{ W}^3/cm^5K$

Neglecting the static heat inleak gives a conservative estimate. The calculated temperature split at  $28.5\text{ W}$  should be about  $30\text{ mK}$ . Or reversed; a  $1.38\text{ mK}$  temperature split requires a cross section of over  $80\text{ cm}^2$ . The static heat inleak is about  $5\text{ W}$  for the short straight section and will further increase the numbers. This discrepancy is still unaccounted for, though subject of several discussions with competent personnel.

The conclusion of the experiment and analysis is that the heat transfer through the interconnections is very efficient and not a source of concern for the performance of the cooling system.

## 6.5 Inverse response

When the JT valve opening is increased to cool down the system, there is a time delay for the temperature to start decreasing to be expected due to the time it takes for the increase in liquid flow to advance and reach the dry part of the heat exchanger. The time delay should be proportional to the wetted length and the velocity with which the liquid is advancing:

$$\Delta t = \frac{L_{\text{wetted}}}{v_{\text{liquid}}} \quad [\text{s}] \quad (6.8)$$

This time delay was sometimes observed to be unexpectedly long. It was also observed that not only did it take long for the temperatures to start decreasing but that the temperature could increase in the period following an opening of the valve. This was especially evident at large jumps in valve opening.

An experiment was devised to investigate this behaviour. The magnet temperature was increased above saturation temperature to allow for large liquid flow without risk of overflowing the heat exchanger. In manual mode the valve was opened from the steady state setting of 32 % to 90 %. The heat exchange started overflowing at 10:26. The resulting behaviour is shown in Figure 6.5. Valve opening is shown in bold line and the temperature of the system in normal line. The marked line is the saturation temperature at the end of the system.

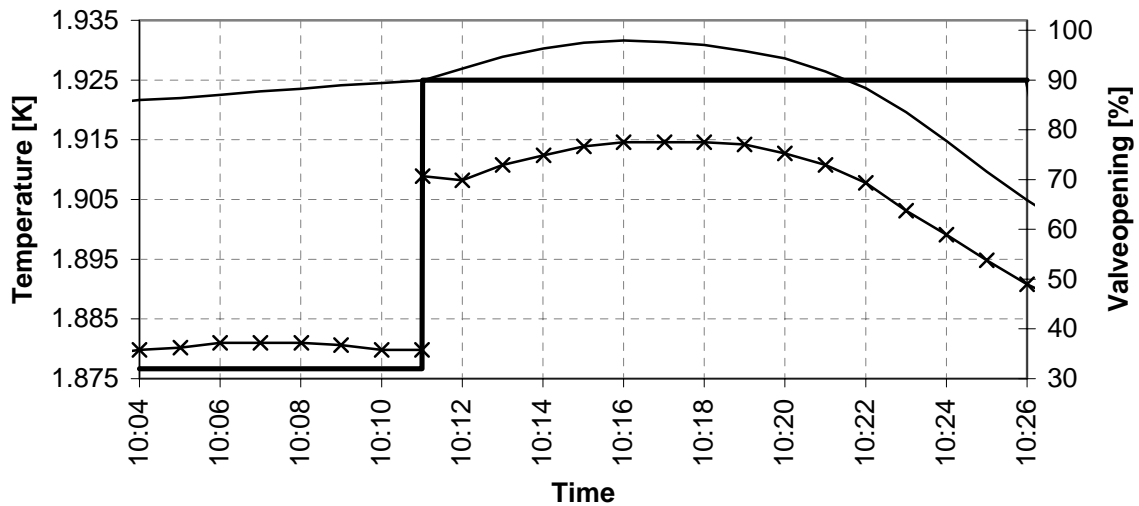


Figure 6.5 Inverse response when opening the JT valve.

The system warms up for five minutes following the opening of the valve, and it takes a full ten minutes for the temperature to start decreasing below the starting temperature. This is a non-desirable characteristic, which upon investigation was found to originate from the flash gas over the valve.

When the overall mass flow over the valve increases, so does the total amount of gas formed in the expansion. This increased gas flow produces higher pressure drop along the

heat exchanger, subsequently increasing the saturation temperature along the tube. This can be observed in the figure where the saturation temperature increases 29 mK following the opening of the valve. The available temperature margin for heat transfer for the wetted part decreases which in turn reduces the cooling power given by:

$$Q = \int_0^{L_{\text{wet}}} T(L) \cdot h_g dL = \int_0^{L_{\text{wet}}} (T - T_{\text{sat}}(L)) \cdot h_g dL \quad (6.9)$$

where  $h_g$  [W/Km] is the global heat transfer coefficient as described in section 6.3.  $T_{\text{sat}}(L)$  is the profile of the saturation temperature along the tube. This reduced cooling leads to the observed warming up of the magnets. Only when liquid advances and covers a long enough part of the HX can the temperature start decreasing.

The dynamics involved in the process is complex. With gas velocity of about 1 m/s at 90 % valve opening the new profile of the saturation temperature develops in about 30 seconds. The increased liquid flow has not yet reached the dry part of the heat exchanger having advanced about 3 meters in this time. However the original liquid front will also start advancing slowly since it is vaporized at a slower rate following the increase in saturation temperature along the tube. At the same time the increasing magnet temperature favourably affects heat transfer.

This inverse response is also present in the opposite case however not so distinct. When the valve is closed a larger temperature difference for heat transfer is created by the reduced saturation pressure resulting from the lesser pressure drop. Cooling power is increased leading to a lowering of the temperature of the system. The liquid front will then vaporize at a faster rate causing the front to retreat and also increasing the gas-flow and consequently the pressure drop. Both these effects counteract the initial cooling down. This is a complex aspect to be taken into consideration.

## 7 First principle modelling the LHC test string

A mathematical model, or simply model, is any complete and consistent set of mathematical equations, which corresponds to some prototype or system. The terms ‘model’ and ‘system’ will be used in the continuation.

There are two main approaches for obtaining a mathematical model of a process. They are commonly known as *white box* and *black box* modelling [26].

White box modelling involves building up a model from equations that express the physical laws or conservation principle, those of mass, momentum and energy. This class is also referred to as first principle models.

Black box models seek to describe the relationship between recorded input and output signals of a system. The term black box model refers to the fact that they do not contain any information about the structure of the system rather than focusing entirely on its observed behaviour. The term grey box model is sometimes used for a model where some physical insight is combined with the black box approach.

The process of modelling might be illustrated by the cycle:

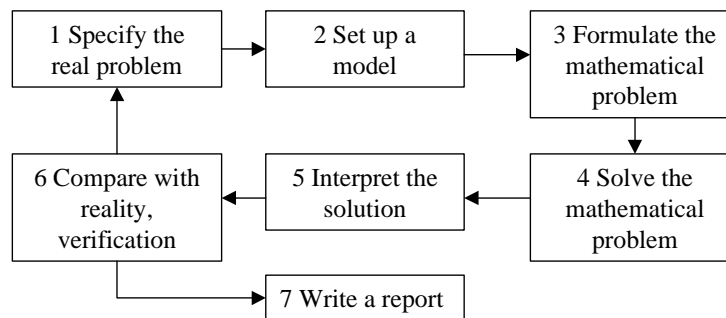


Figure 7.1 Flow chart of the process of modelling [27].

The flow of work follows the arrows but it is usual to return to some boxes several times, in particular from box six to one. Usually the optimum way of working will involve frequent reference forwards and backwards between phases of the modelling cycle, but with focus at any given time more on one rather than the other. The activity of validation should be shown with multiple return paths to all previous stages, thus being regarded as a continuous activity.

Modelling is normally an iterative process, starting from a crude model and gradually improving it until it solves the task. With a simple model at hand it is easier to identify other important aspects, rather than to incorporate a comprehensive list of features from

the start. Revision of ideas is not necessarily towards greater complexity, but might also be towards simplification.

For properly understanding the system to be modelled the first stage should be to collect data and gain experience. This enables the modeller to make sensible assumptions, approximations and estimates and not to be too committed to preconceptions of the problem.

Validation is carried out by comparing predictions from the model with real results. It is sought for the model to be in good agreement with actual data, and not have this purchased at the price of a too complex model. If parameters are determined independently and fed into the model as fixed constants not to be further adjusted, we can have a fair degree of confidence in the data and the model. Both a first principle model and black box models of the 1.9 K cooling loop have been developed.

There are several motivations for creating a first principle model of the 1.9 K cooling loop. Performing experiments on the String is expensive and time consuming with hours required for a single test. Experimental time on the String was limited following the high demand from a number of users since the String was built to investigate a series of aspects beyond single magnet testing as described in section 4.4. The String is subject to a number of disturbances that will not be present in the LHC. In particular the regulation of the suction pressure and the cooling of the thermal shield and magnet support posts. With a reliable model at hand preliminary tests can be carried out in order to utilise the actual experimental time at the String more effectively. Aspects involving very high heat loads, large liquid supply and high temperature can be investigated without jeopardising the system. Stable conditions are easily obtained in simulation and disturbances, both measurable and non-measurable, can be introduced in controlled manner. Also control aspects can be investigated.

Black box models of the system were created to be used as an integrated part of the MPC control structure that has been implemented.

The modelling process of the LHC Test String has followed the above-described methodology. Experiments to gain knowledge and obtain parameters for the model were described in chapter 6 and were performed prior to and during the phase of the modelling. The formulation and structure of the first principle model along with assumptions, simplifications and the validation procedure are presented in section 7.1 through 7.4. The concept of black box modelling is presented in section 7.5 along with candidate models to be used in the MPC implementation.

## 7.1 Assumptions and simplifications

In order for the model not to be of unnecessary high degree of complexity, reasonable assumptions and simplifications must be made. The first principle model of the 1.8 K cooling loop is based on these assumptions:

The velocity of the advancing liquid in the heat exchanger is assumed to be constant 10 cm/s according to the experiment described in section 6.1, and not a function of valve opening. The reason for this is explained in section 7.3.

All magnets are considered to have equal temperature, that of the pressurized superfluid helium. The heat transfer calculation through the interconnections has been suppressed following the argument described in section 6.4.

The friction factor for the gas in the HX is assumed to be 0.077. This value has been measured for the pipe that has been used. The value is consistent with tabulated value in literature for a pipe with the given dimensions.

The thermal conductance of the heat exchanger is considered to be constant 74 W/Km. The degree of wetting of the circumference is neglected according to the argument in section 6.3.

The corrugations of the heat exchanger tube are assumed to constitute a volume that has to be completely filled for the liquid to advance further in the tube. A threshold per unit length has to be exceeded in the calculation for liquid to flow further.

Pressure drop in the heat exchanger pipe is calculated in increments. Gas-flow in each increment is taken as an average of gas-flow in and out of that increment.

Specific heat of the system is assumed to arise solely from the He II. The amount of He II is found to be 180 kg, as described in section 6.2.

The flash over the JT valve is assumed to be constant,  $x=0.12$  corresponding to the design condition for system.

Figure 7.2 illustrates parameters of the system such as it is regarded when building the first principle model.



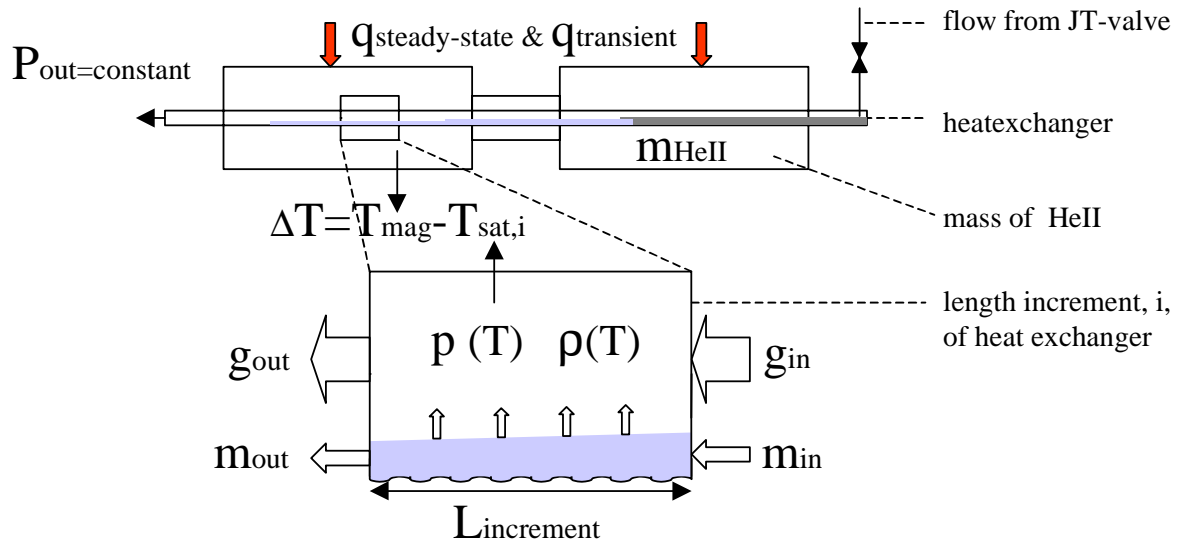


Figure 7.2 Illustration of the parameters used in the first principle modelling of the system.

Helium is sub-cooled from 4.5 K to about 2.2 K by the out-flowing helium gas before it is expanded over the JT-valve and fed to the heat exchanger. The degree of sub-cooling might vary according to the mass-flows on the high- and low-pressure side. Since this will affect the amount of flash over the JT-valve, an attempt was made to include this heat exchanger in the model. Details about this HX were scarce, therefore only a crude model could be established. Inlet conditions on the high-pressure side are assumed constant. Outlet temperature on the low-pressure side is assumed constant and pressure drop on low-pressure and high-pressure side is ignored. An inlet condition on the low-pressure side is given by the pumping pressure and assuming saturated condition.

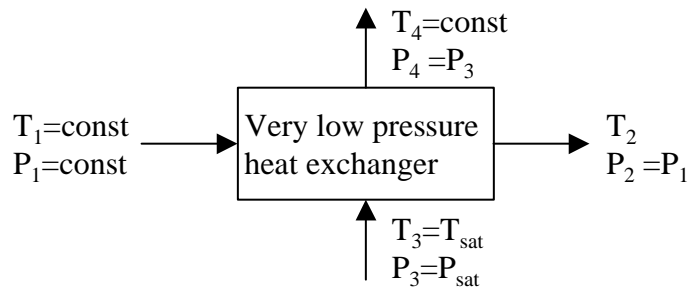


Figure 7.3 Simple model for the very-low-pressure heat exchanger.

There is no measurement of the mass flow on the low-pressure side, and mass flow is assumed to be equal for the two streams. Energy balance over the heat exchanger gives the inlet temperature to the JT-valve. The transfer line from this heat exchanger to the JT-

valve is rather long (several minutes). Time delay from this heat exchanger to the valve is a function of future mass-flow, necessitating the implementation of a variable buffer for storing the temperature history. Heat transfer in the transfer line will smooth out the temperature profile.

Using a fixed time delay and no smoothing of temperature did not improve the model, and further refinement was not given priority. The sub-model was therefore abandoned, and the flash over the JT-valve assumed to be constant in the model and according to design conditions.

## 7.2 The sub-models

The behaviour of the gas and liquid in the 1.8 K heat exchanger was identified to be the most important and challenging aspects of the modelling. This arises from the fact that the flow in the heat exchanger is two-phase, and that the saturated liquid might cover any part of the length of the tube.

Calculation of pressure drop must be incorporated as this affects the local saturation temperature and hence the available temperature margin for heat transfer.

To achieve these goals a strategy was implemented where the heat exchanger tube was discretized along the length. For each length increment the mass-balance and pressure drop is calculated, producing a longitudinal profile of pressure, saturation temperature and liquid distribution.

### 7.2.1 The Joule-Thomson Valve

The state of the helium at the inlet of the JT valve is assumed to be constant at the design value of the machine: 2.2 K at 1.2 bar. The design state after the expansion of 1.9 K at 19 mbar gives a vapour fraction of  $x=0.114$ . The flow of saturated liquid and gas after the valve is then given by:

$$\begin{aligned}\dot{m}_{liquid} &= m(v_{\%}) \cdot (1 - x) \\ \dot{m}_{gas} &= m(v_{\%}) \cdot x\end{aligned}\tag{7.1}$$

Where  $m(v_{\%})$  is the characteristic of the JT valve relating the percentual opening,  $v_{\%}$ , of the valve to a corresponding mass flow. This characteristic is encumbered with quite some uncertainty. The specification from the valve supplier states that the mass flow is linear up to 80 % opening where it supplies 6 g/s. From there it is logarithmic up to 100 % where it supplies 12 g/s as illustrated in Figure 7.4. In the figure also data recorded from a calibration of the valve is shown. There is a considerable mismatch between the data. The third line in the figure is the function:

$$m(v_{\%}) = 0.00044 \cdot v_{\%}^2 + 0.04 \cdot v_{\%} \quad [\text{g/s}] \quad (7.2)$$

This function is partly a compromise between the two sets of data, but more importantly based on experience through operation of the valve. The fit function is to some extent supported by correlating heat inleak measurements with observed valve opening in long duration steady state operation where data has been logged over several nights. It gives confidence that the function gives reasonable results over the most significant range, typically 20-40 %, of valve opening.

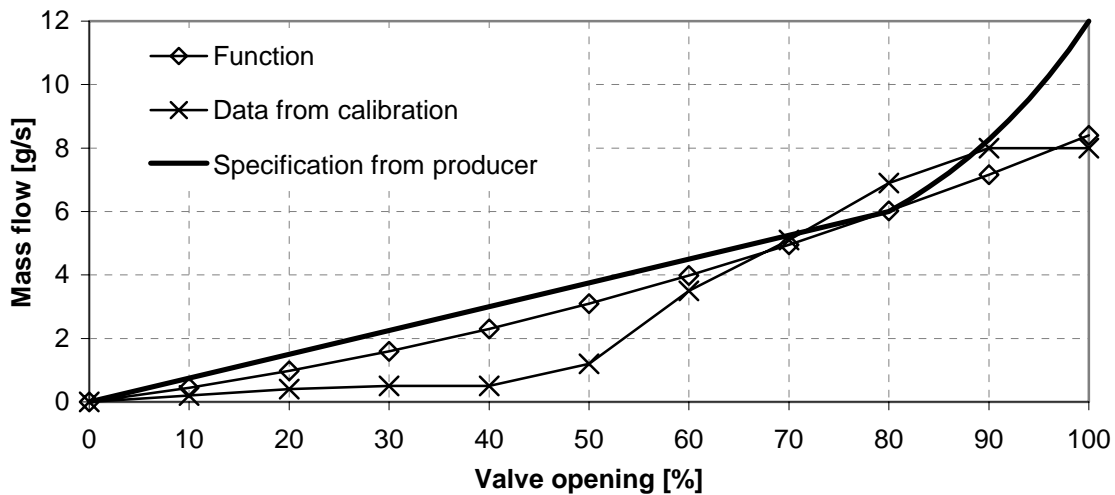


Figure 7.4 Characteristics for the JT valve. Three lines are shown: one is the specification from the supplier of the valve, one is based on measurements in an attempt to calibrate the valve and a fit function based on experience using the valve.

### 7.2.2 Liquid flow in the Heat Exchanger

From the JT valve saturated liquid is fed into the first cell increment at the end of the heat exchanger. Liquid will continue to flow into subsequent cells until the liquid front is completely vaporized. Where this will happen is a function the supply of liquid, heat inleak and available temperature margin for heat transfer. It will typically occur after 1/3 of the length in steady state nominal operating conditions.

Conservation of liquid for one cell increment gives:

$$\frac{dm}{dt} = \dot{m}_{in} - \dot{m}_{out} - \dot{m}_{vaporized} \quad [\text{g/s}] \quad (7.3)$$

where  $m_{in}$  equals  $m_{out}$  from the upstream cell. For the first cell  $m_{in}$  is the mass flow from the JT valve. The mass contained in one cell is assumed to be evenly distributed, and the mass flow out of a cell is given by the relation:

$$\dot{m}_{out} = (m - m_{threshold}) \cdot v_{liq} / L_{cell} \quad [\text{g/s}] \quad (7.4)$$

where  $m$  is the mass present in the cell [g],  $v_{liq}$  and  $L_{cell}$  are velocity of the advancing liquid and length of the cell increments respectively.  $m_{threshold}$  represents the liquid which is needed to fill the corrugations of the tube. After filling the corrugations this liquid does not contribute in bringing liquid into the subsequent cell and is therefore subtracted from the total amount when calculating the liquid flowing out of the cell.

The amount of liquid that is needed to fill one corrugation can be estimated when knowing the dimensions and the shape of the tube. It is assumed that the longitudinal corrugations have the shape of a sine function. The surface of the liquid in a corrugation will be described by an ellipse with dimensions determined by the circular cross section, longitudinal sinus pattern and degree of filling of the corrugation as illustrated in Figure 7.5.

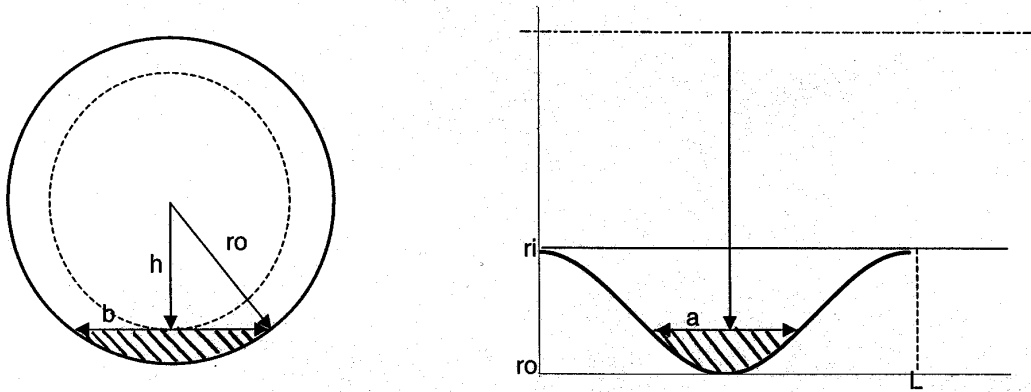


Figure 7.5 Illustration of the parameters used for calculating the volume of one corrugation of the heat exchanger.

The measures  $a$  and  $b$  are given by:

$$b = 2\sqrt{r_o^2 - h^2} \quad a = \frac{4L}{\pi} \arcsin \left[ \frac{\sum r_o - h}{\sum r_o - r_i} \right] \quad (7.5)$$

where  $h$  is the distance from the center of the tube to the surface of the liquid, and  $L$  is the length of the pattern (pitch). The area of an ellipse with dimensions  $a$  and  $b$  is given by  $A = \pi ab/4$  and the volume of the liquid is then given by the integral:

$$V = 2L \sum_{r_i}^{r_o} \sqrt{r_o^2 - h^2} \arcsin \frac{\sum r_o - h}{\sum r_o - r_i} dh \quad (7.6)$$

With dimensions as given in section 4.4.4 the volume of one corrugation is  $0.8842 \text{ cm}^3$ . The density of He II is quite constant  $\mu=0.1456 \text{ g/cm}^3$ . The length of one corrugation is 1.22 cm and the amount of liquid stored in the corrugations per meter tube is then  $m_{HeII}=10.55 \text{ g/m}$ .

### 7.2.3 Gas flow in the Heat Exchanger, Pressure Drop

In each cell increment of the heat exchanger there will be a pressure drop associated with the gas flow. The Reynolds number of the flow determines whether the flow is laminar, turbulent or in the transition zone between them. Reynolds number is defined as:

$$\text{Re}_D = \frac{\rho u_m D}{\mu} \quad (7.7)$$

Where  $\mu$  is the density,  $u_m$  is the mean gas velocity,  $D = 5 \text{ cm}$  is the diameter of the tube and  $\mu$  is the viscosity. With a gas velocity in the order of  $u_m = 1 \text{ m/s}$  after the Joule-Thomson valve in normal conditions the Reynolds number is in the order of 60 000 which is well inside the regime of fully turbulent flow ( $\text{Re}_D > 10\,000$ ). For turbulent flow the hydrodynamic entrance length is approximately independent of Reynolds number and can be assumed fully developed for  $x_{fd} > 10D$  [33]. Thus the flow condition in the pipe is fully turbulent after about 50 cm which is less than 1.5 % of the tube length. Pressure drop correlation for fully developed turbulent flow can be applied and the entrance effect neglected.

For turbulent flow the friction factor is defined as:

$$f = \frac{-(dp/dx)D}{\rho u^2/2} \quad (7.8)$$

where  $D$  is the diameter of the tube,  $\mu$  is the density of the gas and  $u$  the velocity of the gas.

Assuming that the flow is fully developed, the friction factor is constant and the pressure drop may be expressed as:

$$\Delta p = f \frac{\rho u^2}{2D} \sum_{x_1}^{x_2} dx = f \frac{\rho u^2}{2D} L \quad (7.9)$$

where  $L$  is the length of the cell, integrating from  $x_1$  to  $x_2$ .

The mass flow of gas is related to the velocity of the gas through:

$$u = \frac{\dot{m}}{\rho A} \quad (7.10)$$

Where  $A$  is the cross section of the tube. Introducing this relation and  $A = \pi/4 D^2$  the pressure drop is expressed as:

$$\Delta p = f \frac{\dot{m}^2}{\rho \frac{\pi^2}{8} D^5} L = C \frac{\dot{m}^2}{\rho} L, \quad \text{where } C = \frac{8f}{\pi^2 D^5} \quad (7.11)$$

The friction factor  $f$  for this tube has been measured to be 0.077. This number is consistent with the Moody chart friction factor for pipe with rough walls for a tube with relative roughness:

$$\frac{\varepsilon}{D} = \frac{(D_{outer} - D_{inner})/2 - e}{D_{inner}} = 0.08 \quad (7.12)$$

where  $e$  is the wall thickness.

For rough tubes the pressure drop is evaluated using the diameter to the base of the roughness: 50.5 mm [34]. This gives a value of  $C = 2.00 \cdot 10^{-9}$  and the pressure drop given in Pascal [ $\text{g}/\text{mm} \cdot \text{s}^2$ ]. Operating with density in  $\text{g}/\text{cm}^3$  ( $10^{-3} \text{ g}/\text{mm}^3$ ), length of cells in  $\text{m}$  ( $10^3 \text{ mm}$ ) and pressure drop in  $\text{mbar}$  ( $10^{-2} \text{ Pa}$ ) yields a factor of  $C = 2.00 \cdot 10^{-5}$ , which are the dimensions.

The length is introduced as variable in the pressure drop calculation to facilitate varying degree of discretization of the heat exchanger tube.

The density of the gas is calculated by:

$$\rho(T) = 2.321 \cdot 10^{-5} T + 7.53 \cdot 10^{-5} \quad (7.13)$$

This is a fit developed using data produced by Hepak. In the 1.78 – 1.96 K region it matches with an error of less than 0.5 %, and is accurate to within 2.5 % between 1.76 – 2.1 K, see Section B-1.

### 7.2.4 Cooling by the Heat Exchanger

The cooling provided by the heat exchanger is calculated by summation of the liquid that is vaporized from each cell of the discretized heat exchanger during a time increment:

$$\frac{dQ}{dt} = h_{fg} \sum_{i=1}^n (T_{mag} - T_{sat,i}) \frac{h_g L_{cell}}{h_{fg}} \quad (7.14)$$

where  $n$  is the number of increments,  $h_g$  is the global heat transfer coefficient,  $L_{cell}$  is the length of each cell,  $T_{sat,i}$  is the local saturation temperature in each cell, and  $h_{fg}$  is the latent heat of vaporisation of He II. Latent heat of vaporisation is taken to be constant at 23 J/g. According to data taken from Hepak this represents an error of less than 0.5 % in the temperature range 1.74 - 2.08 K.

### 7.2.5 Magnet Temperatures

The longitudinal and transversal heat transfer in the system is good. Assuming that the magnets are isotherm the model for the magnet temperatures takes the form:

$$\frac{dT}{dt} = \frac{q_{ss} + q_{trans} - q_{cooling}}{m_{HeII} \cdot cp(T)_{HeII}}$$

where  $q_{ss}$  and  $q_{trans}$  models the steady state and transient heat loads respectively. The cooling,  $q_{cooling}$  is described in the previous chapter, and the amount of pressurized He II is constant. The temperature dependent specific heat of He II is implemented as mathematical fit to data taken from Hepak:

$$cp(T) = 14.777e^{2.9431T} \quad [\text{J/kgK}] \quad (7.15)$$

This fit has an error of less than 1.25% in the temperature range of 1.7 - 2.07 K, see Section B-2.

### 7.3 Implementation of the Model

The model has been implemented using the graphical interface programming facility of the simulink toolbox of Matlab. Section C constitutes a user manual describing the implementation in more detail

The inputs required for running a simulation are.

- pumping pressure at the outlet of the heat exchanger
- heat load on the system during the simulation
- Supply of helium through the JT valve during the simulation

The program calculates:

- pressure profile in the HX
- saturated temperature profile
- liquid distribution in the HX
- cooling power provided by the HX
- temperature development for the He II of the cold mass hence the magnets
- liquid supply in the case of using a control structure for the valve
- liquid supply as a function of supplied valve-opening.
- specific heat of the pressurized He II in the cold-mass
- density of the helium gas

The calculation of the pressure drop and cooling provided by the heat exchanger contains an algebraic loop. The pressure drop caused by the gas flow determines the profile of the saturation temperature. The saturation temperature in turn determines the amount of liquid that is vaporized hence to calculation of the pressure profile. An algebraic loop must be solved by iteration. Alternatively a holding element can be introduced to break the loop. Using an iterative solution proved very time consuming, and a holding element was introduced. The gas velocity from the previous time step is used in the calculations to break the algebraic loop. The error introduced by a holding element will decrease with shorter time increments, and in steady state it does not introduce an error. A time increment of five seconds was verified as being well within a limit where differences in behaviour could be detected. This is the time increment used in the simulations.

The calculation of the mass flow out of a cell does not contain an algebraic loop. If however the liquid velocity were to be implemented as a function of the overall mass present in the cell, an algebraic loop would be introduced. This would necessitate either resorting to an iterative solution, or introducing another holding element. A constant liquid velocity in the heat exchanger was initially introduced, and no refinement of this assumption was pursued. The possible improvement by introducing liquid flow as a function of overall mass in a cell increment has not been investigated.

There are several possible methods for solving the differential equations of the simulation. In particular there is the choice of using fixed or variable step length. Solvers



based on variable step length are calculating the required step length needed based on specified tolerances. The variable step length routines tended to use extremely short time increments in transients. This however did not alter the simulated behaviour compared to using fixed step length of five seconds as described above. A fixed step length routine was therefore used.

### **7.3.1 Length increments of the heat exchanger tube**

The calculations involved in modelling the two-phase flow in the heat exchanger are by far the most demanding. Deciding the degree of discretisation of the heat exchanger was a trial and error procedure. It was sought to be sufficient to avoid unnecessary errors, but as coarse as possible to minimize the computation burden. Series of simulations were performed with increasingly fine discretisation. When no detectable improvements could be observed it was regarded as sufficient. It was found sufficient to divide the length into 24 parts of 1.46 meters, giving a resolution of about 4 % along the geometry.

## **7.4 Sensitivity Study of Design Parameters**

There are a number of parameters used in the model that have been obtained through the experimental investigation of the system. The parameter and their nominal value are listed in Table 7.1.

Table 7.1 The parameter used in the model and their nominal value.

Parameter	Nominal value	Dimension	Attained by
MHe II	175	[kg]	Experiment
$h_g$	74	[W/Km]	Experiment
$v_{liq}$	0.10	[cm/s]	Experiment
Threshold	10.55	[g/m]	Geometric valuation
Flash	0.12	[-]	Thermodynamic valuation
f	0.077	[-]	Measurement and fluid-dynamic valuation

It is natural to question how the uncertainty related to these parameters affects the performance of the model. In this section the sensitivity of parameters is studied. The parameters are varied around their nominal value according to the uncertainty related to them, and the corresponding effect on the model behavior is analysed.

The input signal that is used is shown in Figure 7.6.

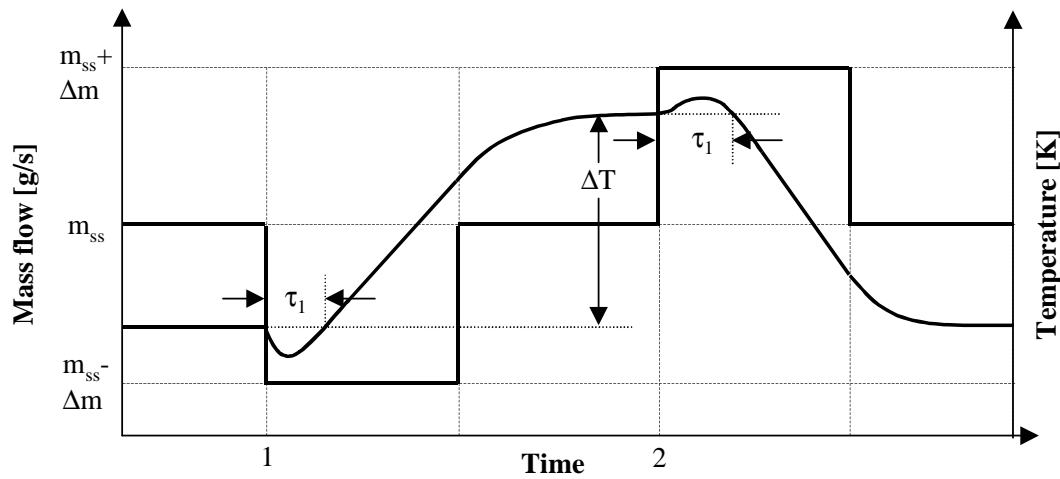


Figure 7.6 The movement of the valve and expected response in magnet temperature.

The change  $\pm \Delta m$  in the input signal and the duration of the change is such that it produces a  $\Delta T$  in the order of 15 mK. Between steps the steady state opening is allowed to persist until a new steady state condition has been attained. The response is qualitatively shown in the Figure 7.6.

The characteristics of the response that are investigated are listed in Table 7.2:

Table 7.2      *Characteristics of the response of the temperature.*

$\Delta T$	[mK]	Overall change in temperature between steady states
$\tau_1, \tau_2$	[s]	Delay from step until inverse response is over
$\Delta p_{\text{sat}1}, \Delta p_{\text{sat}2}$	[mbar]	Change in saturation pressure in the return box

Inverse response is defined to be over when the temperature reaches the temperature before the step was applied. Change in saturation pressure is evaluated in the two steady states at the instants before steps are applied, indicated as time 1 and 2 in Figure 7.6.

The simulations are performed using the same pumping pressure throughout. The initial conditions are set such that the temperature before the first change in the input signal is the same for all the simulations. The conditions are:

Pumping pressure: 18 mbar (1.827 K)  
 Temperature before step: 1.877 K  
 Heat inleak: 23 W

The sensitivity is presented as the observed percentual change of the characteristics described in Table 7.1.

#### 7.4.1 Heat Transfer Coefficient

The heat transfer coefficient affects the part of the heat exchanger that is needed to transfer a given amount of heat for a given amount of temperature drop. A larger coefficient requires a shorter length of the HX to transfer the same amount of heat. This in turn affects how much time additional liquid needs to flow over the already wetted part of the HX to reach the dry area and contribute to increased cooling. Also for a larger value the overall pressure drop will be larger as the mass travels a longer part of the HX as gas thus contributing to the pressure drop.

The effect of a change in this parameter should thus be observed during transients and by observing the pressure drop over the HX. It is not expected to contribute significantly in changing the temperature increase of a step.

The heat transfer coefficient from the saturated to the pressurized He II was measured during an experiment described in section 6.3 It was found to be 74 W/Km with 15 % uncertainty. The resulting relative sensitivity is given in

*Table 7.3 Sensitivity of the heat transfer coefficient*

	$\Delta T$	$\tau_1$	$\tau_2$	$\Delta p_1$	$\Delta p_2$
+ 15 %	0.0	-4.2	0.6	2.7	1.6
- 15 %	0.0	6.2	-0.6	-3.2	-2.7

#### **7.4.2 Amount of helium in the cold mass**

The amount of helium in the cold mass dominates the specific heat of the system and thus the thermal impedance. A change in this parameter is expected to affect to temperature excursion to a change in heat load.

The amount of helium in the cold mass was found to be 175 kg with 15 % uncertainty. The resulting relative sensitivity is given in Table 7.4

*Table 7.4 Sensitivity of amount of helium in the cold mass.*

	$\Delta T$	$\tau_1$	$\tau_2$	$\Delta p_1$	$\Delta p_2$
+ 15 %	-9.3	-0.3	-4.6	0.0	-1.0
- 15 %	12.4	0.0	-5.71	0.0	1.61

#### **7.4.3 Liquid velocity in heat exchanger.**

The liquid velocity in the heat exchanger was found to be 10 cm/s with 25 % uncertainty. The resulting relative sensitivity is given in Table 7.5

*Table 7.5 Sensitivity of liquid velocity in the heat exchanger.*

$\pm 25 \%$	$\Delta T$	$\tau_1$	$\tau_2$	$\Delta p_1$	$\Delta p_2$
0.12	1.55	-9.3	-13.1	0.0	0.3
0.08	-0.8	11.3	14.6	0.0	-0.3

The liquid velocity has the strongest impact in transient mode affecting how fast liquid can advance in the heat exchanger. In steady state it has almost no impact on the overall temperature difference and saturation pressure in the beginning of the tube.

#### 7.4.4 Amount of flash over JT-valve

The flash over the JT valve is calculated to be 0.12 according to design specifications. The variation in this parameter can be in the order of 20 %. The resulting relative sensitivity is given in Table 7.6.

Table 7.6 Sensitivity of the flash over the Joule-Thomson valve.

$\pm 20 \%$	$\Delta T$	$\tau_1$	$\tau_2$	$\Delta p_1$	$\Delta p_2$
0.144	-4.7	12.4	12.6	2.7	3.0
0.96	2.3	-1.4	-17.4	-2.3	-2.4

The flash has an impact on all of the investigated characteristics. The strong impact on the time delay arises from the larger inverse response due to the gas flow and its impact on the saturation temperature along the pipe. Also in steady state the pressure drop is affected however not more than 10-15 % relative.

#### 7.4.5 Friction factor

The friction factor is measured to be 0.077. This agrees with tabulated value with an uncertainty of about 20 %. The resulting sensitivity is given in

Table 7.7 Sensitivity of friction factor.

$\pm 20 \%$	$\Delta T$	$\tau_1$	$\tau_2$	$\Delta p_1$	$\Delta p_2$
0.924	-0.8	16.0	15.7	6.6	9.2
0.616	3.1	-18.8	1.1	-7.8	-10.0

The friction factor directly affects the pressure drop over the heat exchanger. It has an important impact on both saturation pressure in steady state and the time delay during transients. Overall temperature difference is only moderately affected by the friction factor through the change in saturation pressure in the heat exchanger.

### 7.4.6 Threshold of mass in corrugation

The threshold for liquid to advance was from geometrical valuation found to be 10.55 g/m. The uncertainty in this parameter is difficult to estimate, and the sensitivity is controlled with 50 % change.

Table 7.8 Sensitivity of threshold of helium needed to fill the corrugation.

$\pm 50 \%$	$\Delta T$	$\tau_1$	$\tau_2$	$\Delta p_1$	$\Delta p_2$
4.7	-4.7	27.8	10.9	0.0	0.7
3.9	7.8	-19.7	-10.0	0.0	-1.1

As the threshold is the amount of liquid needed to fill the corrugations of the tube it governs how fast the liquid front can advance and retreat in transient mode. As expected it has a noticeable effect on the time delay in transient and only very weak impact on the saturation pressure and overall temperature change.

## 7.5 Validation of first principle model

Validation of the first principle model is performed by comparing simulated behaviour with data logged on the system. Three experiments that emphasise different aspects of the system are used in the validation.

### 7.5.1 Varying the heat load

In the first experiments the electrical heater in the quadrupole is the manipulated variable. The starting condition of the experiment is steady state temperature and valve opening with 10 W of heat added to the quadrupole. The liquid supply is in manual mode. Steady state opening without added heat is 31 %. An additional opening is required to achieve steady state with the heater activated. This opening is calculated using the fit function described in section 7.2.1. Flash over expansion is assumed to be  $x=0.12$

$$m(31 \%) = 1.463 \text{ g/s}$$

Latent heat of vaporisation of He II @ 1.9 K is 23 J/g, consequently 10 W of added heat load requires an increase in liquid supply of  $m=0.435 \text{ g/s}$  and a total mass flow of  $m=1.898 \text{ g/s}$  to be in steady state. The steady state valve opening with the heater activated is:

$$v\%(1.898 \text{ g/s}) = 38 \%$$

The experiment then proceeds by applying a pseudo random binary signal for the heat load. It is set to 20 W for 30 minutes followed by 30 of zero added heat load. This signal is then repeatedly applied with the period of the signal halved for every repetition. The last cycle has a period of 112 seconds. The steady state heat load in the simulation is adjusted such that the overall temperature change during the course of the experiment is the same as what is observed in the recorded data. Figure 7.7 shows simulation and measured temperature evolution.

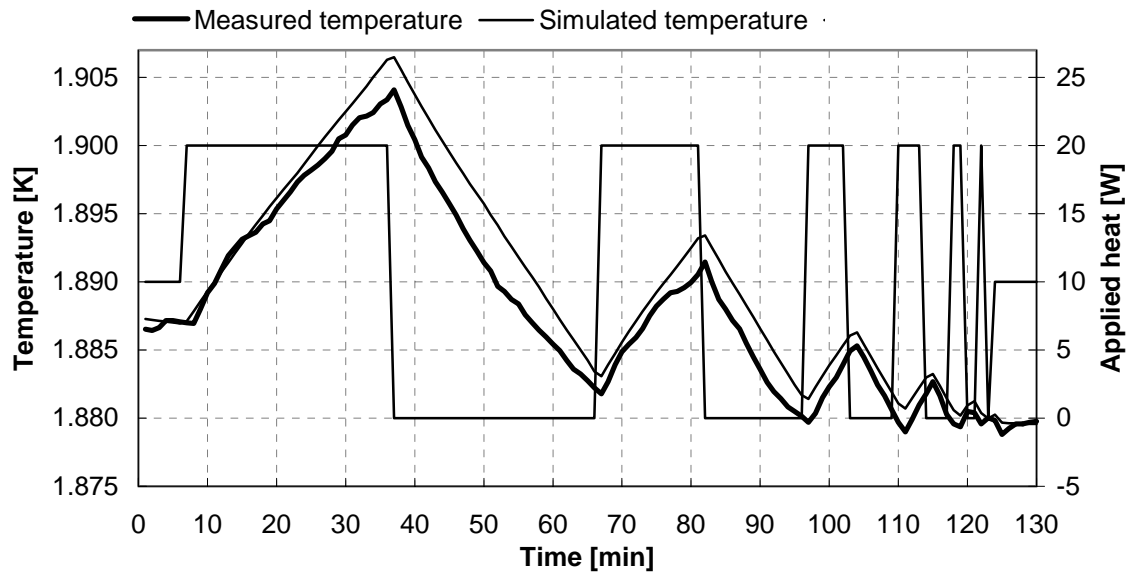


Figure 7.7 The simulated response to changes in heat load compared with measured temperature response of the system.

The transient response of the simulation is similar to that of the measured response. No time delay in the temperature response is observed following a change in heat load. The below table shows the measured and simulated changes in temperature during the first cycle of the experiment.

Table 7.9 Measured and simulated temperature development in first cycle.

	First temperature rise [mK]	First temperature decrease [mK]
Measured	17.5	21.6
Simulated	16.7	21.3

The measured and simulated changes in temperature are within 5 % for the temperature rise and within 1 % for the temperature decrease. The magnitude of the temperature change is primarily governed by the specific heat of the system, hence the amount of He II in the cold mass. The good agreement between simulation and measurement substantiates the experimentally found value of the amount of He II as described in section 6.2.

There is an overall temperature decrease of 7 mK in absolute temperature during the 130 minutes of the experiment. This is because the applied valve opening and supplied mass flow is too high by:

$$\Delta \dot{m} = \frac{\Delta T \cdot m_{\text{HeII}} \cdot cp(T)}{\Delta t \cdot h_{fg}} = 0.027 \quad [g / s]$$

where  $cp=3850 \text{ J/kgK}$  is evaluated at 1.895 K and the amount of He II is 180 kg. The adjustment in mass flow equals a change in the valve opening from 38 % to 37.6 %. This is a small change and substantiates the fit function used for the JT-valve at this valve opening.

### 7.5.2 Manipulating the Joule-Thomson valve

The manipulated variable in this experiment is the Joule-Thomson valve. The experiment starts with the valve in automatic mode and the system in steady state. It then proceeds with the valve in manual mode applying a pseudo random binary signal similar to that of the heat load in the previous section, followed by an additional opening and closing of the valve. The first movement of the PRBS sequence was accidentally set 10 % too low, but this is of no importance for the validation procedure. The steady state heat load in the simulation is adjusted such that the overall temperature change during the course of the experiment is the same as what is observed in the recorded data. Figure 7.8 and Figure 7.9 show simulated and measured temperature evolution. Simulated behaviour is shown in bold lines and the recorded behaviour in normal lines.



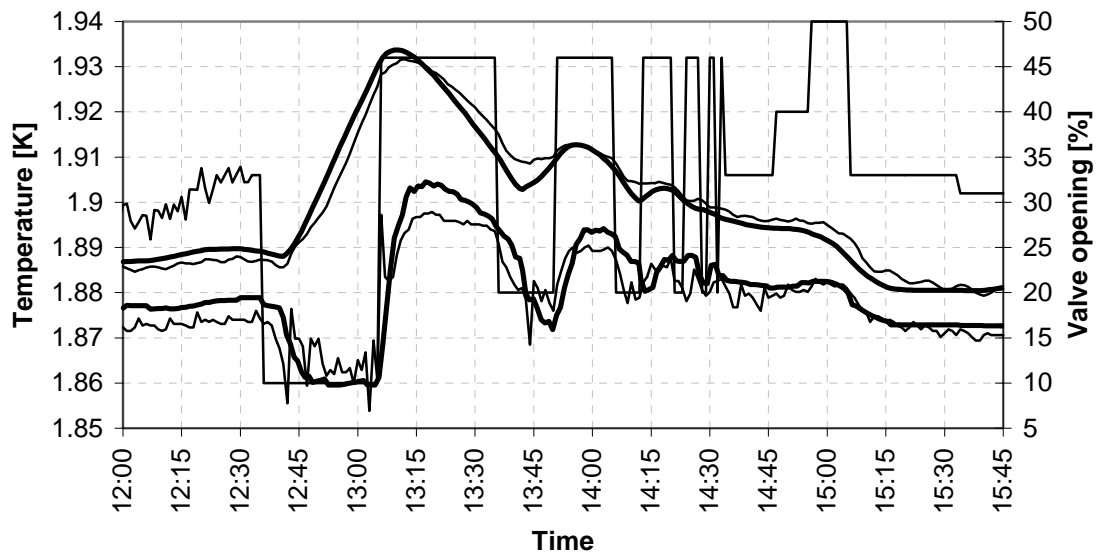


Figure 7.8 Verification I experiment with JT-valve as manipulated variable. The simulated response is shown in bold lines and the measured response in normal lines. The lower set of lines are the pressure measured in the start of the heat exchanger furthest away from the outlet of the system.

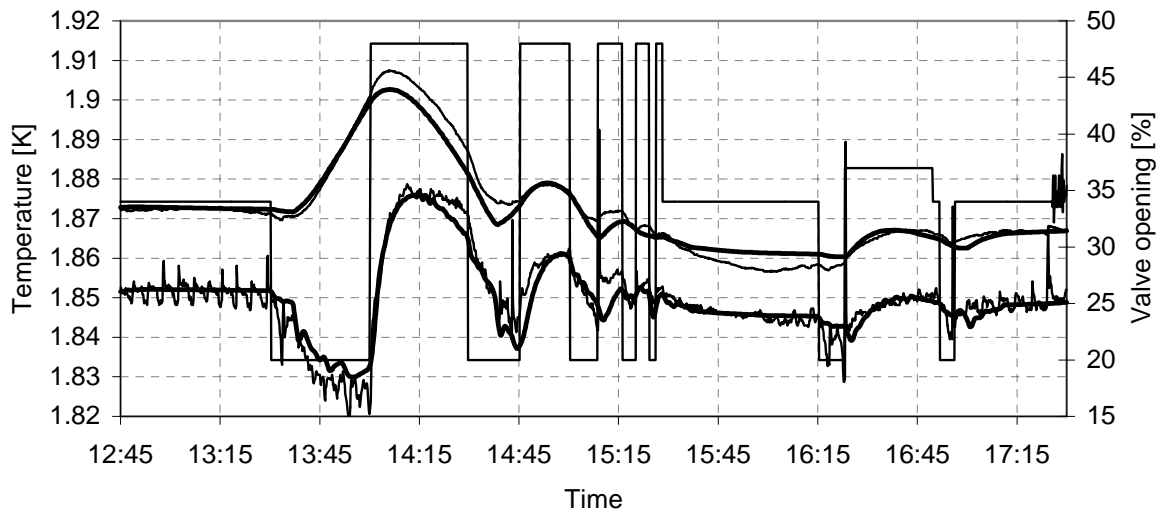


Figure 7.9 Verification II experiment with JT-valve as manipulated variable.

The transient response of the in simulation shows a similar time delay after a change in valve opening as the recorded response.

The development of the saturation pressure in simulation is crucial for the validation of the model. The relative change in pressure in the return box following the changes in valve opening corresponds well with the measured pressure in the return box. However the simulated change in saturation pressure from 10 % to 46 % valve opening is slightly larger than the recorded one. This might be due to a too large value of the friction factor, but not necessarily. The discrepancy might also originate from other dynamic features occurring in the heat exchanger such as the velocity of advance or retreat of the liquid front. The transient behaviour shows a similar development as the recorded one giving confidence that the pressure drop calculation in the model is corresponding well to the characteristics of the real pressure drop.

## 8 Black box modeling of the LHC test string

The theory presented in this chapter is mainly extracted from [35]. It is consistent with other references such as [36] and [37], which have also been consulted.

A model whose parameters are adjusted to fit to data and do not reflect physical considerations in the system is called a *black box model*. The idea of their structure is to have flexible model sets that can accommodate a variety of systems.

The method of obtaining black box models is called *system identification*. The procedure of system identification involves three basic components:

1. a set of recorded input-output data from a system
2. a set of candidate model structures
3. a rule to assess the candidate models

The input output data might be logged through normal operation of the system. The preferred way is however to record the data during specifically designed identification experiments. The experiment design is such that the recorded data contains a maximum of information about the system. The *experiment design* will be treated in section 8.2.

Selecting candidate model structures is an important and difficult choice. Knowledge about the system and engineering insight should be combined with the properties of the models to select sensible candidate structures. This will be treated in section 8.3.

The best model within a set is determined when examining how the models reproduce measured data.

Having arrived at the model that best describes the data according to the chosen criterion, this model must be validated to see if it is adequate for its purpose. *Model validation* involves various procedures to assess how the model relates to observed data, prior knowledge and to its intended use.

System Identification involves a lot of numerical calculation, and a natural evolution of this field is the development of interactive software packages. The next section illustrates the procedure of system identification such as it is implemented in the System Identification Toolbox with Matlab.

### 8.1 The Procedure of System Identification

System Identification using an interactive tool will follow the sequence:

- Specify a model structure

- The computer delivers the best model in this structure
- Evaluate the properties of this model
- Test a new structure

The following flowchart illustrates by rectangles what the software handles, and by ovals what the user must do [38].

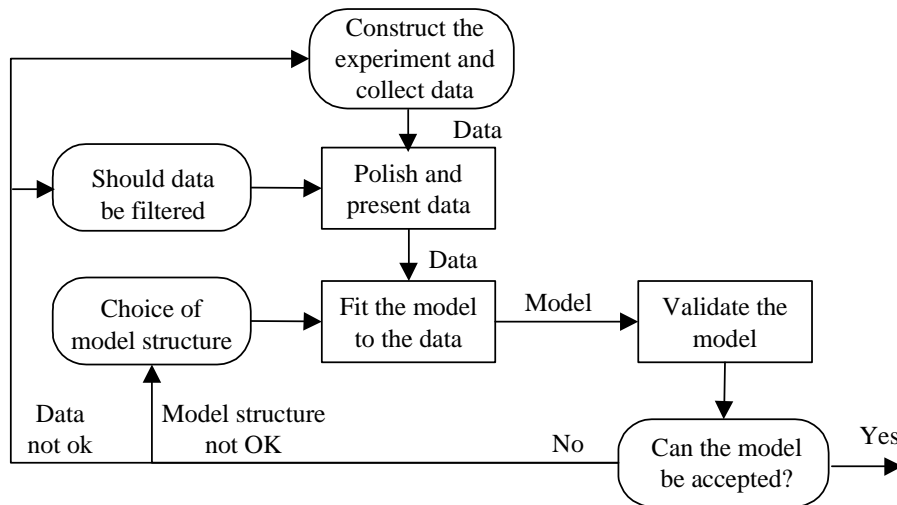


Figure 8.1 Procedure for interactive system identification. Ovals indicate what the user must do, and the squares indicate what is handled by the software.

## 8.2 Design of Experiments for System Identification

As a rule it is wise to let the experiment resemble the situation for which the model will be used. For a non-linear system it is advised that the experiments be performed around the operating point.

The first choices are what to measure and where; which signals to consider as inputs and which as outputs, and which signal to manipulate to excite the system. For the String the inputs and manipulated signals were chosen to be the opening of the JT valve and the heat load to the system provided by the electrical heaters. The output was naturally chosen to be the magnet temperatures.

The next choices are the sampling interval  $T$ , and how many data points  $N$ , that should be collected for each experiment. The situation for the String was that available experiment time was limited, but that data might be sampled at a high rate. From a theoretical point of view it is then advantageous to sample as fast as possible. It is possible later to decimate the data if the sampling rate proves to be too high. When a model is to be used

for control application, the sampling interval should be the same as for the control application. This avoids having to use many sample periods to model time delay in systems with dead time, as this can cause problems in the control design. For model building the optimum choice of  $T$  lies in the range of the time constant of the system. For the String the time constant associated with manipulation of the JT-valve is in the order of minutes and is considerably larger than that of manipulation of the heat load where the response can be argued as being instantaneous due to the heat transfer capability of He II. The sampling time was chosen to be 10 seconds, well within the time constant for manipulation of the valve, yet acceptable regarding the demand for disk space for storage of the data.

Within the constraints of limited experiment time and sampling rate, the number of data points were inherently limited. The experiments were sought kept as long as possible to contain maximum information. Sub-sets of the collected the data can later be chosen if required.

The frequency, amplitude and shape of the input signal are essential choices to make for the experiment to be informative. A binary symmetric signal:  $u(t) = \pm\mu$ , is a common and informative signal. However a binary signal will not allow validation against non-linearities.

Another common choice of input signal, which does not have this disadvantage, is the *Pseudo-Random-Binary-Signal*, *PRBS*. This is a periodic, deterministic signal with white noise properties. The frequency of the signal should include the interesting frequencies of the system. The amplitude of the signals was constrained by the need to keep the magnet temperature safely around the operating conditions and to adequately excite the system. Steady state opening of the valve was in the area of 25-30 %, and it was desired to keep the JT-opening above 10 %. Choosing the longest period for the system to 30 minutes was assumed long enough to include the desired system dynamics. Figure 8.2 shows a typical experiment where the period of the signal is halved after each subsequent step up and down in valve opening. The shortest period for such an experiment was less than 2 minutes, which does not produce a signal detectable above the noise for the output.

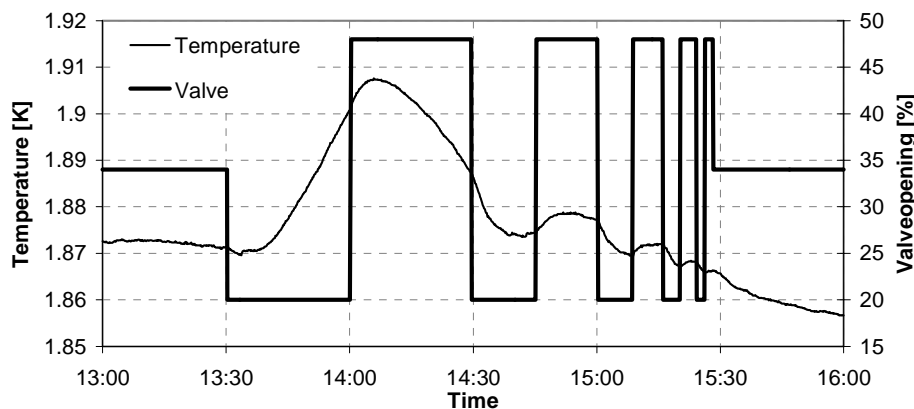


Figure 8.2 Binary input signal for the JT valve and temperature response. The identification experiment I has a duration of 3 hours.

### 8.3 Selection of Model Structure and Order

When the experiments have been performed and the data collected, the first step is to pre-process the data to remove drifts, trends, outliers in the data, pre-filter and to examine the data and if necessary choose useful subsets.

The next major step is to choose the structure and order of the model to be identified. This is the most crucial step in identification procedure, since the wrong structure cannot yield a ‘good’ model no matter what the amount and quality of the experiments and the data. The next sections describe the family of model structures and the choices made when identifying the model for the String.

#### 8.3.1 Models of Linear Time Invariant (LTI) Systems

A system with scalar input  $u(t)$  and output  $y(t)$  is time invariant if its response does not depend on absolute time. It is linear if its output response to a linear combination of inputs is the same as the linear combination of output responses of the individual inputs. It has the property of being causal if output at a certain time depends on input up to that time only. With these assumptions the linear theory for dynamic systems can be applied. An LTI system subject to disturbance is shown in Figure 8.3

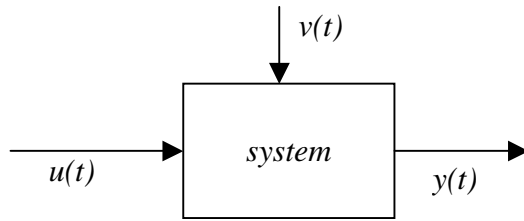


Figure 8.3 An LTI system subject to disturbance.

The disturbance,  $v(t)$ , can be measurement noise or some uncontrollable input to the system. The impulse response for such a system in discrete time is described by:

$$y(t) = \sum_{k=1}^{\infty} g(k)u(t-k) + v(t) \quad \text{where} \quad v(t) = \sum_{k=0}^{\infty} h(k)e(t-k) \quad (8.1)$$

the noise term  $v(t)$  is assumed to be driven by white noise  $e(t)$ .

Introducing the backward shift operator  $q^{-1}u(t)=u(t-1)$  and the notations

$$G(q) = \sum_{k=1}^{\infty} g(k)q^{-k} \quad \text{and} \quad H(q) = \sum_{k=0}^{\infty} h(k)q^{-k} \quad (8.2)$$

the description for an LTI system can then be written:

$$y(t) = G(q)u(t) + H(q)e(t) \quad (8.3)$$

where  $G(q)$  and  $H(q)$  are the transfer functions for the input and the noise respectively.

A particular model for the system corresponds to finding the two functions  $G$  and  $H$ . Working with infinite sequences,  $g(k)$  and  $h(k)$  is impractical, and  $G$  and  $H$  should be parameterized using a finite number of numerical values. Determining these parameters is done in the estimation procedure. A common way is to represent  $G$  and  $H$  as rational functions and let the parameters be the numerator and denominator coefficients. A generalized model structure, which may give rise to 32 different model sets, is:

$$A(q)y(t) = \frac{B(q)}{F(q)}u(t) + \frac{C(q)}{D(q)}e(t) \quad (8.4)$$

where the five polynomials have either of the forms:

$$A(q) = 1 + a_1 q^{-1} + \dots + a_{n_a} q^{-n_a} \quad B(q) = b_1 q^{-1} + \dots + b_{n_b} q^{-n_b}$$

where  $A$ ,  $C$ ,  $D$  and  $F$  have leading 1's. The structure is illustrated in Figure 8.4.

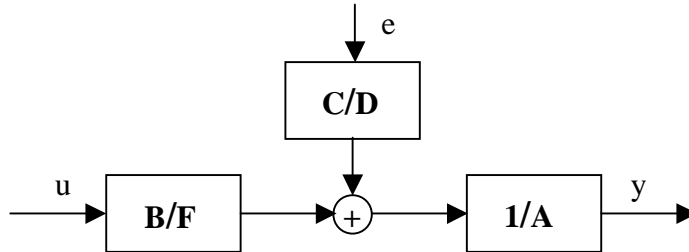


Figure 8.4 A generalized model structure for an LTI system.

The polynomial  $A$  corresponds to poles that are common between the dynamic model and the noise model. This polynomial is appropriate if the noise enters system "close to" the input. Likewise  $F$  determines the poles that are unique for the dynamics from input, and  $D$  the poles that are unique for the noise. This structure is too generalized for most purposes, and one or several of the polynomials can be set to unity. This gives rise to more common special black box SISO models listed in Table 8.1.

*Table 8.1 Some common Black Box SISO models.*

Polynomials used	Name of Model Structure
AB	ARX
ABC	ARMAX
BF	OE (Output Error)
BFGD	BJ (Box-Jenkins)

### 8.3.2 LTI Models for the String

The choice of model structure is closely linked to the nature of the noise that enters the system.

The ARX structure does not allow the noise to have an effect on the system different than the effect coming from of the input. This could correspond to noise on the reading of the position of the JT-valve, or from effects such as hysteresis in the valve movement or uneven flow of liquid through the valve for some reason.

If one suspects that the measurement of the output is burdened with white noise, this would come as a direct addition to the signal from the process, and the polynomials  $C$ ,  $D$  and  $A$  would be set to unity, thus yielding the OE model structure. This situation would correspond to a disturbance affecting the temperature sensor or noise generated by the processing of the signal from the temperature sensors.

If the noise has the nature of some uncontrollable input to the system, it will be filtered by the same dynamics as the contribution from the input. This implies using the same denominator  $A$  for the input signal as for the disturbance, thus making  $D$  and  $F$  redundant. This corresponds to the ARMAX model. Variation of the heat inleak to the String would have this effect.

If the uncontrollable input to the system not only filters through as the input signal, but has a more complex affect it would have to be described by the polynomials  $C$  and  $D$ , yielding the BJ model structure. This could be envisaged to happen because of some disturbance affecting the temperature sensor itself as well acting as an uncontrollable variation of the heat inleak.



For the String all of the above-indicated sources of disturbance can be imagined to occur to a greater or lesser extent. As there are no measurements or sensible prediction of either of the disturbances, the only way to go about it was to try all the structures and interpret which disturbance has the dominating effect. This procedure is also in compliance with recommendations in literature which advises a generous attitude to the choice of model structure [L.Ljung]

## 8.4 LTI models and validation

Three experiments were used in the system identification and model validation procedure. The experiment used for creating the modes is shown in Figure 8.2. Two experiments were used for model validation. They are shown in Figure 8.5 and Figure 8.6 below. The working point in the identification experiment is 1.87 K compared to the working points of 1.88 K and 1.895 K for the validation experiments. This allows for testing against the non-linearity of  $c_p(T)$  which experiences a 7.5 % increase from 1.87 K to 1.895 K .

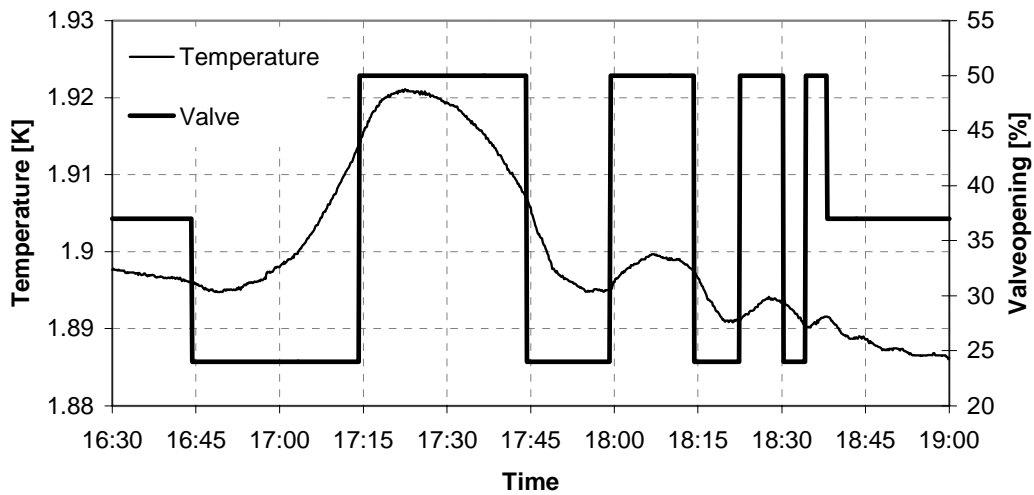


Figure 8.5 Validation experiment I, 2 1/2 hours duration.

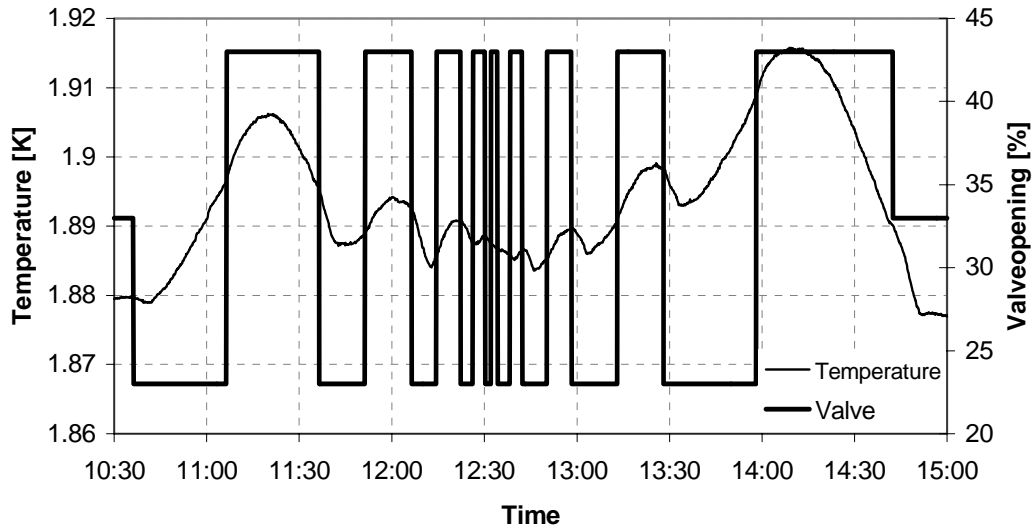


Figure 8.6 Validation experiment II, 4 ½ hours duration.

The four model structures in Table 8.1 have been investigated. The orders of the polynomials in the structures have been varied to identify the best model in each structure. The best candidate from each structure is then compared in the validation procedure.

Several aspects of the models are examined.

The simulated *model outputs* of the models are compared with the actually measured output. The comparison is performed against the data used to create the model.

The autocorrelation of the model *residuals* (prediction errors) and the crosscorrelation between inputs and residuals are examined to test if they are contained within a specified confidence interval.

*Transient response* of the models resulting from a step in the input signal is examined.

*Frequency response* of the models, known as Bode plots, is examined. The bandwidth of the model decreases according to how fast the phase of the model drops. A lower bandwidth means that the system is slower, and higher frequency inputs will be smoothed out in the response of the model.

The *poles and zeros* of the models are examined. The poles of the system are the zeros of the denominator polynomial in the transfer function from the input to the output. Operating with the q-transform the criterion for the stability is that the unit circle must lie inside the region of convergence (ROC) shown in Figure 8.7. One of the properties of the ROC is that it does not contain any poles (property 2 p635 signals and system). Consequently the poles of the system must lie inside or on the unit circle, otherwise the system is unstable. The zeros of the numerator polynomial are the zeros of the system. If

a zero is located positively on the outside of the unit circle, it indicates that the system is non-minimum phase. [seborg 132] The presence of complex conjugate poles indicates that the response will contain sine and cosine modes, that is, it will exhibit oscillatory modes. Zeros in the numerator are said to exhibit *numerator dynamics*. Processes with a higher degree in the denominator than in the numerator exhibit some sort of inertia, and no jump in the output will be observed.

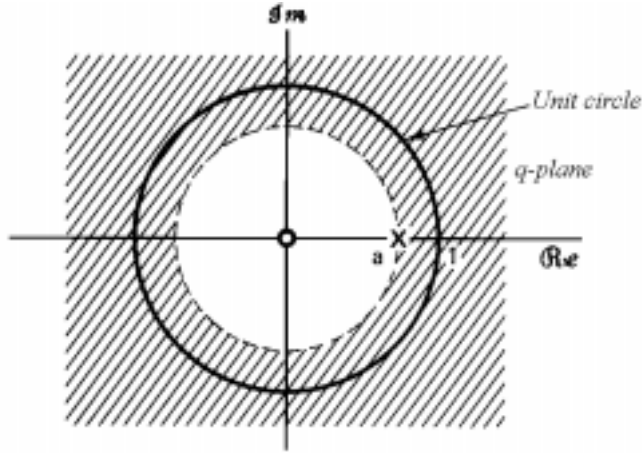


Figure 8.7 Region of convergence in the  $q$ -plane indicated by the dashed area. The unit circle must lie in the ROC for the model to be stable.

The sampling time used in the identification that is presented here is 20 seconds.

#### 8.4.1 Parameter estimation

[37] A system described by an ARX model is written:

$$A(q)y(t) = B(q)u(t) + e(t) \quad (8.5)$$

It is assumed to be no time delay in the model. The polynomials  $A(q)$  and  $B(q)$  are given by:

$$A(q) = 1 + a_1 q^1 + a_2 q^2 + \dots + a_{na} q^{na}$$

$$B(q) = b_1 q^1 + b_2 q^2 + \dots + b_{nb} q^{nb}$$

where  $n_a$  and  $n_b$  are the order of the  $A$  and  $B$  polynomials respectively. By defining:

$$\psi_t = [-y_{t-1} - y_{t-2} \dots - y_{t-na} u_{t-1} u_{t-1} \dots u_{t-nb-1}]^T \text{ - regressor vector} \quad (8.6)$$

$$\theta = [a_1 a_2 \dots a_{na} b_1 b_2 \dots b_{nb}]^T \text{ - parameter vector} \quad (8.7)$$

the model is expressed as:

$$y(t) = \psi^T(t) \theta + e(t) \quad (8.8)$$

The goal of the estimation procedure is to find the estimate for  $\theta$  that best describes the data. A loss function that sums up the square of the error between the estimated output and the measured output is introduced:

$$J(\hat{\theta}) = \sum_{t=1}^N [y(t) - \psi^T(t) \hat{\theta}]^2 \quad (8.9)$$

where the superscript  $\hat{\cdot}$  denotes estimate.  $N$  is the number of data samples. Derivation of the loss function gives:

$$\frac{\partial J}{\partial \hat{\theta}}(\hat{\theta}) = -2 \sum_{t=1}^N \psi(t) [y(t) - \psi^T(t) \hat{\theta}] \quad (8.10)$$

By setting the derivative to zero and solving for the estimated parameter vector the estimate becomes:

$$\hat{\theta} = \frac{\sum_{t=1}^N \psi(t) \psi^T(t)}{\sum_{t=1}^N \psi(t) \psi^T(t)} \sum_{t=1}^N \psi(t) y(t) \quad (8.11)$$

which is the least square estimate of the model that is solved in the estimation procedure. The least square model of other structures proceeds along similar lines starting with the relevant model structure.

### 8.4.2 ARX and IV models

The regular ARX model with time delay has the structure:

$$A(q)y(t) = B(q)u(t - nk) + e(t) \quad (8.12)$$

where  $e(t)$  is white noise. In a case where the noise is coloured the ARX structure will not give an unbiased estimate [37]. An alternative form for achieving an unbiased estimate in the presence of coloured noise is called instrumental variables method has the form:

$$A(q)y(t) = B(q)u(t - nk) + v(t) \quad \text{where } v(t) = H(q)e(t) \quad (8.13)$$

and  $H(q)$  is a rational transfer function. The idea of the IV structure is to find consistent estimates for  $A(q)$  and  $B(q)$  while not regarding the coloured noise and its transfer function in the estimation procedure. This is achieved by defining a set of alternative regression variables which are denoted the *instrumental variables*.

Figure 8.8 Shows the simulated output compared with measured output for three models in the classes of ARX and IV models. The orders of the polynomials are indicated as  $ARX_{n_A n_B n_k}$ .

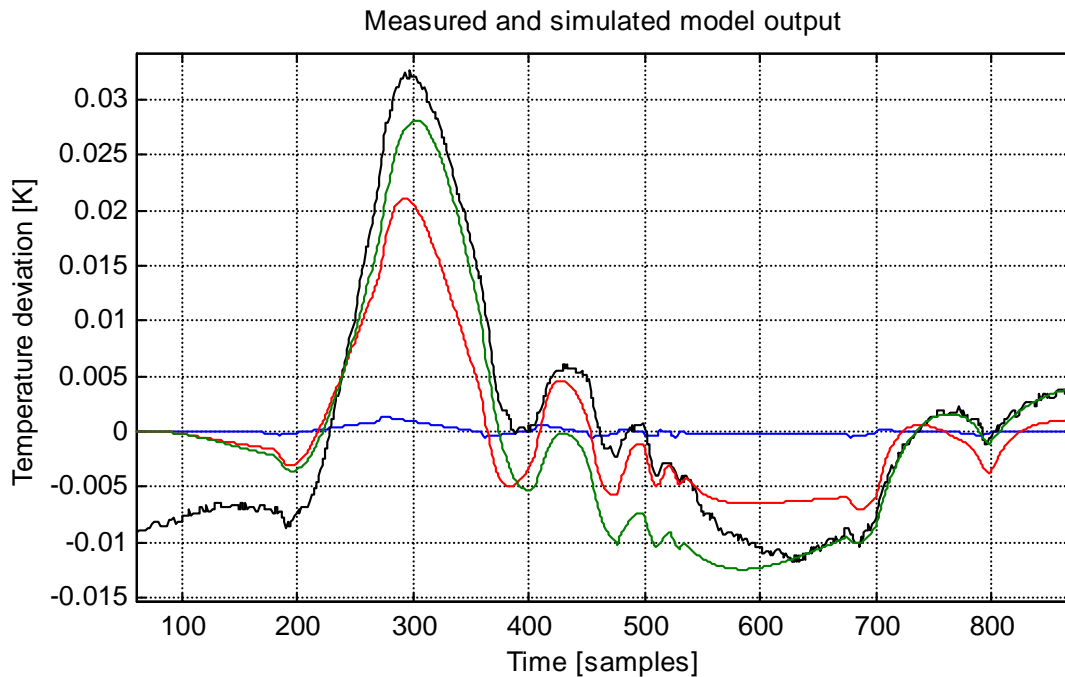


Figure 8.8 Model outputs. Blue:  $ARX_{221}$ , red:  $ARX_{10\ 10\ 1}$ , green:  $IV_{221}$

The ARX model of order 2 does not even remotely reproduce the data, and only a model of high order ( $>10$ ) is moderately successful in describing the dynamics of the data. This is an unacceptably high order for a model. The IV model of order 2 (green line) does a much better job of reproducing the data. It is clear that the noise in the system is not white, and a simple ARX model will not be satisfactory. The IV structure is sensitive to the order of delay, and  $IV_{223}$  gives an diverging output. Higher order of the A

polynomial give poles in origo signalling that the order is too high, and also give a degradation in the model output. IV221 is thus the only order of the structure with satisfactory properties

### 8.4.3 Output error (OE) models

The output error structure has the form:

$$y(t) = \frac{B(q)}{F(q)}u(t - nk) + e(t) \quad (8.14)$$

Figure 8.9 shows the simulated output of three OE-models. The orders of the polynomials are indicated as  $OE_{n_B n_F n_k}$ .

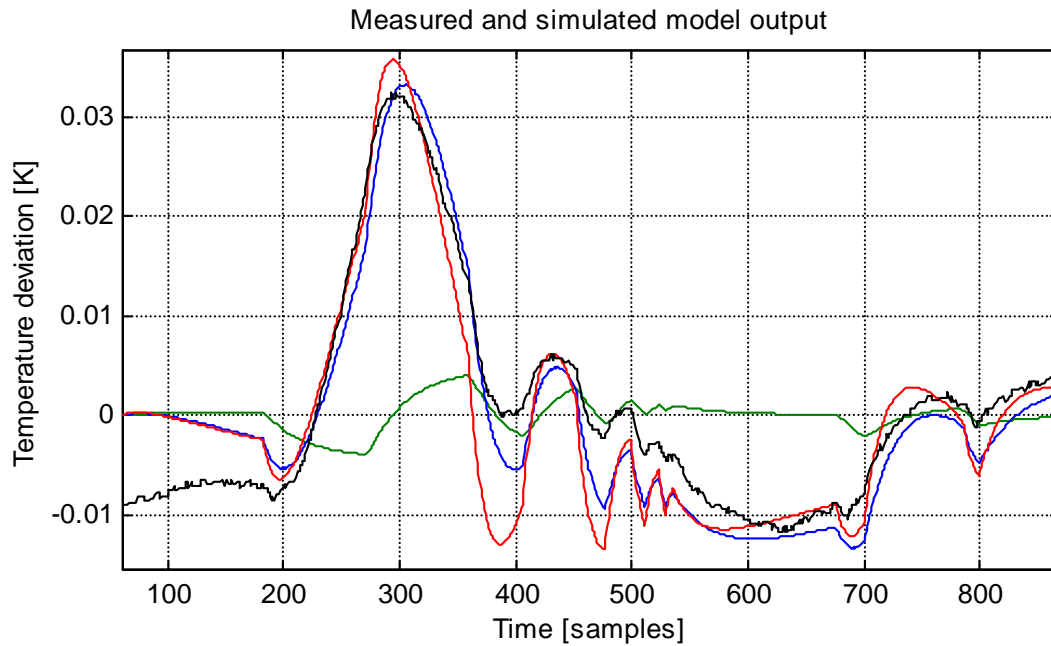


Figure 8.9 Model outputs. Blue:  $OE_{331}$ , red:  $OE_{221}$ , green:  $OE_{121}$

The model  $OE_{221}$  does a moderately good job in describing the data. It has two stable poles and a zero outside the unit circle, indicating a non-minimum phase system as would be expected. A model order 3 does a better job in reproducing data, however it has an additional negative zero outside the unit circle as well as a pole in minus 1. Higher order models yield totally unacceptable high frequency oscillation around the output trajectory produced by complex poles. The structure is also sensitive to the order of delay  $n_k$ . Both  $OE_{331}$  and  $OE_{221}$  shows a degradation in performance if increasing the order of delay

by one. This does not inspire confidence in the structure, and no acceptable model is identified.

#### 8.4.4 ARMAX models

The ARMAX structure has the form:

$$A(q)y(t) = B(q)u(t - nk) + C(q)e(t) \quad (8.15)$$

Figure 8.10 shows the simulated output of three ARMAX-models. The orders of the polynomials are indicated as  $\text{ARMAX}_{n_A n_B n_C n_k}$ .

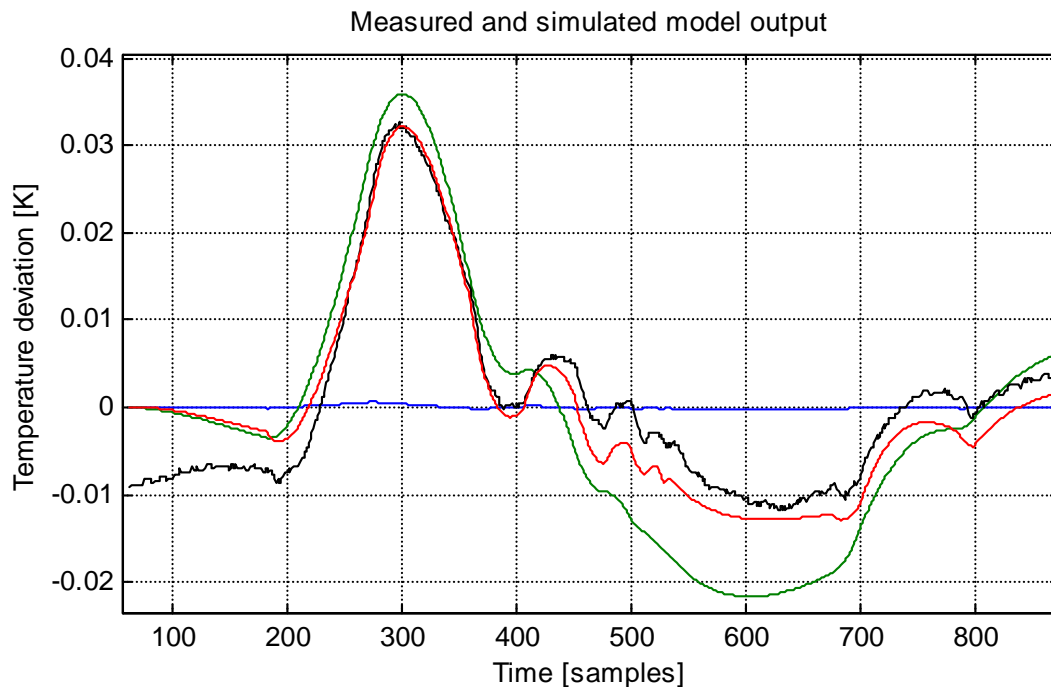


Figure 8.10 Model outputs. Red:  $\text{ARMAX}_{2211}$ , green:  $\text{ARMAX}_{1211}$ , blue:  $\text{ARMAX}_{2111}$

Assuming second order for all parameters in an ARMAX model yields a much better response. Reducing parameters until a noticeable degradation in behaviour occurs gives the simplest acceptable model in the class:  $\text{AMX}_{2211}$  (red line). Increasing any of the model parameters does not noticeably improve the model output. Increasing the order of the  $A$  polynomial gives additional poles close to origin signal that the order is too high. Reducing either the polynomial  $A$  (green line) or  $B$  (blue line) gives a noticeable degradation in performance. Decreasing the  $C$  polynomial yields an unacceptable performance.

Increasing the time delay in the ARMAX221 $n_k$  model does not significantly alter the simulated output. A delay of 8 samples moves the zero inside the unit circle to indicating minimum phase system. It is hence the delay identified as necessary to account for the combined effect of the system being non-minimum phase and a transport delay. Additionally the 8-sample delay smooth out the higher frequencies, and signals with a time constant of less than five minutes are filtered out. The model AMX2211 is the best model in the structure.

### 8.4.5 Box-Jenkins (BJ) models

The Box-Jenkins structure has the form:

$$y(t) = \frac{B(q)}{F(q)} u(t - nk) + \frac{C(q)}{D(q)} e(t) \quad (8.16)$$

Figure 8.11 shows the simulated output of three Box-Jenkins-models. The orders of the polynomials are indicated as BJ $n_B n_C n_D n_F n_k$ .

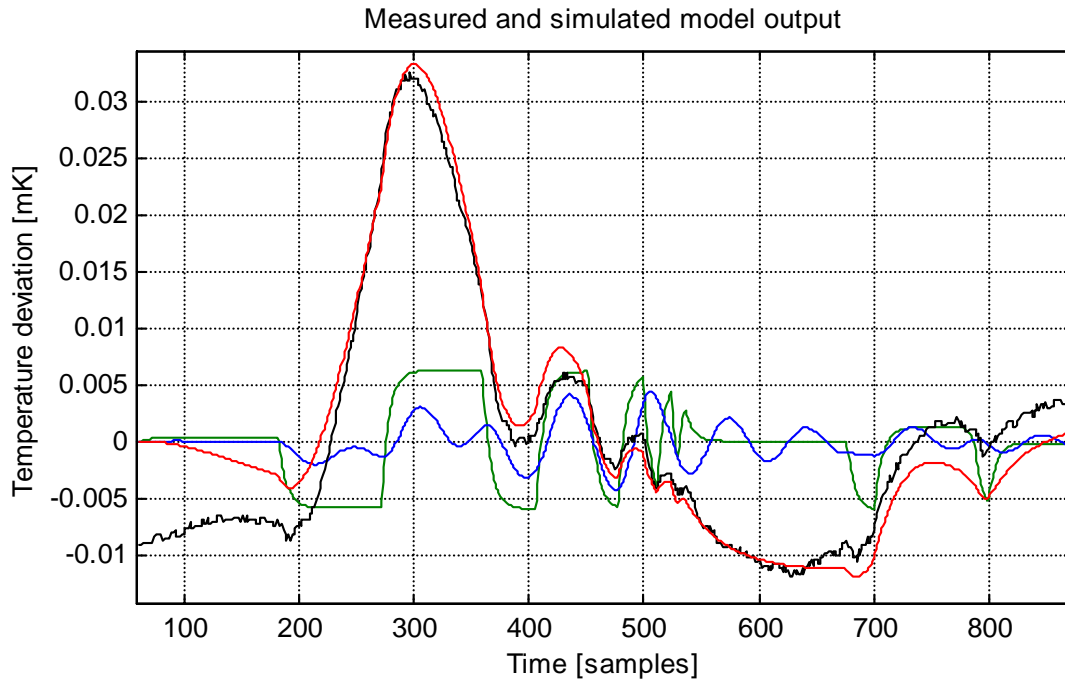


Figure 8.11 Model outputs. Red: BJ21121, blue: BJ11121, green: BJ21111



Assuming second order for all parameters (BJ22221) gives a response very similar to that of the ARMAX model. Reducing model parameters until the behaviour noticeably degrades gives the simplest model in the class: BJ21121. Increasing any of the model parameters does not noticeably improve the model output. Reducing either the polynomial  $A$  (green line) or  $B$  (blue line) gives an unacceptable performance. Decreasing the  $C$  or  $D$  polynomials does not noticeably change the model output, however the autocorrelation is significantly outside the confidence interval.

Increasing the time delay in the BJ2112 $n_k$  model does not significantly alter the simulated output. A delay of 15 samples moves the zero inside the unit circle indicating minimum phase system. The phase margin decreases with increasing specified dead time. The model BJ21121 is the best model in the structure.

#### 8.4.6 Verification of the models

The model output of the best models plotted against the identification data set in

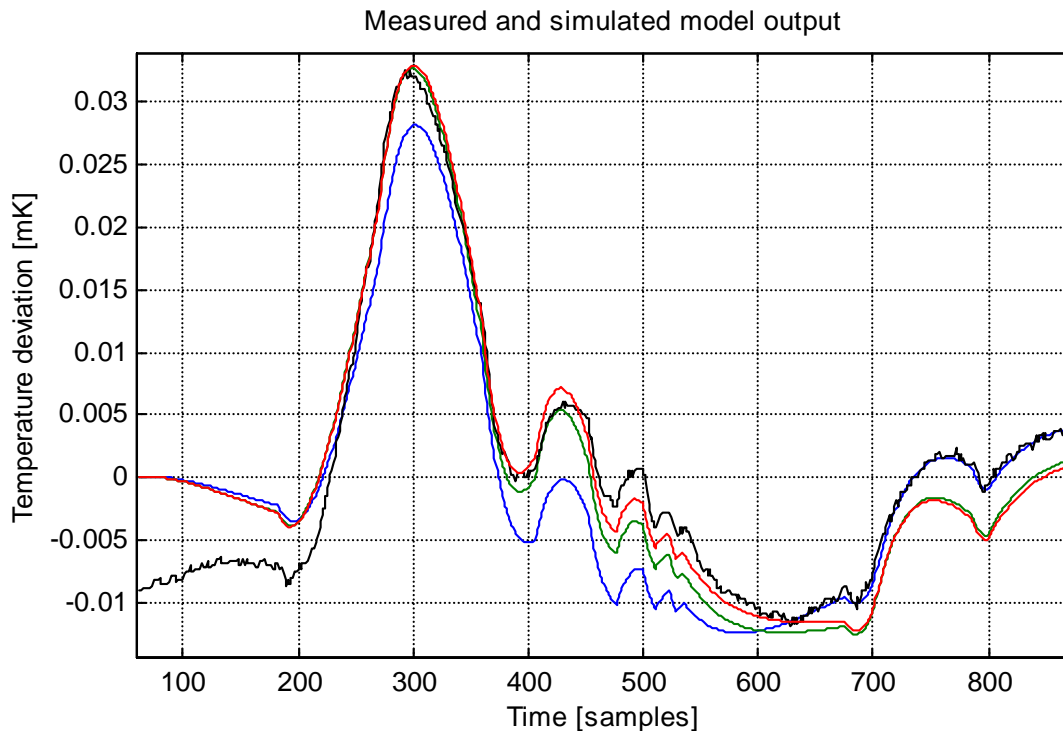


Figure 8.12 Model outputs of the best model in each structure. blue:IV221, green: ARMAX2211, red: BJ21121

All the models have real and stable poles and a zero outside the unit circle indicating a non-minimum phase system. One of the poles is practically at the unit circle signalling an integrating system. The models also have second pole close to the unit circle indicating that the system is close to being unstable. Table 8.2 shows the zeros and poles for the three models. The duration of the inverse response is also shown. All the models have a phase of  $-180^\circ$  at 0.5 Hz.

*Table 8.2 Zeros and poles and duration of step response for IV221, ARMAX2211 and BJ21121.*

	Pole I	Pole II	Zero	Step response
ARMAX	0.998	0.975	1.098	6 m 30s
BJ	0.999	0.974	1.096	6 m 40 s
IV	0.992	0.985	1.076	8m 20 s

Figure 8.13 and Figure 8.14 shows the performance of the best model in each structure plotted against the two verification experiments shown in Figure 8.5 and Figure 8.6.

*Measured and simulated model output*

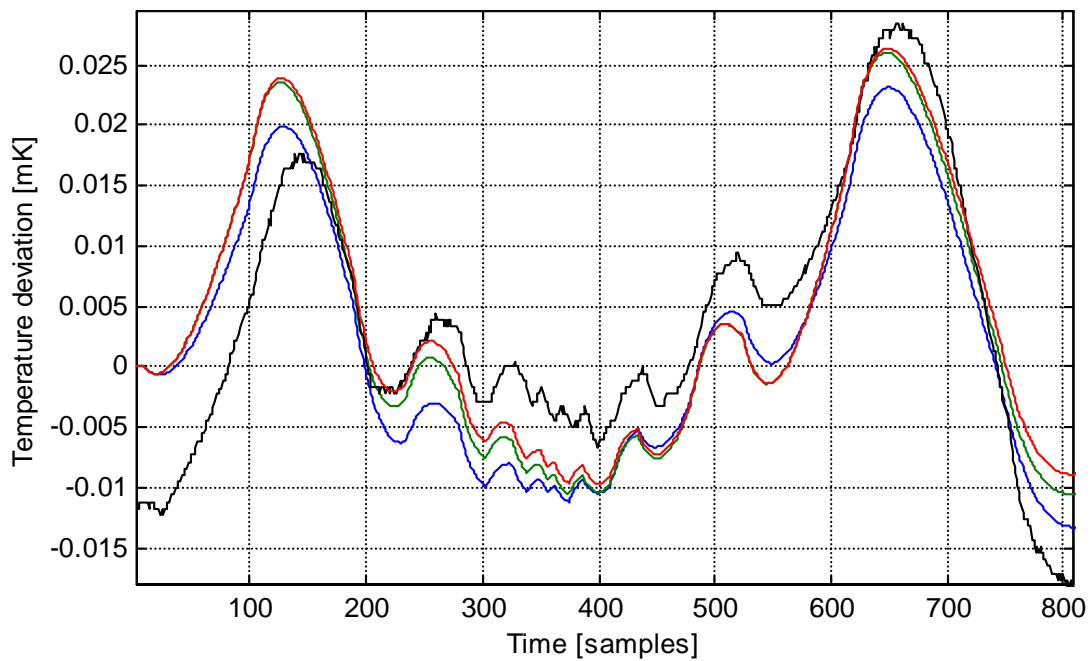


*Figure 8.13 Model outputs shown against verification experiment I. Blue: IV221, green: ARMAX2211, red: BJ21121.*

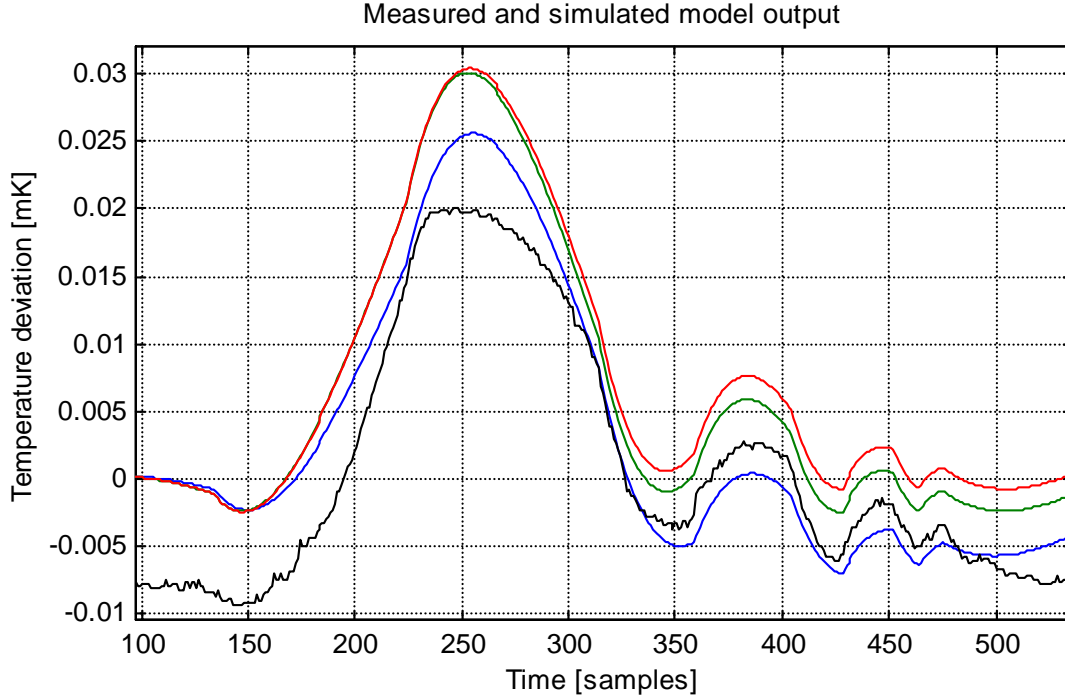


Figure 8.14 Model outputs shown against verification experiment II. Blue: IV221, green: ARMAX2211, red: BJ21121.

The transfer function of the three models are:

$$\text{ARMAX2211: } \frac{B(q^{-1})}{A(q^{-1})} = \frac{10^{-5}(1.211q^{-1} - 1.330q^{-2})}{1 - 1.9726q^{-1} + 0.9726q^{-2}} \quad (8.17)$$

$$\text{BJ: } \frac{B(q^{-1})}{F(q^{-1})} = \frac{10^{-5}(1.230q^{-1} - 1.348q^{-2})}{1 - 1.9723q^{-1} + 0.9723q^{-2}} \quad (8.18)$$

$$\text{IV: } \frac{B(q^{-1})}{A(q^{-1})} = \frac{10^{-5}(1.228q^{-1} - 1.321q^{-2})}{1 - 1.9770q^{-1} + 0.9771q^{-2}} \quad (8.19)$$

The performance of the BJ model is very similar to that of the ARMAX model indicating that no improvement is gained by using a separate polynomial for describing the nature of the noise. This indicates that the dominant factor in the noise is the variation in the heat inleak to the system.

## 9 MPC control of the 1.8 K cooling loop

In chapter 5 the concept of Model Predictive Control was introduced. An MPC controller has been implemented on the 1.8 K cooling loop of the Magnet Test String. This chapter describes in more detail the concept of MPC and the implementation on the String. Figure 9.1 shows schematically how an MPC is functioning. The theory presented in this chapter is consistent with literature e.g. [39], [40] and [41].

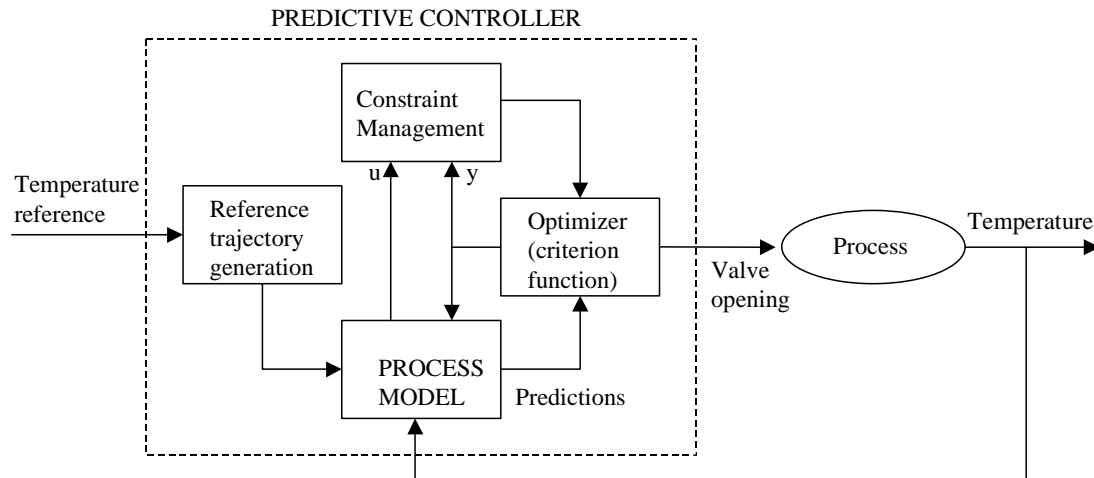
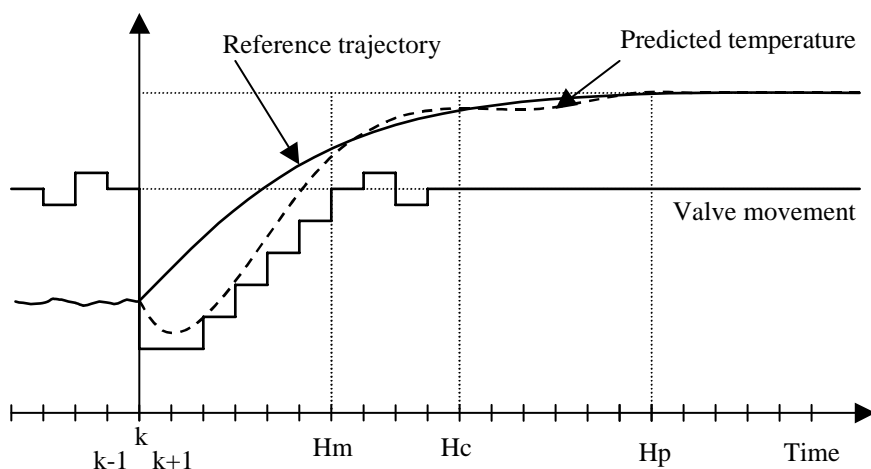


Figure 9.1 The parts that constitute a model based predictive controller.

At each sample time first a reference trajectory is created according to the present state of the system and a predefined rule for the shape of the trajectory. Then an optimized sequence of movements of the manipulated variable is found according to a predefined criterion function. This is the sequence that drives the process ‘as close as possible’ along the reference trajectory. The optimization might be subject to a set of predefined constraints which would have to be taken into consideration. The process output used in the optimization is calculated according to a process model which is embedded in the controller.

The first value of the sequence of movements of the manipulated variable, the valve opening in the case of the String, is fed to the process. The whole procedure is then repeated at the next sample time using updated information recorded from the process. The concept of predicting the process output at each sample time using updated information is referred to as receding horizon control.



*Figure 9.2 The reference trajectory, valve sequence and predicted temperature response of the MPC. Receding horizon control: process output at each sample time using updated information.*

Three design parameters are marked in Figure 9.2 and Table 9.1 shows the range in which the parameter must lie.

*Table 9.1 Ranges where to choose design parameters [42].*

$H_p$	Prediction horizon	$\geq H_m$
$H_m$	Minimum cost horizon	$d+1 \leq H_m \leq H_p$
$H_c$	Control horizon	$1 \leq H_c \leq H_p-d$

The control horizon  $H_c$  is the number of allowed movements of the manipulated variables that can be used to create the predicted temperature development. The discrepancy between the reference trajectory and the predicted temperature is evaluated between minimum cost horizon  $H_m$  and the prediction horizon  $H_p$ .  $d$  is the dead time of the process. It can be argued that the lower limit of  $H_m$  should be 1 and not  $d + 1$  as listed. This is indeed the case

## 9.1 Reference trajectory

The reference trajectory defines how the process should move from one set point to another and is an arbitrary sequence of point. However for many processes a simple first order trajectory can be used. The trajectory can be created according to:

$$w(k+i) = (1-\alpha)Sp + \alpha w(k+i-1) \quad (9.1)$$

where  $\alpha$  is a factor defining the gradient of the reference trajectory. The set point  $Sp$  is the desired temperature of the magnets. The starting point for  $w(k)$  is chosen as either  $y(k)$  or the initial value of  $w(k)$  as illustrated in Figure 9.3.

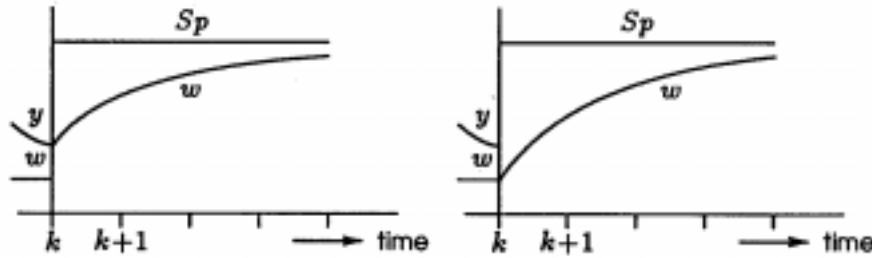


Figure 9.3 Two ways of initiating the reference trajectory: either at the measured output or at the previous value of the reference trajectory [43].

By using  $y(k)$  an extra feed-back loop is activated, as an updated value of the starting point of the trajectory is fed back to the controller from the process. This is the reference trajectory used in the String implementation.

Choosing a reference trajectory is a way of defining the desired closed-loop response. In the String implementation this was a matter of choosing the value of  $\alpha$ . As no satisfactory guideline was found this was a matter of trial and error.  $\alpha$  was chosen such that the reference trajectory was in order of the maximum gradient attainable for the process.

## 9.2 Criterion function

In predictive controllers, minimization of a criterion function yields the predictive control law. The choice of the criterion function is therefore important.

The simplest form of criterion function is:

$$J = \sum_{i=1}^{H_p} [\hat{y}(k+i) - w(k+i)]^2 \quad (9.2)$$

It can be shown [Soeterboek, R, p49] that this criterion will yield a minimum variance controller. This type of controller might give a badly damped or unstable control system.

This is improved by putting the output in the criterion function, and the criterion becomes:

$$J = \sum_{i=1}^{H_p} [\hat{y}(k+i) - w(k+i)]^2 + \rho u(k+i-1)^2 \quad (9.3)$$

The weighting factor  $\mu$  is used to make a trade-off between the conflicting objectives of minimizing the tracking error and minimizing the controller output. Increasing  $\mu$  puts more weight on the controller output and gives a less active output and a slower process output.

Using this weighting factor has two major disadvantages:

1. choosing  $\mu$  such that the system behaves as desired. Since  $\mu$  depends on the process, the choice must be done either based on simulation or by trial and error.
2. For processes with a constant nonzero  $u(k)$  in steady state conditions, the use of  $\mu$  will give a steady state error when set point and disturbances are constant. Since  $u(k)$  is nonzero in steady state conditions it affects the criterion function in steady state and hence the steady state controller output.

Weighing the controller increment instead of the output itself will avoid steady state errors since the control increments in steady state are zero. It does not however make the choice of  $\mu$  any easier.

If a minimum value of the dead time is known or the process is non minimum phase, the minimum cost horizon should be equal to or larger than the dead time or inverse response. The criterion function that is used in the MPC implemented on the String then becomes:

$$J = \sum_{i=H_m}^{H_p} [\hat{y}(k+i) - w(k+i)]^2 + \rho \sum_{i=1}^{H_c} \Delta u(k+i-1)^2 \quad (9.4)$$

### 9.3 The predictive control law

The optimal control law is derived by minimization of the criterion function with respect to the controller output sequence over the control horizon. When there are no constraints and the process model is linear, the minimization can be done analytically. Subject to constraints the minimization is done by an iterative method.

If the criterion function  $J$  is optimized with respect to the vector  $u$ , then any local optimum  $u$  satisfies:

$$g = \frac{\partial J}{\partial u} = 0 \quad (9.5)$$

where  $g$  denotes the gradient and  $\partial$  denotes the partial derivative. A local optimum is global minimum if the Hessian  $J$

$$J = \frac{\partial^2 J}{\partial u^2} \quad (9.6)$$

is positive definite. This is the optimization that yields the predictive control law.

### 9.4 Constraints

Constraints are classified as either soft or hard constraints. Soft constraints might be violated temporarily to satisfy other criteria. These can usually be taken care of by the minimization of the criterion function. The weighting factor  $\mu$  can be selected such that the soft constraint is satisfied most of the time. For the String the magnet temperature is a soft constraint: it might temporarily be allowed to exceed a defined maximum. For the results presented later in this chapter the upper limit for the temperature is set such that this constraint is never violated.

Hard constraints on the other hand cannot be violated at any time. Typically there are hard constraints on the input of the process. For the MPC implantation at the String the valve has constraint with a lower limit of 5 % opening and an upper limit of 100% opening. Hard constraints must be taken into account explicitly and an unconstrained minimization is no longer possible. This results in an optimization solution that must be found iteratively at each sample time by quadratic programming (QP).

In addition to level constraints there might also be constraint on the rate of change  $\mu u$ . The control of a process subject level constraints might become rather bad, and if rate of change constraints are present even unstable. Taking into account the effect of constraints



has been shown to result in much better system performance: the controller anticipates the constraints becoming active in the future.

The optimal operation point for a process often lies at the intersection of constraints. The control must avoid violations and still operate close to the constraints. This is one of the strong points of predictive controllers, since they can incorporate the handling of constraints in a systematic way. Hence a predictive controller which takes hard constraints into account allows to operate closer to the physical limitations of the process safely. Up until now, predictive control is the only controller design concept that can handle hard constraints in a natural and systematic way.

## 9.5 System model for the MPC

In Chapter 8 the concept of black box models was discussed. The models that were implemented in the MPC algorithm were developed in the system identification procedure. The ARMAX model was identified as the structure that best describes the system. The BJ structure performed very similar to the ARMAX structure was implemented in the algorithm. No difference in performance between the two structures was detected. An OE model was also tested giving an unstable closed loop performance. The ARMAX model that was developed is:

$$\frac{B(q^{-1})}{A(q^{-1})} = \frac{10^{-5}(1.211q^{-1} - 1.330q^{-2})}{1 - 1.9726q^{-1} + 0.9726q^{-2}} \quad (9.7)$$

## 9.6 Design parameters

Model Predictive Control is an open methodology that can contain a number of design parameters according to the desired properties and the implementation at hand. A unified approach to MPC involves ten design parameters. However not all parameters are relevant for each implementation. This chapter treats the relevant design parameters for the String implementation. Also treated are guidelines how to choose them and their effect on the robustness and stability of the controller.

To investigate the effect of the design parameters the MPC controller was run off line without temperature feedback from the system. The temperature observed by the controller was constant throughout the procedure. However for a period of about five minutes a real temperature evolution is not expected deviate much from the initial temperature due to the inverse response. Consequently the predictions made by the controller and the applied valve sequence corresponds reasonably well with a real situation for this period. As time advances the discrepancy will increase. From steady state condition with 28 % valve opening a step down in the temperature reference of 15

mK was introduced. The subsequent valve response with different settings of the design parameters was studied. The sampling time for the simulations is 10 seconds.

### 9.6.1 Controller output weighting

The criterion function, equation (9.4), shows that the weighting factor  $\rho$  and the filter  $\Delta$  realize the controller output weighting. A rule of thumb on how to choose  $\rho$  does not exist. However a large value of  $\rho$  results in an unstable closed-loop system because there is no longer any feedback. The value of  $\rho$  must therefore be chosen with care. The below figure shows the evolution of the valve opening following the procedure described above. The three parameters  $H_m$ ,  $H_p$  and  $H_c$  are constant in each of the two figures respectively. The weighting factor  $\rho$  is varied.

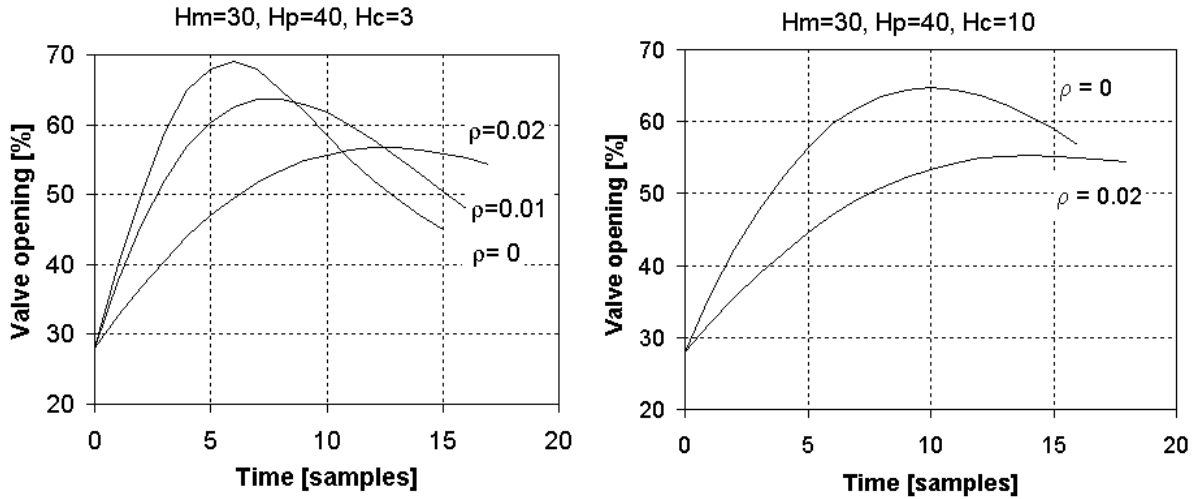


Figure 9.4 Valve response using different values for the weighting factor  $\rho$ .

Values up to  $\rho = 0.02$  give reasonable limitation of valve movement. For larger values the restriction in the valve movement becomes increasingly severe, and this value was considered as an upper limit.

In discrete time  $\Delta$  is expressed:

$$Q_n = 1 - q^{-1} \quad (9.8)$$

The use of  $\Delta$  eliminates steady state offset and does not influence the steady-state behavior if the reference trajectory and disturbances are constant. This is the reason for

the use of  $\Delta$  in many predictive controllers. However there is a danger that weighting the controller increment the closed-loop can lead to a badly damped or even unstable system. Since the criterion function is minimized over a finite number of samples the controller is still optimal with respect to the criterion function. Low frequency oscillations result in small values of the controller increments hence the corresponding part of the criterion function remain small. However the system will exhibit low frequency oscillations corresponding to the disturbance. If the criterion function is minimized over a larger horizon the situation improves. This effect will not occur when weighting the controller output directly since both parts of the criterion function go to infinity if the closed-loop system is unstable.

The situation can be improved by introducing in addition to  $\Delta$  the filter:

$$Q_d = 1/(1 - \mu q^{-1}) \quad (9.9)$$

where  $\mu=0.95$  is a typical value. Now  $\Delta$  still satisfies the steady-state requirements for constant set points and disturbances, while the dynamic behavior is approximately equal to that when the controller output is weighted directly.

For the MPC implementation of the String, both  $\rho$  and  $\Delta$  as well as the described  $Q_d$  have been used. Zero steady state offset was achieved as well as low variance of the controller output. The results of using  $Q_d$  were inconclusive.

### 9.6.2 Prediction, minimum cost and control horizon

In this section the influence of the prediction horizon ( $H_p$ ), the minimum cost horizon ( $H_m$ ) and the control horizon ( $H_c$ ) is examined.

These parameters can be used to select different well-known controllers. With  $\rho = 0$  choosing  $H_p = 1$  yields a minimum variance controller, and  $H_p \rightarrow \infty$  yields a mean-level controller. A large value of  $H_p$  is normally chosen for robustness reasons, and it can then no longer be considered as a tuning parameter. However the behavior of the closed-loop system can be influenced by  $H_c$  in a similar way to that when using  $H_p$ . If  $H_c = n_d + 1$  a dead-beat controller is approximated, while for  $H_c = H_p - d$  a minimum-variance controller is obtained. Normally however predictive controllers are not used as pole placement controllers and the parameters are chosen differently.

For a stable process the prediction horizon can be chosen according to the settling time of the closed-loop system:

$$H_p = \text{int}(t_{s,\mu}/T_s) \quad (9.10)$$

Where  $\text{int}(\cdot)$  is a function that converts real value to an integer, and  $T_s$  is the sampling time. For badly damped or unstable processes such as the string this rule of thumb cannot be used, and instead  $H_p$  can be related to the bandwidth of the open-loop process:

$$H_p = \text{int}(2\mu_s / \mu_b) \quad (9.11)$$

Where  $\mu_b$  is the bandwidth of the open-loop system and  $\mu_s$  is the sampling frequency. The bandwidth of the String is about  $\mu_b = 0.003 \text{ Hz}$  (333 sec). This value has been identified by examining the filtered output of the identification and validation experiments presented in Chapter 8. Input signals with frequencies higher than  $\mu_b$  are not detectable above the noise of the output signal. Sampling period should as a rule of thumb be chosen 10 – 20 times smaller than the settling time. Combining equations (9.9) and (9.10) the sampling period should be chosen 5 - 10 times smaller than the inverse of the bandwidth e.g. 33 – 66 seconds. According to equation (9.10) the prediction horizon should be chosen as  $H_p = 20 - 40$ . If the sampling time of the system is chosen different from this rule, then  $H_p$  should be adjusted accordingly for to apply. With this value the sensitivity of the closed-loop system to changes in  $H_p$  is small, and consequently  $H_p$  can no longer be used as a tuning parameter. In the simulations presented here the sampling time is ten seconds the prediction horizon should be chosen  $H_p = 67 - 133$  (11 – 22 minutes).

Figure 9.5 shows the valve response in simulated according to the procedure described above.

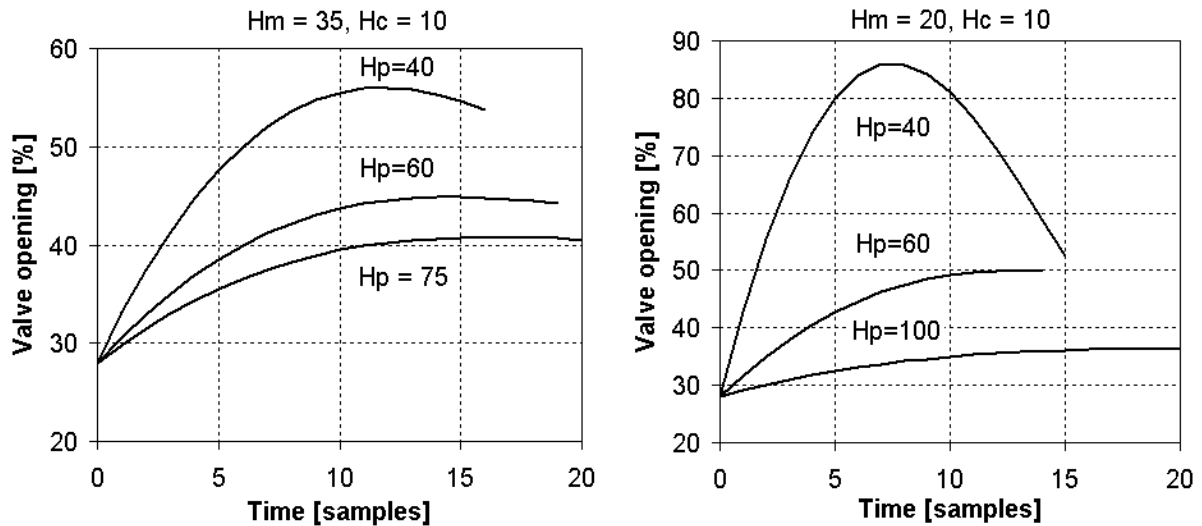


Figure 9.5 Valve response using different values for the prediction horizon.

On the left graph with  $H_m = 35$  there is a small difference when increasing the prediction horizon from 60 to 75 and the lower value of the rule of thumb seems appropriate. However with  $H_m = 20$  there is still a considerable change in valve response when increasing the prediction horizon from 60 to 100. A larger value than  $H_p = 67$  should be chosen to eliminate  $H_p$  as a tuning parameter.

Figure 9.6 shows the response of the valve using different values of the control horizon  $H_c$ .

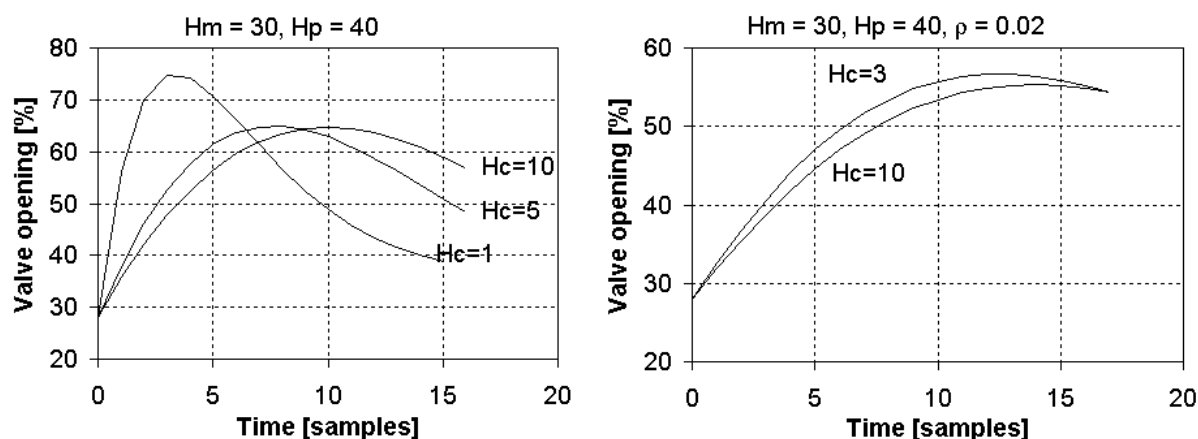


Figure 9.6 Valve response using different values for the control horizon.

Tuning rules states that in general increasing  $H_c$  with  $H_p \rightarrow \rho$  makes the controller more active. Figure 9.6 shows that the valve becomes less active when increasing the control horizon. This is contrary to the general tuning rule making the choice of  $H_c$  more difficult. Increasing the control horizon from 5 to 10 has a limited effect. On the right hand figure it is seen that introducing the weighting factor  $\mu$  reduces the effect of changing the control horizon.

Tuning rules states that for a minimum phase process, increasing  $H_m$  makes the closed-loop system respond more slowly to set point changes. [68] When controlling a non-minimum phase process, increasing  $H_m$  yields a faster closed loop system. Figure 9.7 shows the response of the valve using different values of the minimum cost horizon  $H_m$ .

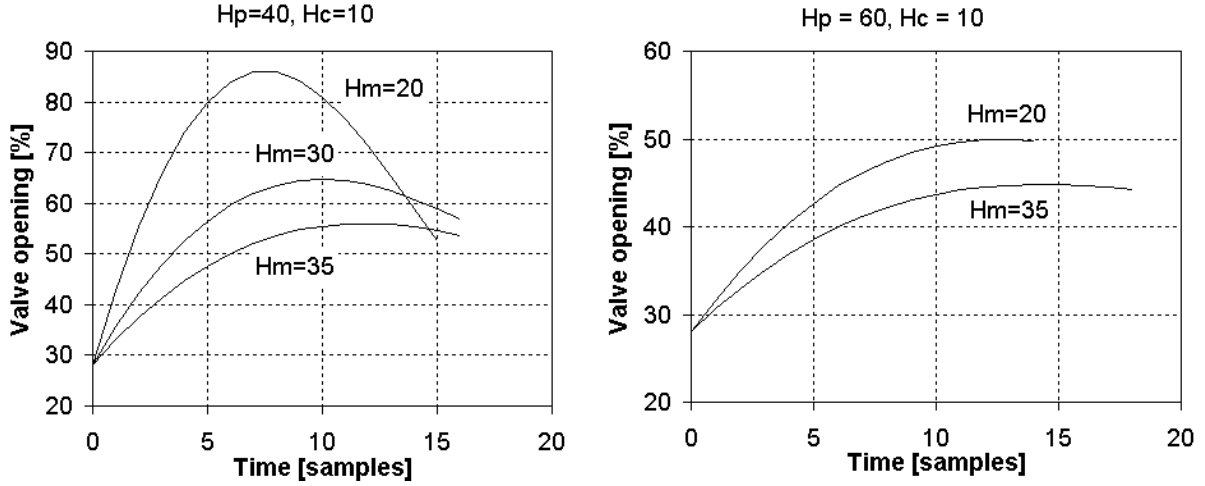


Figure 9.7 Valve response using different values for the minimum cost horizon.

Decreasing the minimum cost horizon makes the controller more active. Again this is contrary to the tuning rules making the choice of  $H_m$  more difficult.

A possible choice is  $H_m = H_p$ . In this case the tracking error is considered at only one point in the future. However assuming  $H_c = 1$  then choosing  $H_p$  is quite difficult when the system is non-minimum phase. This setting was attempted and as expected did not yield a satisfactory performance.

### 9.6.3 The disturbance model

Tuning rules states that the disturbance model is a powerful tool for tuning the regulator behaviour. When the model is different from the process the choice of the disturbance model is essential for obtaining a stable closed-loop system. The disturbance model:

$$T = (1 - \mu q^{-1})^{n_a} \quad (9.12)$$

can be used for unstable processes. The order of the  $A$  polynomial is  $n_a = 2$ . The choice of  $\mu$  depends on the sampling period.  $\mu = 0.8$  yield acceptable results in most cases. Increasing  $\mu$  makes the closed-loop system react more slowly to set point changes if the model is different from the process. This is not the case when the model is correctly modelled. Using a small value for  $\mu$  usually results in unacceptable regulator performance because the controller output variance is very large. Using  $T = (1 - \mu q^{-1})^{n_a}$  the response to a load change will be smooth.

Another choice for the disturbance model is:

$$T = A \quad (9.13)$$

However this is not advised when the model has badly damped poles, as is the case for the model of the String. It has

## 9.7 Performance of the MPC controller

*In view of the poor agreement between tuning rules and the behaviour of the valve obtained in simulation the tuning of the MPC controller was not straightforward. A trial and error approach was employed using both the tuning rules and the experience from simulation as guidelines. The sampling time used in the controller was varied between 20 seconds and 2 minutes.*

*The results presented here are extracts from the tuning procedure. The first three figures show the response of the valve and the temperature following a 15 mK step up and down in the reference with a steady state between. This is compared to a similar step when the PID controls the system which is show in Figure 9.11. It should be noted that for the MPC implementation the temperature reference is a constant temperature, while for the PID implementation the reference is based on the saturation pressure in the overflowing pot, as described in section 5.1. The last two figures show the response of the system when 7 W heat load was applied and using 20 seconds and 2 minutes as sampling time. In the figures the temperature is shown in red, the valve response in blue and the reference black line.*

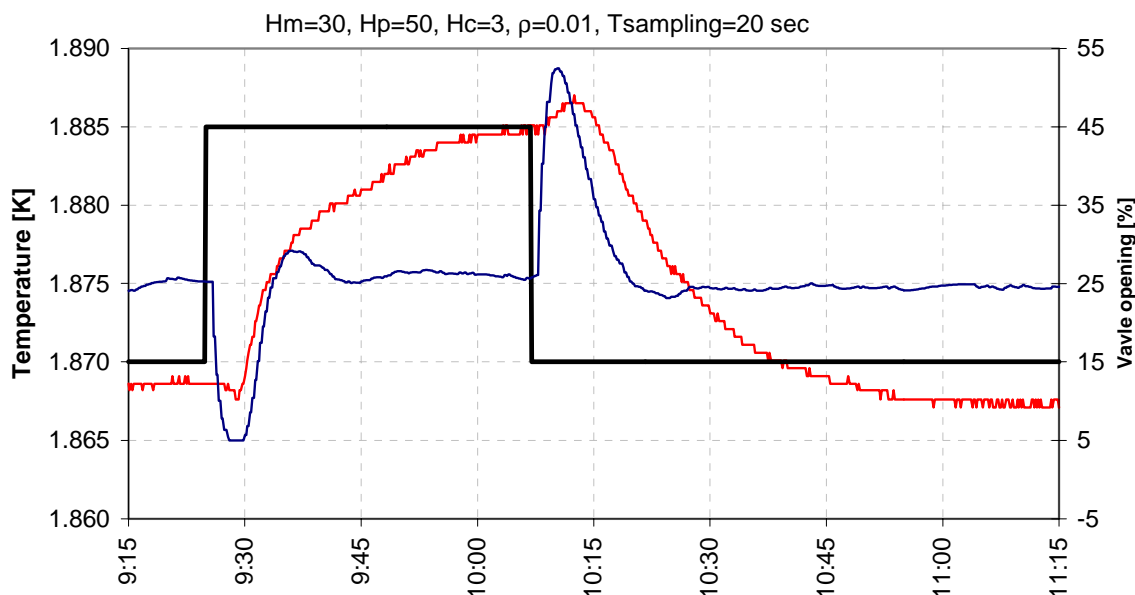


Figure 9.8 MPC performance following a 15 mK step up and down in the reference.

The controller output is quite active and reaches the hard constraint at 5 % valve opening after eight samples. The valve starts opening again even before the inverse response is over and the temperature starts increasing beyond the starting temperature. Such a behaviour cannot be obtained by a PID controller. The temperature is within 5 mK of the set point after 15 minutes, however the valve is opened too much and it takes 35 minutes to fully reach the set point. The step down induces an inverse response lasting for 10 minutes with a maximum temperature increase of 2 mK. The temperature reaches the set point after 32 minutes.

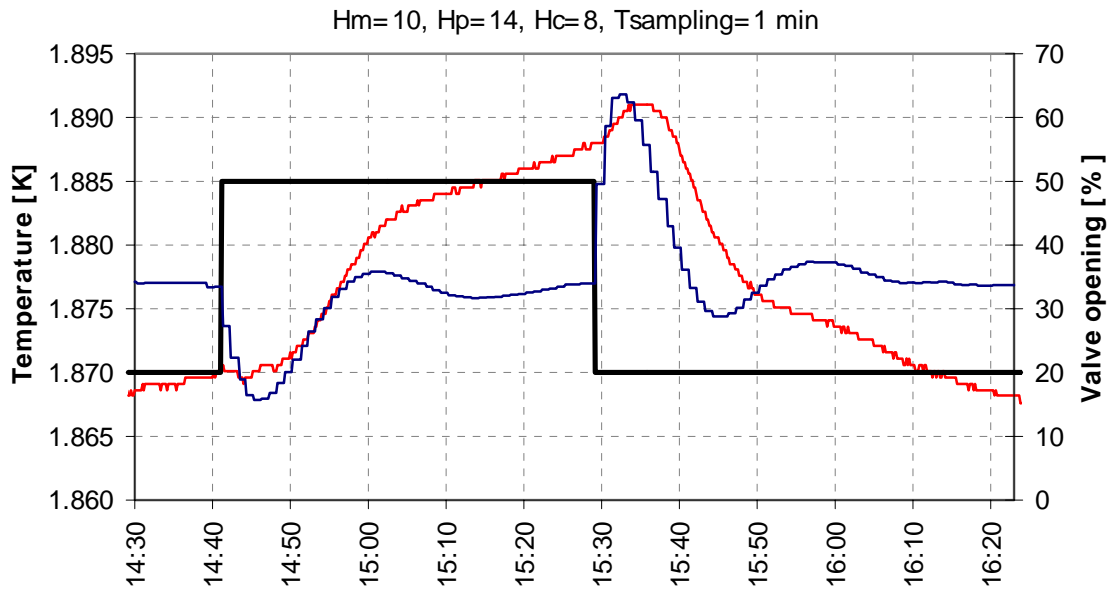


Figure 9.9 MPC performance following a 15 mK step up and down in the reference.

With this setting the valve output is less active and the adjusting movements of the valve last for a longer period than in the previous figure. The temperature is within 5 mK of the set point after 21 minutes and reaches the set point in 30 minutes. In the step down the valve is opened more than in the previous figure inducing an inverse response lasting for 11 minutes with a maximum temperature increase of 3 mK. It takes 40 minutes for the temperature to reach the set point since the final valve adjustment towards the set point are not well performed. In general the performance of the controller to a step down in temperature is poorer than for a step up.



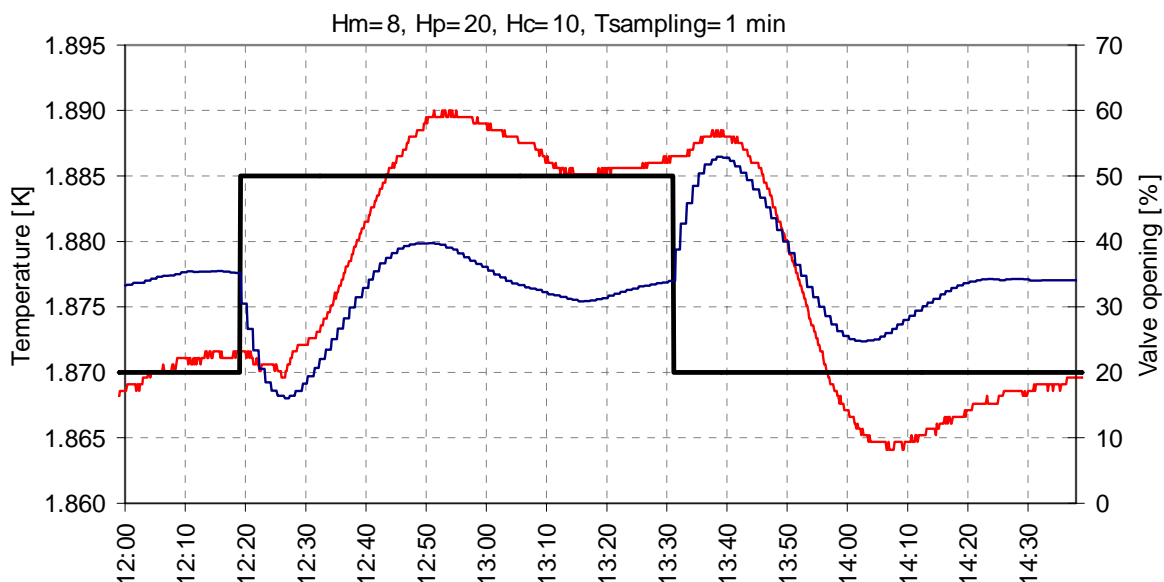


Figure 9.10 MPC performance following a 15 mK step up and down in the reference.

The temperature is within five mK of the set point after 20 minutes and reaches the set point in 25 minutes which is the fastest of the three performances. However the temperature overshoots with five mK and is not stable at the set point until 50 minutes. The step down induces an inverse response lasting for 13 minutes with a maximum temperature increase of 2 mK. This long inverse response is induced by the temperature being slowly increasing prior to the step. The maximum valve opening is 10 % smaller than in the previous figure. But again the final valve adjustment towards the set point are not well performed and the temperature passes the set point after 25 minutes and undershoots with 5 mK before being stable at the set point after one hour.

The performance observed by the MPC controller in the previous three figures can be compared with the performance of the PID controller to a similar step in the reference as shown in Figure 9.11.

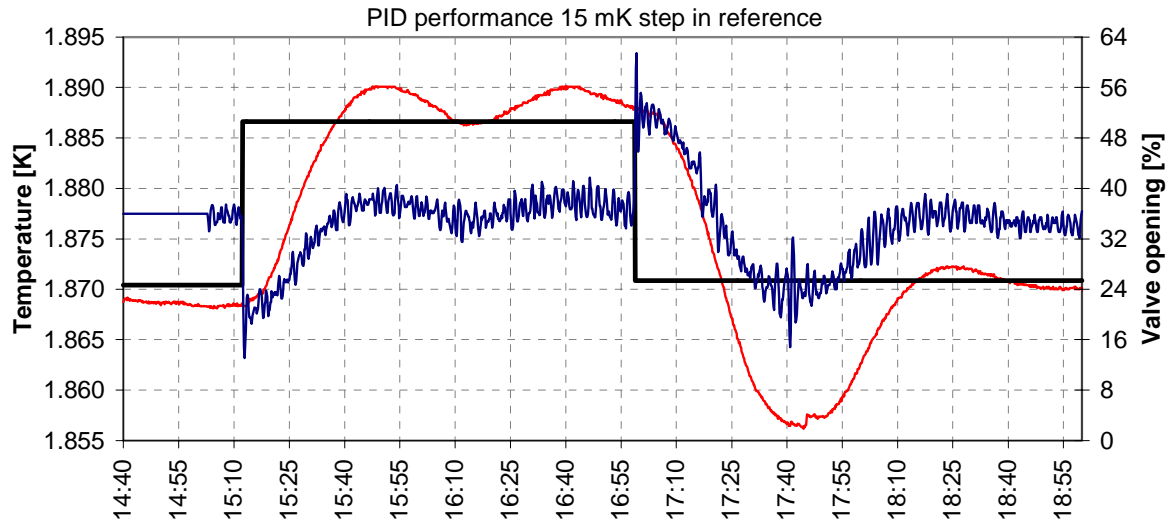


Figure 9.11 ID performance following a 15 mK step up and down in the reference.

The temperature is within 5 mK after 19 minutes and reaches the set point in 26 minutes which is the same as the fastest MPC response. However the temperature overshoots the set point with 4 mK and then shows an oscillatory behaviour. The step does not produce an inverse response and the temperature starts decreasing after 6 minutes. The absence of inverse response induced by the temperature being slowly decreasing prior to the step. The maximum valve opening is similar to the maximum valve opening of the MPC controller in the previous figure. The undershoot for the PID is significantly larger than what is observed with the MPC controller. The temperature is at the set point after 20 minutes but is followed by an undershoot of 14 mK. As is the case for the MPC controller also the performance of the PID controller to a step down in temperature is poorer than for a step up.

The next two figures show the MPC performance subject to an added heat load of 7 W which is equivalent to the heat load expected when ramping the magnet current. The sampling time is 20 seconds in Figure 9.12 and 2 minutes Figure 9.13.

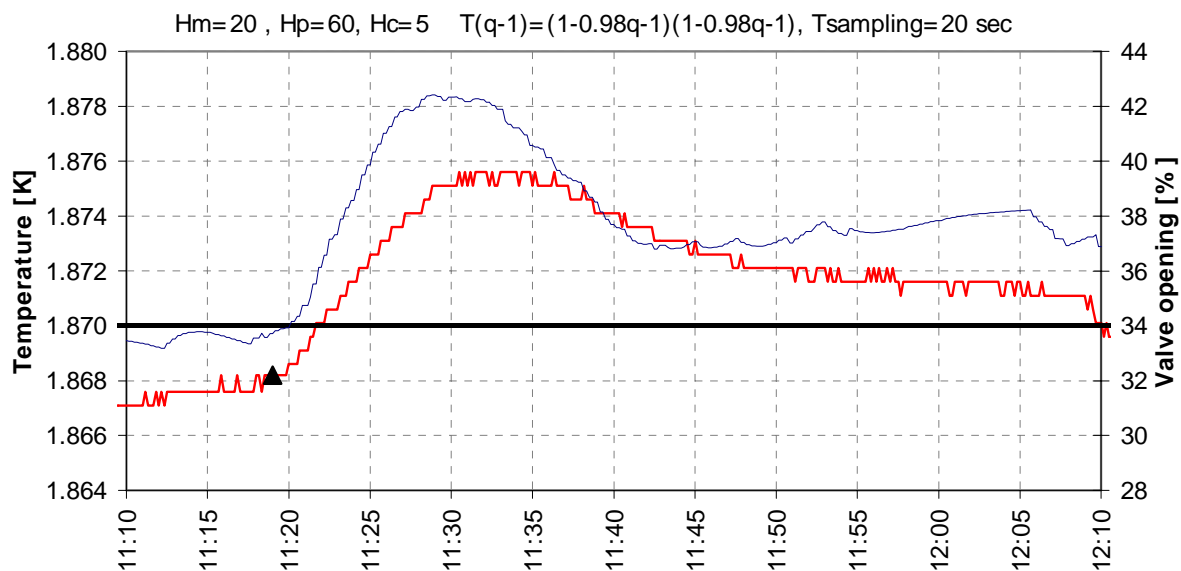


Figure 9.12 PC performance following a 7 W applied heat load.

Steady state valve opening is 33 % before and 38 % after the heat load is applied. The maximum temperature excursion is 6 mK after 12 minutes with a maximum valve opening of 42 %. The system is brought back to within 2 mK of the set point after half an hour.

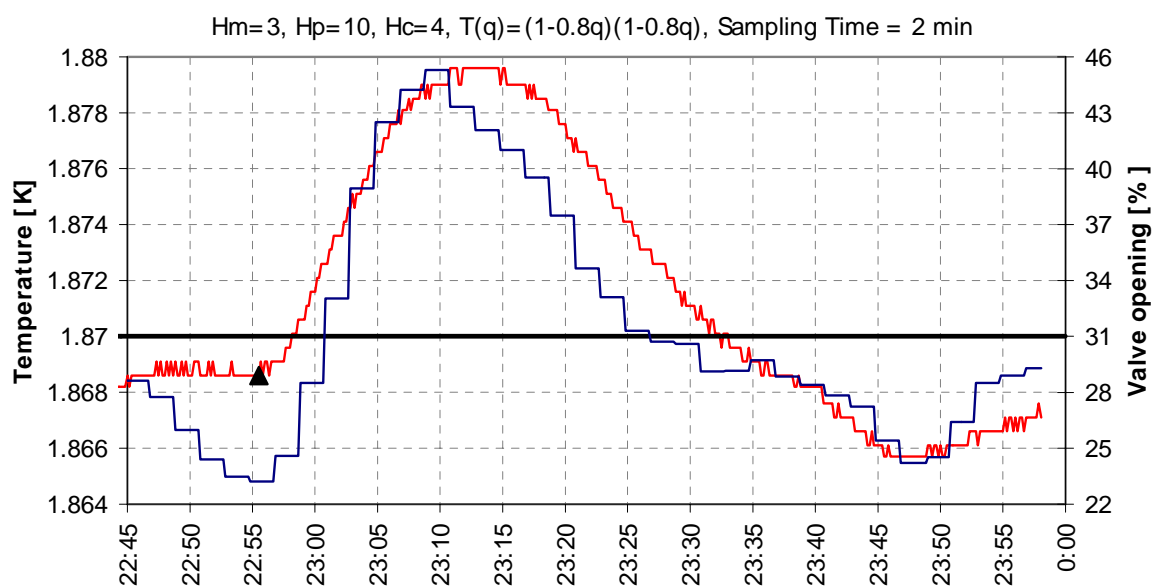


Figure 9.13 MPC performance following a 7 W applied heat load.

Steady state valve opening is 25 % before and 30 % after the heat load is applied. The maximum temperature excursion is 10 mK after 15 minutes. The temperature is back at the set point after 37 minutes and undershoots

## 10 Discussion and Conclusion

The Large Hadron Collider is the next generation particle accelerator presently under construction at CERN. It will make use of superconducting cryomagnets operating in pressurised He II at 1.9 K throughout its circumference of 27 kilometres. The scope of this work was to investigate the properties of the 1.9 K level of the 35-m full-scale model of the LHC, and initiate the process of designing a control scheme adapted to the challenges posed by the system.

On the basis of this investigation a first principle simulation program is constructed and validated. Black box models of the system are developed, and used as an integral part of a model predictive controller implemented at the magnet test string for controller the magnet temperature.

### 10.1 Investigation of the 1.9 K level

The 1.9 K level of the Magnet Test String has been subject to series of experiments determine the process characteristics. It is found to be an integrating (non self-regulating) process since a new steady state will not be reached following a change in either the manipulated variable (Joule-Thomson valve) or the disturbance (heat inleak). The process is strongly non-linear in particular governed by the change in specific heat of He II and density of helium gas with temperature. The process has a variable transport delay (dead time) in the flow of helium to reach the dry part of the heat exchanger. The process is non-minimum phase (inverse response) due to the competing dynamic effects of pressure drop and advance of liquid in the heat exchanger.

Classical control such as PID in the case of the String, are not optimal when one or more of the above mentioned characteristics are present in a process. A narrower control band can in principle be achieved when using an advanced, also denoted modern, control technique. The MPC methodology has been identified as the most promising for tackling the challenges present in the process of the 1.9 K level of the Magnet Test String. MPC is an open methodology in the class of predictive control algorithms. MPC can be used to control a variety of processes.

A series of experiment to gain knowledge about the properties and dynamic characteristics of the 1.9 K cooling loop of the magnet test string has been carried out. The velocity of the advancing liquid in the heat exchanger pipe is measured to be in the order of 10 cm/s. There is an increase in the velocity observed with increasing mass flow. The interaction between the liquid and gas phase is found to be weak, and the two phases are considered to flow independent of each other.

The mass of He II present in the cold mass is the determining factor of the thermal property of the system. Although the helium constitutes less than one percent of the total

weight at this temperature level it still dominates the heat capacity of the system owing to the extreme specific heat of He II. The amount of He II is measured to be 185 kg. The accordance of results in simulation with the observed behaviour supports this measured quantity.

Heat transfer at low temperature is governed by the Kapitza conductance between the He II and surrounding parts. The total thermal conductance of the 1.9 K heat exchanger tube has been measure in an experiment involving heat loads from 0 - 2 W/m. The conductance was measured to be 74 W/Km. The degree of wetting of the circumference of the tube was not taken into account in the calculation, and the heat transfer coefficient is assumed to be a function of length only. This assumption is justified by the corrugated geometry of the tube, which ensures good wetting at low mass flow. Separate work has found the Kapiza conductance of the tube to be 304 W/Km, indicating a wetted perimeter of 25 %. The numbers agree well with a geometrical consideration of the liquid in the tube, and indicate that liquid entrainment and creeping of liquid up the wall does not contribute significantly in improving heat transfer.

The vessels of the cold masses are connected by interconnection tubes with a length of 52 cm and having a cross section of 66 cm<sup>2</sup>. Due to instrumentation feed through the efficient cross section of helium for heat transfer is about 30 cm<sup>2</sup>. The heat transfer through them magnet interconnections has been measured to be very good. The measured temperature difference measure a cross section of the tube larger than the cross section of the unobstructed tube. This discrepancy is unaccounted for, but it is concluded that the heat transfer capability of the interconnections is not a limiting factor in the temperature control of the system.

An inverse response is observed during temperature transients. Opening the Joule-Thomson valve from steady state opening of about 30 % to 90 % will provoke an inverse response lasting for about eight minutes and the magnet temperature will increase about 5 mK before the system starts to cool down. This undesirable behaviour is inherent in the system and not a characteristic that can be eliminated by the control system. The inverse response is originating from the pressure drop characteristic of the heat exchanger tube. When the amount of flash gas increases following the opening of the valve, the pressure drop along the heat exchanger increases with a resulting lower temperature margin available for heat transfer. Consequently the cooling power of the heat exchanger decreases until a longer part of the tube is wetted.

## 10.2 First principle modelling

A first principle model of the 1.9 K level of the magnet test string has been constructed. The assumptions underlying the model are:

- friction factor of the heat exchanger tube is  $f = 0.077$
- thermal conductance of the heat exchanger is  $h_g = 74 \text{ W/m}$

- amount of He II in the cold mass is  $m = 180 \text{ kg}$
- the characteristic of the Joule-Thomson valve is assumed to be:

$$m(v_{\%}) = 0.00044 \cdot v_{\%}^2 + 0.04 \cdot v_{\%}$$

where  $m$  is the mass flow as a function of valve opening  $v_{\%}$

The simplifications are:

- the velocity of the advancing liquid in the heat exchanger tube is regarded as being constant 10 cm/s
- all magnets are assumed to be of equal temperature, thus neglecting the longitudinal heat transfer in the mode
- the corrugations of the tube are assumed to constitute a volume that has to be filled in order for the liquid to advance further. An amount of 10.55 g/m is assumed required to fill the corrugations
- pressure drop over a part of the tube is calculated on basis of the average of the gas flow in and out of that part of the tube
- the flash created during the expansion over the Joule-Thomson valve is assumed to be constant  $x = 0.12$
- the latent heat of vaporisation of He II is regarded as constant 23 J/g

The heat exchanger is divided into length increments in order to obtain a longitudinal profile of the liquid distribution along the tube, and to calculate the pressure drop resulting from the increase in gas flow as the liquid absorbs the heat load and vaporises.

The characteristic of the Joule-Thomson valve is a compromise between the specification from the supplier of the valve, results obtained in a calibration procedure on site and experience obtained through operation of the valve. Most emphasis is placed on experience gained through operation of the valve. For the most significant range of opening of the valve, 20 - 40 %, the characteristic agree well with results calculated from long duration observation of steady state liquid consumption compared with measured heat inleak. Operation of the valve in manual mode is based on this characteristic. The experience of using this fit function supports its validity.

The volume of one corrugation of the tube has through a geometrical consideration been calculated to be  $0.8842 \text{ cm}^3$ . This equals a stored mass in the corrugation of 10.55 g/m. The consideration is based on the assumption that the circumference of the tube is that of a circle, and the longitudinal pattern is that of a sine curve.

The pressure drop calculation is assuming the tube to be a pipe with a relative roughness of 0.08 and using the outer diameter of the corrugation in the calculations. The density of the helium gas is calculated using a fit function accurate to within 0.5 % of tabulated values in the 1.78 K – 1.96 K region.

Cooling provided by the heat exchanger is calculated for each length increment and summed up over the length. Assuming constant latent heat of vaporisation of He II represents an error of less than 0.5 % in the 1.74 K – 2.08 K region.

When all the magnets are assumed to be isotherm only one differential equation is needed for the overall energy balance. The specific heat of He II is implemented as a fit function with an error less than 1.25 % in the 1.7 K – 2.07 K region.

The model has been implemented using the mathematical program Matlab. The inputs required for running a simulation are:

- pumping pressure at the outlet of the heat exchanger
- heat load on the system during the simulation
- supply of helium through the JT valve during the simulation.

The program calculates:

- pressure profile in the HX
- saturated temperature profile
- liquid distribution in the HX
- cooling power provided by the HX
- temperature development for the He II of the cold mass hence the magnets
- liquid supply in the case of using a control structure for the valve
- liquid supply as a function of supplied valve-opening
- specific heat of the pressurised He II in the cold-mass
- density of the helium gas

The degree of discretisation of the heat exchanger was a trial and error procedure. It was sought to be sufficient to avoid unnecessary errors, but as coarse as possible to minimise the computation burden. Series of simulations were performed with increasingly fine discretisation. When no detectable improvements could be observed it was regarded as sufficient. It was found sufficient to divide the length into 24 parts of 1.46 meters, giving a resolution of about 4 % along the geometry.

A sensitivity study of the design parameters is performed. The parameters were varied according the uncertainties related to the respective parameter. The effect was evaluated by examining the response of the system following a step down and up in the valve producing a 15 mK step up and down in temperature. Three characteristics of the response were evaluated: the overall change in temperature, the time delays associated with the inverse response and the pressure drop during the steady states between the steps.

The temperature excursion following a pulse input in the manipulated variable is affected the most by the uncertainty related to the amount of He II in the cold mass. About 10 % uncertainty in the magnitude of the excursion is introduced by the 15 % uncertainty of this parameter. Also the threshold of mass in the corrugations has moderate effect on the temperature excursion. This is due to the amount of cooling power ‘stored’ in the liquid



in the heat exchanger. The other parameters only weakly affect the overall temperature excursion between steady states.

The time delay associated with changes in the manipulated variable is noticeably affected by several parameters. The threshold of mass in the corrugations has the most significant effect with up to 30 % increase in time delay observed after reducing the valve opening. The friction factor introduces 15 - 20 % uncertainty in the time delay, and an increase of the flash over the valve lead to 10 % increase in delay time.

The pressure drop in steady states is affected only by the friction factor, which causes a 10 % uncertainty. All the other parameters have a neglectable effect on the pressure drop.

Model validation:

The first principle model is validated against data recorded from dedicated experiments on the real system. For a situation with actively applied heat load on the system the performance of the model is in good agreement with recorded behaviour. The transient response shows no time delay to a change in the heat load, and the simulated temperature excursions are within 5 % of the real response. This supports the value used in the simulation program for the amount of He II in the cold mass, and is within the 10 % uncertainty found in the sensitivity analysis.

For simulations where the Joule-Thomson valve is the manipulated variable the results are more complex. Both time delay following changes in valve opening and temperature excursions in general agree well.

The pressure drop is identified as playing a vital part of transient behaviour of the system. A good agreement of the changes in pressure drop, both in transient and steady state conditions, is therefore of fundamental importance for the validation of the simulation program. The pressure measurement in the real system is plagued by noise arising from the active control of the pumping pressure in the overflow pot. In addition there is a cyclic disturbance occurring at 2 – 3 minutes interval and lasting for some tens of seconds, and whose origin has not been determined. These disturbances are not present in the simulated behaviour of the pressure. When neglecting the effect of these disturbances the simulated and measured temperature behaviours correspond well, and gives confidence in the implemented pressure drop model. Both overall changes in pressure drop between steady states and the transient behaviour between them shows a good correlation.

### **10.3 Black box modelling**

Linear time invariant (LTI) black box models of the system have been identified on the basis of data recorded on the real system through specially designed experiments. A pseudo random binary signal with signals ranging from 30 to 2 minutes in period of the valve opening around the steady state opening have been used. This includes all

foreseeable significant frequencies for the system. Models have been identified in several structures and compared. The ARMAX structure is found to be the structure best suited for describing the system. Judging from which model structure that best describes the behaviour of the system the disturbance affecting the system is variations of the heat inleak.

## 10.4 Model predictive control of the system

An model predictive control (MPC) has been implemented to control the temperature of the 1.9 K cooling loop of the Magnet Test String. Models obtained through the black box modelling have been used in the controller. The code of the controller is developed at the University of Valladolid in Spain and intended for use in the sugar industry. The code is used in agreement with the licence holder, and for proprietary reasons this code cannot be published. The controller allows specifying the reference trajectory as any mathematical expression and using the feedback of the output or the previous value of the reference trajectory. The criterion function can include controller output weighting and polynomial filtering of the output sequence. It allows implementation of polynomial models for the disturbance. The prediction horizon ( $H_p$ ), the minimum cost horizon ( $H_m$ ) and the control horizon ( $H_c$ ) are all allowed as tuning parameters. In addition controller output weighting and polynomial filtering of the output is allowed.

In the String implementation the following settings have been used. The reference trajectory is implemented as a first order filter from the feedback of the output and the set point temperature. The generation of the trajectory includes a tuning parameter to decide the slope of the curve. This parameter is in simulation chosen such that the shape of the trajectory corresponds as close as possible with the free response of the system. A more active controller can be achieved by choosing a steeper reference trajectory.

To avoid steady state errors the controller weights the increments rather than the controller output itself. A polynomial filter for the controller increments is used in addition to avoid low frequency oscillations through the system. The results of using this polynomial are inconclusive.

Rules of thumb how to choose the weighting factor of the controller output do not exist. Literature states that this must be done through trial and error or in simulation. A value of  $\rho = 0.02$  has in simulation been found to give reasonable restriction in the valve movement. This value is used in the controller and observed to give reasonable results. The weighting factor must be used with caution since it affects the robustness of the closed loop system, and a larger value is not advisable.

The choices of prediction horizon ( $H_p$ ), minimum cost horizon ( $H_m$ ) and control horizon ( $H_c$ ) are based on rules of thumb and adjusted in simulation and through experiments. Rules of thumbs are based on system that are open loop stable, have no dead time and are minimum phase or systems containing one of the negative of these three features. Rules that apply to open loop unstable, non-minimum phase are not specified. There is not a

good agreement between tuning rules and results obtained in simulation. Consequently a degree of adjustment and trial and error is involved in tuning the controller for the String. The result of choosing these parameters is not completely conclusive, but sets of parameters giving acceptable performance have been identified.

The use of the disturbance model for tuning the MPC controller has only been subject to preliminary investigation. The disturbance model is a powerful tool for tuning predictive controllers and should be studied more in detail. An improvement in regulator performance is expected using a properly tuned noise model

The introduction of a first principle model that takes into account the non-linearity of the system, and specially the behaviour of the two phase flow in the heat exchanger tube, should improve the performance of a MPC controller.

Sampling time of 2 minutes is too long and allows disturbances to have an unnecessarily large effect. Since heat load on the system has practically an immediate effect it will be advantageous to operate with a much shorter sampling time. The use of a sampling time of 20 seconds was well within the capability of the implemented hardware and software. A sampling interval shorter than 20 seconds will not be an improvement since none of the foreseeable heat load will have a detectable effect over such a short time span. A heat load of 30 W will need 24 seconds to produce a temperature increase of 1 mK at 1.9 K

The study of the implemented MPC controller performed during about one month is incomplete, and the results are partly inconclusive. Nevertheless the performance of the MPC controller is observed to be as good or better than the PID control structure presently implemented. This in spite of the PID having been in operation and subject to tuning for a period of three years. The MPC controller shows promising properties for tackling the dynamic challenges of the system. The response of the MPC to set point changes is observed to be good, and the controller possesses properties superior to that of the PID. The results regarding noise rejection are less well documented. The increased challenges imposed by increasing the length of the geometry from 35 meters to 100 meters will enhance the advantages of predictive control over classical control.

In view of the incomplete development and tuning of the controller that has been undertaken, it is the conviction that the performance of a predictive controller that has been dedicatedly developed for this process will offset the increased initial cost and add to a robust and fault tolerant operation of the LHC machine.

## 11 References

- [1] J P Gourber, *Status of the LHC*, LHC Project Report 167, Presented at the International Europhysics Conference on High-Energy Physics, Jerusalem, 19-26 August 1997
- [2] L Evans, Ph Lebrun, *Progress in Construction of the LHC*, LHC Project Report 239, 1998 , Presented at HEACC'98- XVII International Conference in High Energy Accelerators -7 - 12 September 98 Dubna
- [3] D R Tilley & J Tilley, *Superfluidity and Superconductivity*, Adam Hilger Ltd 1986
- [4] S W van Sciver, *Helium Cryogenics*, Plenum Press, New York, 1996
- [5] E Emren, *Feasibility Study of Designing Tuning Quadrupole using Double Pancake Winding*, LHC/ICP, 1997
- [6] S W van Sciver, *Helium Cryogenics*, Plenum Press, New York, 1996, 46
- [7] L Evans and Ph Lebrun, *Progress in Construction of the LHC*, LHC Project Report 239, 1998 , Presented at HEACC'98- XVII International Conference in High Energy Accelerators -7 - 12 September 98 Dubna
- [8] S W van Sciver, *Helium Cryogenics*, Plenum Press, New York, 1996
- [9] D R Tilley & J Tilley, *Superfluidity and Superconductivity*, Adam Hilger Ltd 1986
- [10] D R Tilley & J Tilley, *Superfluidity and Superconductivity*, Adam Hilger Ltd 1986, 2
- [11] Cryodata Inc., *Hepak*, P.O. Box 558, Niwot, Colorado 80544
- [12] D R Tilley & J Tilley, *Superfluidity and Superconductivity*, Adam Hilger Ltd 1986, 10
- [13] S W van Sciver, *Helium Cryogenics*, Plenum Press, New York, 1996,144
- [14] P L Kapitza, *The Study of Heat Transfer on Helium II*, J. Phys. (USSR) **4**, 181 (1941)
- [15] M Kado, *Thermal conductance measurements on the LHC helium II heat exchanger pipes*, LHC Note 349, CERN-AT-95-34 CR, 1995

- [16] The LHC Study Group, *The Large Hadron Collider Conceptual Design*, CERN/AC/95-05 (1995)
- [17] The LHC Study Group, *The Large Hadron Collider Conceptual Design*, CERN/AC/95-05 (1995), 6
- [18] F Bordry et al., *The LHC Prototype Full-Cell: Design Study*, LHC Project Report 170, 1998, 6
- [19] The LHC Study Group, *The Large Hadron Collider Conceptual Design*, CERN/AC/95-05 (1995), 95
- [20] The LHC Study Group, *The Large Hadron Collider Conceptual Design*, CERN/AC/95-05 (1995), 83
- [21] J P Gourber, *Status of the LHC*, LHC Project Report 167, Presented at the International Europhysics Conference on High-Energy Physics, Jerusalem, 19-26 August 1997
- [22] A Bézaguët et al. *The Superfluid Helium Cryogenic System for the LHC Test String: Design, Construction and First Operation*, LHC Note 357 CERN AT/95-40, 1995
- [23] Official web site of the LHC Project, <http://www.lhc.cern.ch/ACR/Synop.html>
- [24] Ph Lebrun et al., *Cooling strings of superconducting devices below 2 K: the helium II bayonet heat exchanger*, Cryogenic Engineering Conference – International Conference on Cryogenic Materials – Portland OR, 27 July – 1 Aug 1997
- [25] C Balle, Instrumentation and Process Control Section in LHC/ACR, Personal communication, November 1999
- [26] C de Prada, *Introduction to Modelling and Identification*, paper within J Richalet et al., *Model Based Predictive Control*, Compendium from two day training course 10-11/3 1997, Initiative of the working group CIDIC, Dresden 10 – 11 March 1997
- [27] Aris, R., *Mathematical Modelling Techniques*, Pitman Publishing Limited 1978
- [28] J J van den Boom, *Comparison of MBPC with other Techniques*, paper within J Richalet et al., *Model Based Predictive Control*, Compendium from two day training course 10-11/3 1997, Initiative of the working group CIDIC, Dresden 10 – 11 March 1997
- [29] D E Seborg et al., *Process Dynamics and Control*, John Wiley Son Inc. 1989

- [30] R Soeterboek, *Predictive Control A Unified Approach*, Prentice Hall International (UK) Limited, 1992
- [31] D E Seborg et al., *Process Dynamics and Control*, John Wiley Son Inc. 1989, 191
- [32] R Soeterboek, *Predictive Control a Unified Approach*, Prentice Hall International (UK) Limited, 1992, 5
- [33] F P Incropera et. al, *Fundamentals of Heat and Mass Transfer*, P. DeWitt. .3<sup>rd</sup> ed., 469
- [34] R L Webb, *Principles of Enhanced Heat Transfer*, John Wiley & Son Inc., 1994, 232 and 281
- [35] L Ljung, *System Identification, Theory for the User*, Prentice Hall PTR Prentice-Hall Inc., 1999
- [36] A V Oppenheim et al., *Signals and Systems*, Prentice Hall Inc., 1983
- [37] R Henriksen, *Stokastiske Systemer, Analyse, Estimering og Regulering*, Institutt for Teknisk Kybernetikk The Norwegian University of Science and Technology, 98-12-X, 1998
- [38] L Ljung, *System Identification, Theory for the User*, Prentice Hall PTR Prentice-Hall Inc., 1999, 520
- [39] R Soeterboek, *Predictive Control A Unified Approach*, Prentice Hall International (UK) Limited, 1992
- [40] D W Clarke et al., *Generalized Predictive Control – Part I. The Basic Algorithm*, Automatica, vol. 23, No. 2, 1987, 137-148
- [41] D W Clarke et al., *Generalized Predictive Control – Part II. Extensions and Interpretations*, Automatica, vol. 23, No. 2, 1987, 149-160
- [42] R Soeterboek, *Predictive Control A Unified Approach*, Prentice Hall International (UK) Limited, 1992, 97
- [43] R Soeterboek, *Predictive Control A Unified Approach*, Prentice Hall International (UK) Limited, 1992, 95
- [44] T A Badgwell S J Qin, *An Overview of Industrail Model Predictive Control Technology*, Chemical Process Control - V, Jan. 7-12, 1996, Tahoe, California

## 12 A-1 Data and measurement for calculating liquid velocity

The measurement used to calculate the velocity of the advancing liquid in the heat exchanger tube was performed when the String consisted of two dipoles and one quadrupole. The flash is calculated on the basis of conservation of enthalpy over the expansion. The liquid flow is calculated on the basis of the fit for the characteristic of the Joule-Thomson valve:

$$m(v_{\%}) = 0.00044 \cdot v_{\%}^2 + 0.04 \cdot v_{\%} \quad [g/s]$$

Length of heat exchanger tube: 27.5 m

Steady state valve opening: 25%

State of the liquid before expansion: 2.2 K at 1.2 bar

Amount of flash over the valve:  $x = 0.1182$  at 21 mbar,  $x = 0.1441$  at 10 mbar

Table A- 2      *Measurements of time for the liquid to flow through the heat exchanger at different valve opening and saturation pressure.*

	Opening of JT valve [ % ]	Saturation pressure [mbar]	Saturation temperature [K]	Delay for wave to arrive [s]	Velocity of liquid [cm/s]	Liquid flow [g/s]
21 mbar	40	21	1.873	457	6.02	2.08
	50	21	1.873	287	9.58	2.75
	60	21	1.873	284	9.68	3.48
	70	21	1.873	257	10.70	4.27
10 mbar	50	10	1.670	274	10.04	2.73
	80	10	1.670	224	12.28	5.06

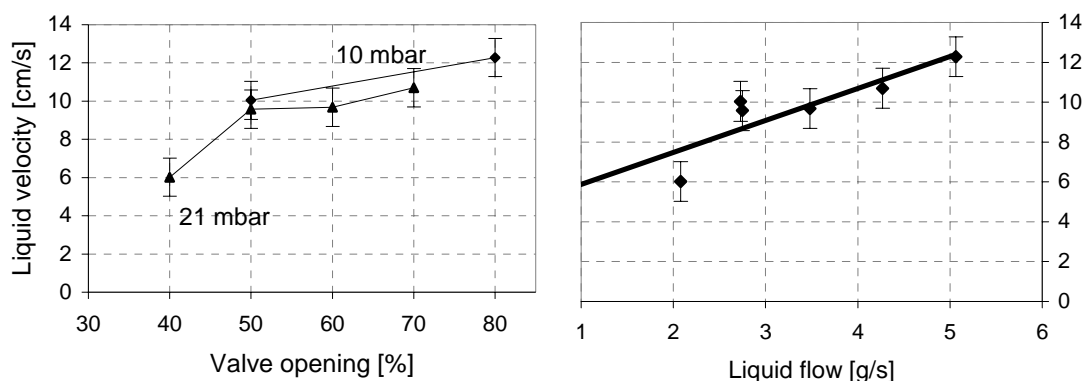


Figure A-1      *Measurement in Table A-1 represented graphically.*

### 13 A-2 Amount of helium in the cold mass

*Table A-3*

*Temperature measurements and the average  $c_p$  for temperature intervals used to calculate the amount of helium in the cold mass.*

Time	Temperature [K]	Time	Temperature [K]
17:15	1.8867	17:46	1.9258
17:16	1.8860	17:47	1.9288
17:17	1.8856	17:48	1.9315
17:18	1.8849	17:49	1.9346
17:19	1.8844	17:50	1.9373
17:20	1.8842	17:51	1.9399
17:21	1.8841	17:52	1.9431
17:22	1.8844	17:53	1.9478
17:23	1.8847	17:54	1.9535
17:24	1.8850	17:55	1.9589
17:25	1.8852	17:56	1.9639
17:26	1.8855	17:57	1.9692
17:27	1.8850	17:58	1.9742
17:28	1.8843	17:59	1.9794
17:29	1.8838	18:00	1.9843
17:30	1.8837	18:01	1.9887
17:31	1.8839	18:02	1.9933
17:32	1.8852	18:03	1.9983
17:33	1.8875	18:04	2.0025
17:34	1.8905	18:05	2.0064
17:35	1.8929	18:06	2.0053
17:36	1.8956	18:07	2.0033
17:37	1.8977	18:08	2.0047
17:38	1.9000	18:09	2.0060
17:39	1.9029	18:10	2.0064
17:40	1.9063	18:11	2.0065
17:41	1.9095	18:12	2.0059
17:42	1.9129	18:13	2.0060
17:43	1.9161	18:14	2.0056
17:44	1.9191	18:15	2.0052

Temperature range [K]	Average $c_p$ at 1.2 bar [J/kgK]
1.888-1.940	4.0986
1.906-1.940	4.2024
1.948-2.005	4.9127
1.953-2.003	4.9256



## 14 A-3 Data for the thermal conductivity of the heat exchanger

Table A-4 Temperature measurements as a function of heat load for calculating the thermal conductivity of the heat exchanger.

Applied heat load [W/m]	Measured temperature for the six sensors					
	TTCM01	TTCM02	TTCM11	TTCM12	TTCM12	TTCM22
	[K]	[K]	[K]	[K]	[K]	[K]
0	1.862	1.862	1.861	1.859	1.861	1.862
0.2	1.863	1.863	1.863	1.861	1.862	1.864
0.4	1.865	1.864	1.864	1.863	1.863	1.866
0.5	1.867	1.867	1.866	1.865	1.866	1.867
0.6	1.867	1.867	1.866	1.865	1.866	1.867
0.8	1.869	1.869	1.868	1.866	1.867	1.869
0.9	1.872	1.871	1.871	1.869	1.870	1.872
1	1.874	1.873	1.873	1.871	1.872	1.874
1.2	1.877	1.876	1.875	1.873	1.875	1.876
1.3	1.878	1.877	1.876	1.874	1.876	1.878
1.4	1.879	1.878	1.878	1.876	1.877	1.879
1.6	1.881	1.881	1.880	1.878	1.880	1.882
1.8	1.885	1.884	1.884	1.881	1.883	1.885
2	1.889	1.889	1.888	1.886	1.888	1.890

Table 5 Temperature deviations in mK from a chosen temperature  $T_{base}=1.861$  K. The average temperature deviation for the six sensors is shown in the last column.

Applied heat load [W/m]	Temperature deviation from 1.861 K						
	TTCM01	TTCM02	TTCM11	TTCM12	TTCM12	TTCM22	Average
	[mK]	[mK]	[mK]	[mK]	[mK]	[mK]	[mK]
0	1	1	0	-2	0	1	0.17
0.2	2	2	2	0	1	3	1.67
0.4	4	3	3	2	2	5	3.17
0.5	6	6	5	4	5	6	5.33
0.6	6	6	5	4	5	6	5.33
0.8	8	8	7	5	6	8	7.00
0.9	11	10	10	8	9	11	9.83
1	13	12	12	10	11	13	11.83
1.2	16	15	14	12	14	15	14.33
1.3	17	16	15	13	15	17	15.50
1.4	18	17	17	15	16	18	16.83
1.6	20	20	19	17	19	21	19.33
1.8	24	23	23	20	22	24	22.67
2	28	28	27	25	27	29	27.33

## 15 A-4 Heat transfer in the interconnections

The figure and table show the recorded temperature splits between the two temperature sensors mounted on either side of the interconnection.

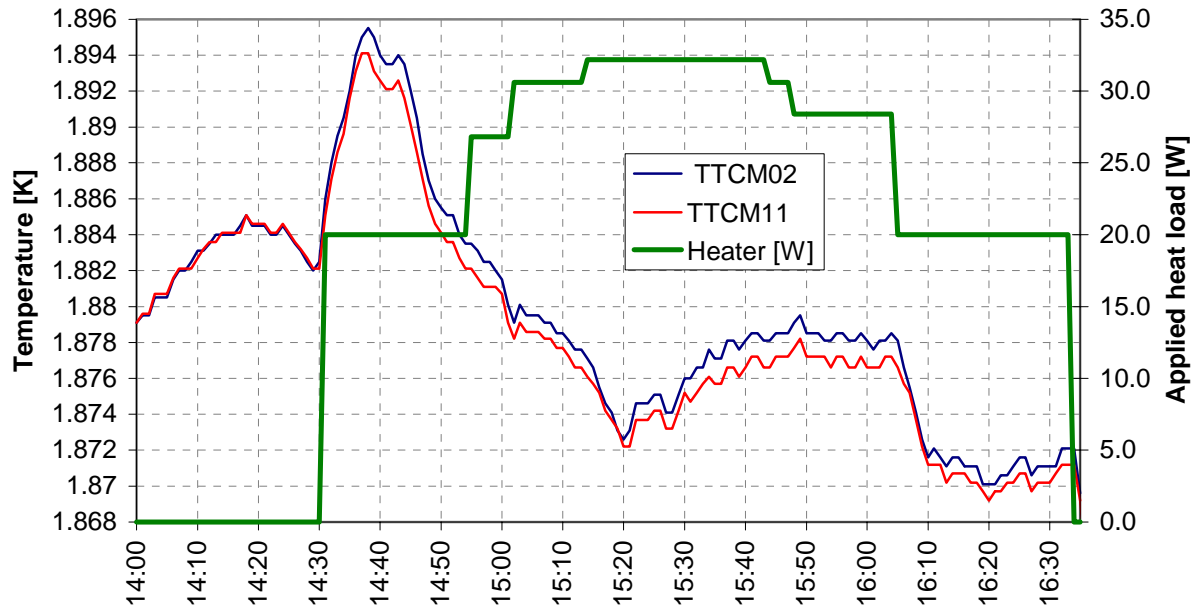


Figure A-2 Recorded temperature splits between the two temperature sensors

Table A-6 Recorded temperature splits between the two temperature sensors

Time	TT02-TT11	Time	TT02- TT11		
15:50	1.330	16:10	0.430	16:22	0.930
15:51	1.330	16:11	0.930	16:23	0.430
15:52	1.330	16:12	0.430	16:24	0.930
15:53	0.930	16:13	0.930	16:25	0.930
15:54	1.530	16:14	0.930	16:26	0.930
15:55	1.330	16:15	0.930	16:27	0.930
15:56	1.330	16:16	0.430	16:28	0.930
15:57	1.530	16:17	0.930	16:29	0.930
15:58	1.530	16:18	0.930	16:30	0.930
15:59	1.330	16:19	0.430	16:31	0.430
16:00	1.530	16:20	0.930	16:32	0.930
16:01	1.030	16:21	0.430	16:33	0.930
16:02	1.530				
16:03	0.930				
16:04	1.330				

## 16 B-1 Fit function for density of helium gas

The below figure shows the value of the density such that it is given by Hepak. This data is compared with data generated by the fit function:

$$\rho(T) = 2.321 \cdot 10^{-5} T + 7.53 \cdot 10^{-5}$$

The error between the fit function and the data from Hepak is also shown.

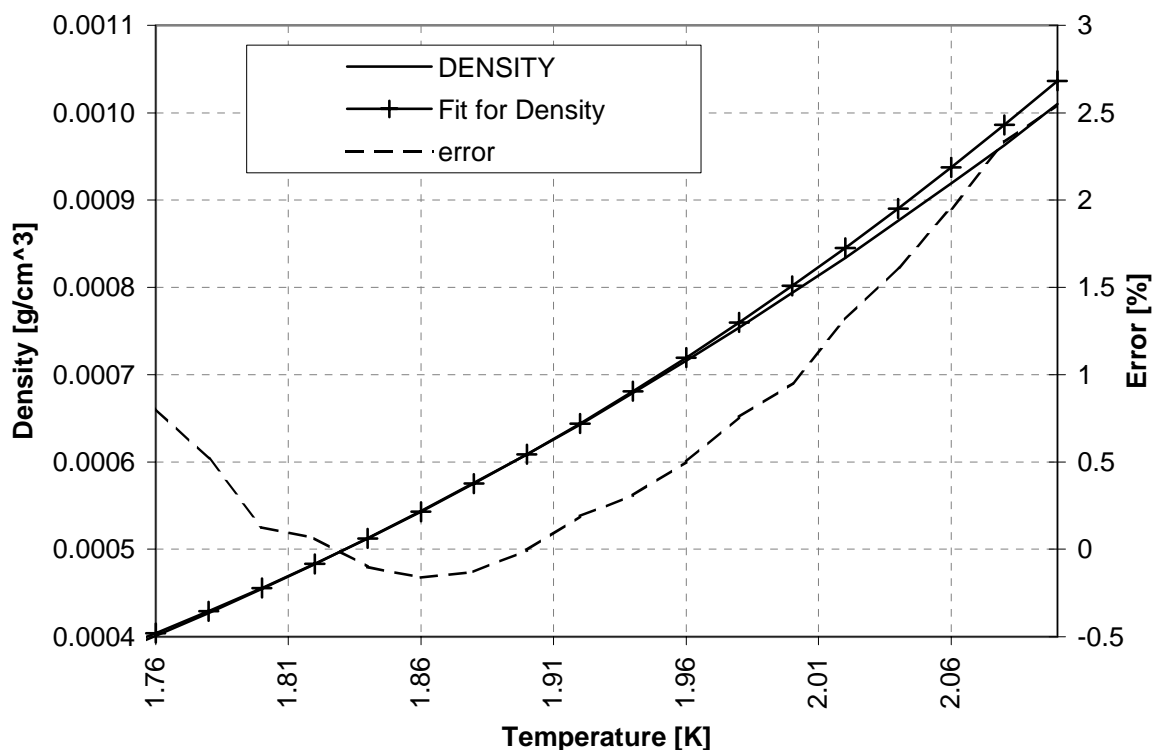


Figure B-1 The density of the saturated helium gas and error between data from Hepak and values by the fit function

## 17 B-2 Fit function for specific heat of He II

The below figure shows the value of the specific heat of pressurized He II at 1.2 bar such as it is given by Hepak. This data is compared with data generated by the fit function:

$$cp(T) = 14.777e^{2.9431T}$$

The error between the fit function and the data from Hepak is also shown.

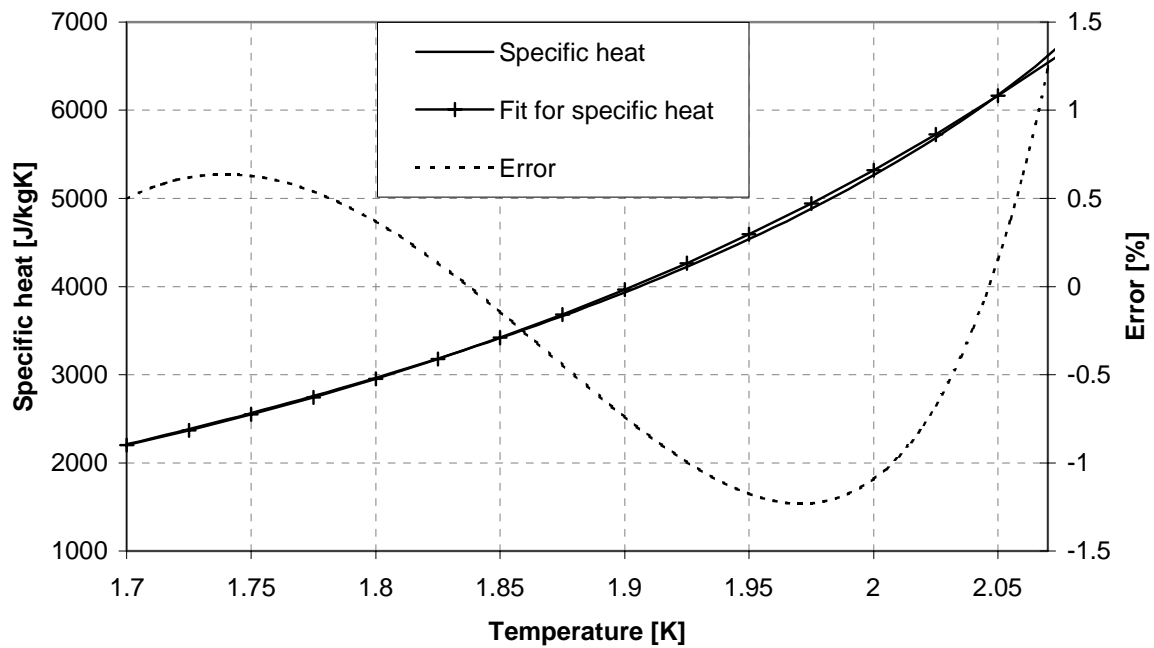


Figure B-2 The specific heat of pressurised He II at 1.2 bar and error between data from Hepak and values by the fit function

## 18 C-1      **Manual for Simulation Program**

This is a manual described how to open, edit, run and present results from The 1.8 K Cooling Loop Simulation Program.

The program is written using the Matlab Simulink Toolbox. This is a graphical interface to the functionality of the Matlab programming language. Editing and running the program is done through the Simulink interface. Presenting results is done through the Matlab Command Line.

To be able to use the program the user need to have Matlab and the Simulink Toolbox installed. Running the program requires only a basic knowledge of Matlab. Editing the program requires some knowledge and experience using Simulink.

### 18.1 C-1.1    **Opening and Understanding the Program**

Start Matlab, and go to the right directory where the program files are stored. Type 'start' at the command line and press <enter>. This command calls an .m file called 'initialconditions' which sets the constants used by the simulation program. It then starts the main program.

#### 18.1.1 The Main Window

The main window of the program is constructed to mimic the design of the LHC Magnet Test String. It has three main components, which can be seen in Figure C.1.

JT-valve  
Magnets (pressure vessel)  
Heat exchanger

In addition it contains four more block:

Pumping pressure  
Heat inleak  
Output file (with a multiplexer to gather the data into one matrix)  
Clock



This block represents the Joule Thomson valve supplying liquid and flash gas to the heat exchanger. The input can be any of the blocks in ‘sources’ library. The outputs from this block must have dimension [g/s]. This block has three outputs: ‘*gas from JT*’ and ‘*liquid from JT*’ that goes to the ‘*Heat exchanger*’ block. The ‘*mass from JT*’ that goes to the ‘*Dataoutput*’ block.

The input is split into two parts simulating the formation of saturated liquid and gas over the JT-valve. This is done by the two gain-blocks ‘*flash*’ and ‘*1-flash*’. Flash is by default set to 0.12 corresponding the nominal operation conditions (2.3 K @ 1.15 bar before and 19 mbar @ 1.85 K after the valve).

In Figure C.2 the input is a block that reads data in the workspace of Matlab. [T,U] can be a matrix of logged data from a String experiment. *U* is a vector of recorded values of JT valve opening in %. *T* is the corresponding time vector where time is given in seconds. Since the output must be in g/s the value of the valve opening must be converted to mass flow. This is done by the function block ‘*valve characteristic*’ which contains the function  $[0.00044*u^2 + 0.04*u]$  corresponding to the valve characteristic  $m(\%) = 0.00044\% ^2 + 0.04\%$ .

The block is also equipped with a ‘*Manual Switch*’, which when double-clicked on switches to a step input (this is only done to enable the user to easily change the mode of input).

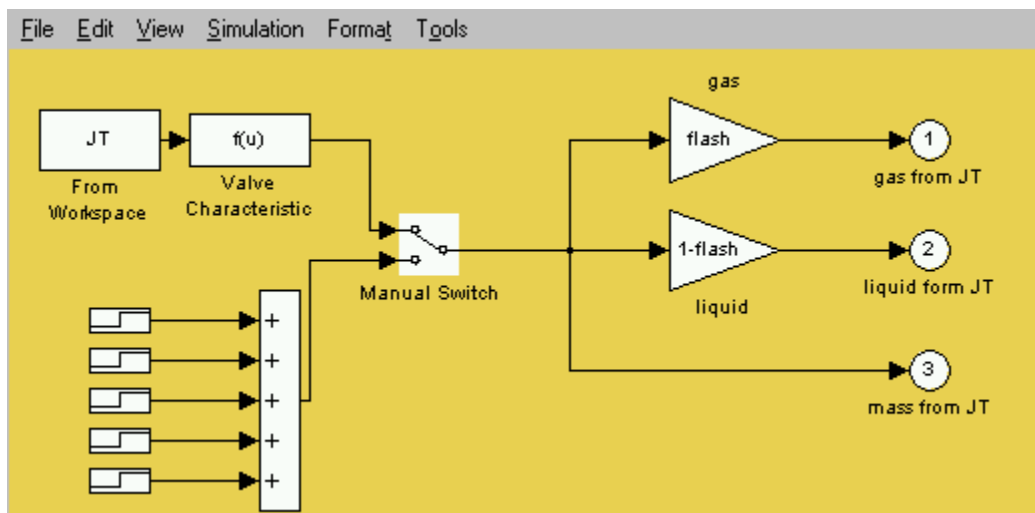


Figure C.2 The JT valve-block

### 18.1.5

#### 18.1.6 Magnet (Pressure Vessel)

This block represents the magnets and the cold mass at 1.8 K. The whole cold mass is considered to be isotherm.

The block does not have any input controlled by the user. It has the two inputs ‘*Cooling from HX*’ coming from the ‘*Heat exchanger*’ block, and ‘*Heat inleak*’ coming from the block with the same name. Both have dimensions [W]. The string of commands corresponds to the differential equation describing the magnet temperatures:

$$\frac{dT}{dt} = \frac{(q_{in} - q_{cooling})}{m_{HeII} cp(T)}$$

The ‘*Magnet Temperature*’ is fed back to the multiplexer (Mux) and used to calculate  $cp(T)$ .

The output is the temperature of the cold mass and has dimension [K]. It goes to the ‘*Magnet (pressure vessel)*’ block and to the ‘*Dataoutput*’ block.

*Figure C.3 The block representing the magnet temperature.*

#### 18.1.7 Heat Exchanger

This block represents the inside of the heat exchanger.



The block does not have any input controlled by the user. It has four inputs and four outputs.

**Inputs:**

'*Pumping pressure*' coming from the block with the same name. Dimension [*mbar*]

'*gas in*' coming from the '*JT valve*' block. Dimension [*g/s*]

'*liquid in*' coming from the '*JT valve*' block. Dimension [*g/s*]

'*Tmag*' coming from the '*Magnet (pressure vessel)*' block. Dimension [*K*]

**Outputs:**

'*Pressure in return box*' going to the '*Dataoutput*' block. This is the calculated pressure in the return box of the system. Dimension [*mbar*]

'*gas out*' going to the '*Dataoutput*' block. This is the amount of gas that is being pumped out of the system. Dimension [*g/s*]

'*liquid out*' going to the '*Dataoutput*' block. This is the amount of liquid flowing through the system without evaporating. Dimension [*g/s*]

'*cooling*' goes to the '*Dataoutput*' block and the '*Magnet (pressure vessel)*' block. This is the cooling power provided by the heat exchanger. Dimension [*W*]

### *Figure C.4 The Heat exchanger*

The heat exchanger is discretized into a number of cells (of which only the first three and the last two are shown in Figure C.4). The last cell represents the part of the heat exchanger closest to the end where the vapor is pumped out. The first cell represents the first part of the heat exchanger where liquid and gas is fed in from the JT valve.

Each cell has four inputs and four outputs with dimensions as described above. All the cells are identical.

The '*Pumping pressure*' input goes into the last cell. At each time step this pressure plus the calculated pressure drop over this cell is the input pressure to the previous cell. This procedure is repeated backwards through all the cells resulting in the '*Pressure in return box*' in the start of the heat exchanger, thus the total pressure drop over the length of the heat exchanger.

The '*gas in*' and '*liquid in*' from the JT-valve goes into the first cell. If an amount of liquid is calculated to evaporate from this cell, the '*gas out*' and '*liquid out*' from this cell are incremented and decremented by that amount respectively. They then form the '*gas in*' and '*liquid in*' to the next cell, and this procedure is calculated forward through all the cells. '*gas out*' and '*liquid out*' from the last cell forms the corresponding outputs from the '*Heat exchanger*' block and goes to the '*Dataoutput*' block as described.

The amount vaporized from all the cells is summed up and multiplied by the latent heat of vaporization,  $h_{fg}$ , to give the cooling provided by the heat exchanger.

The magnet temperature is an input to all of the cells in order to calculate the local saturation pressure and density of the gas.

#### 18.1.7.1 Inside a Cell

Each cell might be regarded as divided in two parts: one dealing with the liquid phase and one with the gas phase.

The gas part has as input the pressure in the downstream (next) cell [*mbar*] and the gas coming from the upstream (previous) cell [*g/s*]. Pressure drop is calculated by the '*dp*'-function according to:

$$dp = C \frac{\dot{m}^2}{\rho(T)} L_{cell}$$

where  $C$  and  $L_{cell}$  [*m*] are constants. The mass flow used in the pressure drop calculation is the mass flow from the previous cell plus half of the vaporized amount in this cell. There is an algebraic loop in the equation as the pressure drop depends on the density of the gas and vice versa. To break this algebraic loop the density,  $\rho(p)$ , is calculated using the pressure from the previous time step.

Instabilities in the pressure drop calculations necessitated averaging the present value with the previous value. This can be seen following the '*gas from previous cell*' input. Conservation of mass is preserved during simulation.

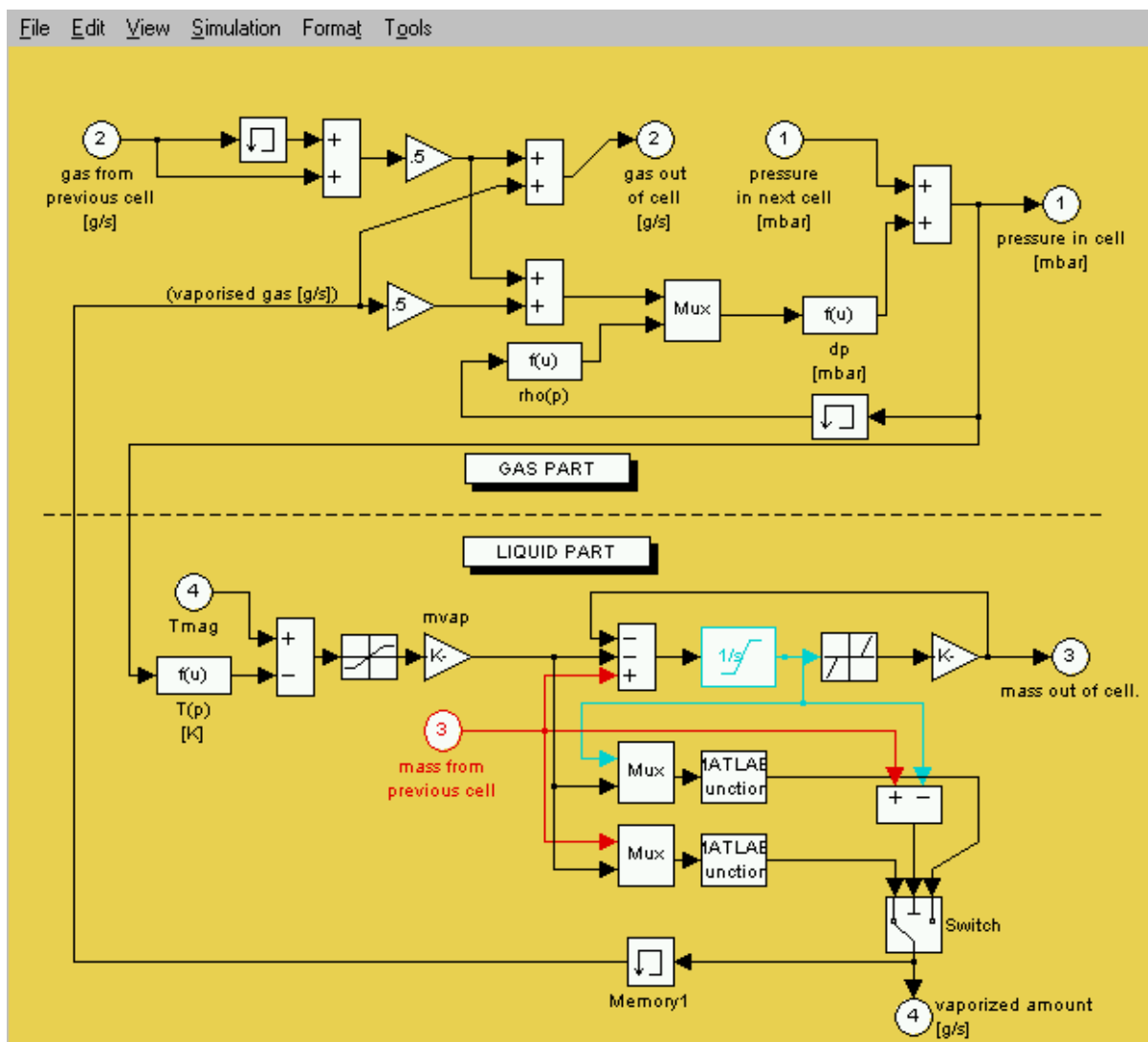


Figure C.5 A cell of the heat exchanger

The part dealing with the liquid phase has two inputs: the magnet temperature, ' $T_{mag}$ ', and the liquid flowing from the previous cell, '*mass from previous cell*'. It contains an integrator, which calculates the amount of liquid present in the cell. The amount of liquid that is being vaporized is calculated according to:

$$m_{vap} = (T_{mag} - T_{sat}) \cdot h_g \cdot L_{cell} / h_{fg}$$

A saturation block is needed to avoid a negative vaporized amount in the case that the saturation temperature exceeds the magnet temperature. Conservation of mass is preserved by the limited integrator:

$$\frac{dm}{dt} = m_{in} - m_{out} - m_{vap}$$

The integrator has a lower bound equal to zero since there cannot be negative mass in the cell. The dead zone block accounts for the amount of liquid needed to fill the corrugations before any liquid can flow out of the cell.

The lower part of the cell involving the '*Switch*' block is needed in the case when the cell is about to dry out or is just starting to fill. In these cases the calculation of the amount that should vaporize might yield a larger value than what is actually present in the cell. The switch-routine ensure that this value is not applied by only allowing what is in the cell and flowing into it to vaporize.

### 18.1.8 Output File and Clock

This block stores the result of the simulation. It produces a 7x'length of simulation' matrix by the name of '*Dataoutput*' in the Matlab workspace. Its consists of seven columns vectors containing:

Time: the time in seconds when the row was created

Temperature: the magnet temperature

Pressure in return box: Saturation pressure at the start of the HX

Gas out: the gas flow out of the system

Liquid out: the liquid flow out of the system

Cooling power: the total cooling power provided by the heat exchanger [W]

Mass from JT valve: the mass that was supplied by the JT valve.

One row is added to the matrix at every time step during the simulation. How many rows that are created depend on the simulated time and the method of integration that is chosen.

## 18.2 C-1.2 Editing the Program

There are three inputs that the user would want manipulate in order to use the program under different conditions:

The input to the JT-valve

The heat inleak to the system

The pumping pressure

All of these three can get their values from either of the blocks in the '*Sources*' library of *Simulink*.

The *Simulink* is started by entering the command <simulink> on the command line in Matlab. This opens the simulink libraries, of which one is the '*Sources*' library. This is opened by double-clicking its icon. The desired block can be transferred either by copy-paste or drag-and-drop to the desired page in the program. The block is attached by dragging the mouse from the output port of the block to the desired input port of another block.

### 18.3 C-1.3 Running the Program

Selecting the <Start> option in the <Simulation> pull-down menu in Simulink starts the program. By selecting the <Parameters> option of the same menu some choices might be made:

**Simulation Time:** a start time and a stop time can be specified. The unit is seconds. Normally a period of ~2000 seconds is required to obtain steady state conditions in the heat exchanger tube. This is needed for the profile of liquid and pressure drop to develop.

**Solver options:** this concerns the way the differential equations are solved. Either a fixed step length or a variable step length can be selected and several options for solvers exits for both choices. It is advised to choose the 'Fixed-step' option with a step length of 10 seconds. This has proven sufficiently short, and no improvement is obtained by choosing it shorter. Longer step length (~30 seconds) can be used for initial investigations. No significant difference is observed using the different option for solver and the fastest (and simplest) is the Euler.

When choosing the 'Variable-step' option, the program is in danger of running very slowly due to the solver requiring very short time increments.

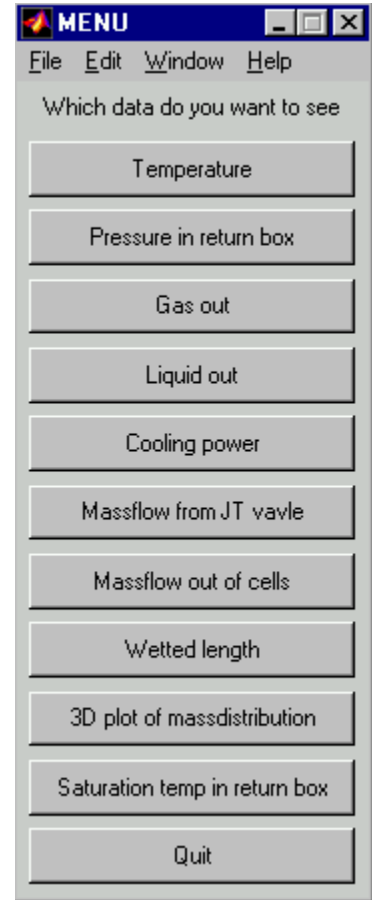
## 18.4 C-1.4 Viewing the simulation result

The result from a simulation is stored as a matrix in the Matlab workspace. The name of the matrix is specified in the <To workspace> block of the main window (called 'Dataoutput' in Figure C.1).

By typing 'show' on the Matlab command line and pressing <Enter> the menu shown to the right is opened. Selecting a button in the menu a figure with the desired data is created. The data-matrix must have the name 'aa' for this script to recognize it. (to create a matrix called 'aa' simply type `aa=dataoutput;` on the command line).

The data that can be shown in a figure as a function of time is:

1. temperature of the system
2. saturation pressure in the return box (corresponding to the pressure drop through the heat exchanger)
3. flow of helium gas out of the system
4. flow of helium liquid out of the system (overflow)
5. cooling power provided by the heat exchanger
6. mass flow from the Joule Thomson valve
7. mass flow out of each individual cell
8. the wetted length of the heat exchanger (as an integer number of cells)
9. a 3-D plot of distribution of liquid in the heat exchanger over length and time
10. saturation temperature in the return box (corresponding to the saturation pressure).



### **18.5 D-1 Paper submitted to ICEC 17**

The following paper was submitted to and presented at the *Seventeenth International Cryogenic Engineering Conference and Exhibition* held 14 – 17 July 1998 in Bournemouth, England.

The only change that has been made to the originally submitted paper is the inclusion of page numbers.

## 18.6 Applying Advanced Control Techniques for

## 18.7 Temperature Regulation of the LHC Superconducting Magnets

Bjørn flemsæter<sup>1</sup>, Enrique Blanco<sup>2</sup>, Juan Casas-Cabillos<sup>2</sup>, Steinar Sælid<sup>3</sup>

<sup>1</sup>LHC Division, CERN, Geneva (Switzerland)

<sup>2</sup>SIA Uiversidad de Valladolid, Valladolid (Spain)

<sup>3</sup>ITK Norwegian University of Science and Technology (Norway)

The temperature of the superconducting magnets for the future LHC accelerator is a control parameter with strict operation constraints imposed by (a) the maximum temperature at which the magnets can operate, (b) the cooling capacity of the cryogenic system, (c) the variability of applied heat loads and (d) the accuracy of the instrumentation. A temperature regulation with narrow control band can in principle be achieved by implementing a Model Predictive Control (MPC)-type controller. For this purpose, and for investigating the behavior of the cooling system, a simulation program has been developed. A prototype MPC controller has been installed and completed its first run.

### 1 INTRODUCTION

The Large Hadron Collider (LHC) [1] project will be the next major research facility for high-energy physics. It will provide proton-proton collisions based on a 27-km ring of high field superconducting magnets operating in superfluid helium at about 1.9 K. It represents a major challenge in applied superconductivity and cryogenics, and imposes hard constraints and a strict range of the temperature for operation of the machine.

### 2 SYSTEM DESCRIPTION AND PROCESS CHARACTEREISTICS

#### 2.1 The 1.9 K cooling loop

The superconducting magnets operate in static baths of pressurized HeII at 1.9 K and 1 bar. The generated or deposited heat is transported by conduction to a heat exchanger tube (Hx) threading its way along the magnet string, thus constituting a linear cold source. Inside the tube, a flow of saturated HeII absorbs the heat load by gradual vaporization [2].



The superfluid helium cooling scheme for the future LHC will be implemented in independent cooling loops (cell), each constituted of eight separated but thermally linked magnets totaling 107 meters. The configuration of the present test facility roughly represents a half-cell, consisting of four slightly shorter magnets with a total length of 35 meters, but with the basic cryogenic cooling concept being identical (see figure 1). It is mounted on a 1.4 % slope, representing the maximum slope inside the LHC tunnel [3].

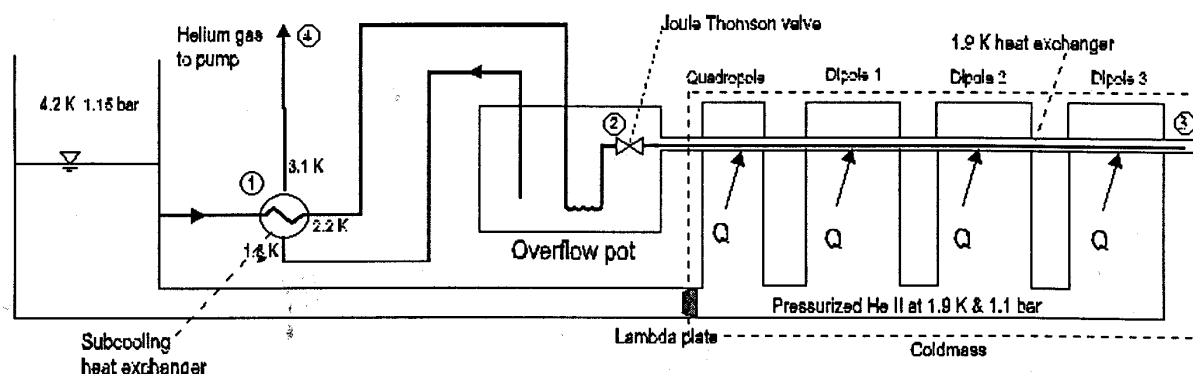


Figure1 The 1.9 K cooling loop

Subcooled helium I (1) is expanded to saturation by throttling through a Joule Thomson valve (2) and fed to the far end of the corrugated heat exchanger tube (3). The liquid gathers heat and vaporizes as it flows back in co-current flow with the vapor, and is then pumped out (4).

## 2.2 Process characteristics

The mass of pressurized HeII in the cold mass is about 160 kg compared to the several tons of metal, but it still constitutes 99 % of the specific heat ( $C_p$ ) at 1.9 K. Most physical parameters are highly nonlinear in the temperature range of interest, for example  $C_p$  more than doubles its value from 1.8 to 2.1 K.

The Hx-tube is only partly wetted over its length during normal operation. When more cooling power is required, the JT valve opens and the additional liquid will have to flow over the already wetted length to participate in the cooling. At the same time both the amount of flash gas from the JT-valve and the pressure drop along the Hx-tube increase, leading to a higher saturation temperature. This effect leads to an inverse response where the cooling *decreases* in a transient period (typically 5-10 min).

## 3 MODELLING & SIMULATION

Models of real systems are based on hypotheses and approximations and are therefore never perfect. Models are helpful in process analysis and control by improving the understanding of the process, to design the control law, and finally to optimize the process operation conditions.

There are in principle two main approaches of obtaining mathematical models of a system. (a) First principle models (white box) constructed from fundamental physical

laws such as conservation of mass, balance of energy and momentum. They are able to explain process behavior under different operation conditions, but are in general difficult to embed in a linear model based controller. (b) Identified models (black box), describing the relationship between input and output measurements of a plant. They are obtained from experiments on the plant, and can only describe the operational band and the dynamics that are present during the observation period.

### 3.1 Assumptions and simplifications

The velocity with which the liquid flows in the Hx-tube has been observed to be fairly constant and in the model taken as constant. The latent heat of vaporization of helium, the percentage of flash over the JT-valve and the heat transfer coefficient ( $k_{global}$ ) from saturated to pressurized HeII along the wetted perimeter inside the Hx-tube are assumed constant. Cooling is thus a function of wetted length and  $\Delta T$  from saturated to pressurized helium.  $k_{global}$  includes the solid conduction through the Hx-wall and Kapitza conductance

on the two solid-liquid interfaces. The magnets are assumed to be isothermal thanks to the good heat transfer along the half-cell.

### 3.2 Challenges and solutions

The dynamic behavior of the saturate liquid helium flow along the Hx-pipe has proved to be one of the most complex parameters to model. A good understanding of liquid quantity and location and the pressure profile along the Hx-pipe is important, as this determines the cooling provided to the system. For this the Hx-pipe is discretized longitudinally and in each element mass and energy balance and pressure drop is calculated. A tradeoff between accuracy and complexity has to be made. When the cooling provided by the Hx is known, the calculation of the magnet-temperature is straightforward. The differential equations for pressure drop, magnet temperature and mass balance respectively:

$$\begin{aligned} \frac{dp}{dt} &= f \frac{\rho(T) \cdot v_{gas}^2}{2 \cdot d} \sum^{L_{incr}} dx & \frac{dT}{dt} &= \frac{q_{heatloads} - \sum q_{cooling}}{m_{HeII} \cdot Cp(T)} \\ \frac{dm}{dt} &= \dot{m}_{in} - \dot{m}_{out} - q_{cooling} / h_{fg} \end{aligned}$$

The cooling power, mass and gas flow out of each element are found from these relationships respectively:

$$\begin{aligned} q_{cooling} &= \Delta T \cdot L_{increment} \cdot k_{global} & \dot{m}_{out} &= (m - m_{threshold}) \cdot v_{liq} / L_{increment} \\ g_{out} &= g_{in} + q_{cooling} / h_{fg} \end{aligned}$$

During each time step, these calculations are performed for each length increment, except  $dT/dt$  as the geometry is assumed isothermal. ( $f$  -friction factor,  $d$ -tube diameter,  $v_{gas}$  -gas velocity,  $q_{heatloads}$  -heat loads,  $m$  -mass of helium in increment,  $h_{fg}$  -latent heat of vaporization,  $L_{increment}$  -length of discretization increments,  $m_{threshold}$  accounts for corrugations in the Hx-tube).

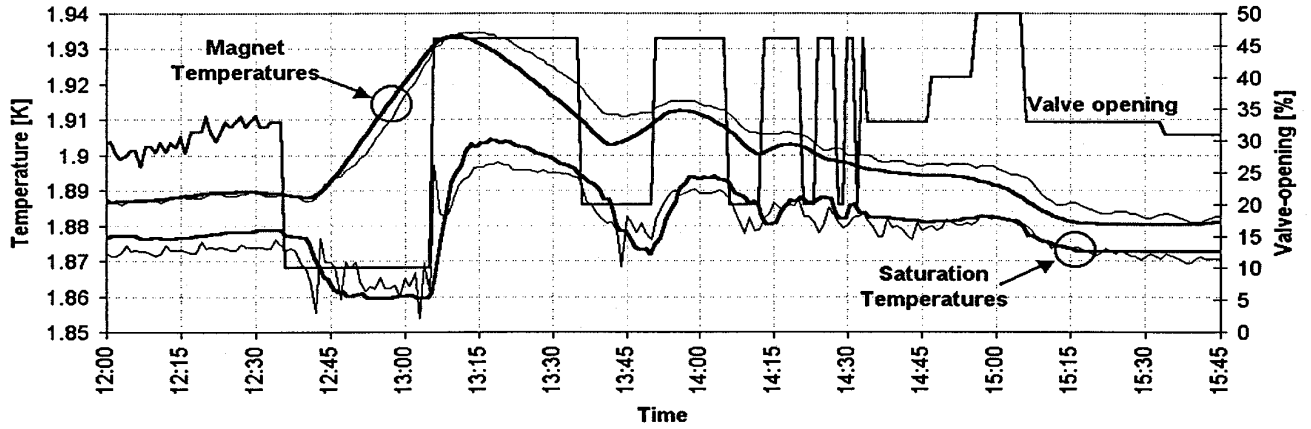


Figure 2 First principle model simulation (bold lines) versus measurement (thin lines)

Figure 2 shows the comparison between simulation with a first principle model and experimental data, and a good agreement is obtained. To calculate magnet temperatures and pressure profile along the Hx-pipe the model requires the JT-valve position, pressure in the overflow pot and the heat load on the system.

#### 4 PROCESS REGULATION

The process is characterized by being non-self regulating (integrating process), having a variable dead time (transport lag in the Hx-pipe), exhibiting inverse response (as the temperature initially rises when the valve is opened and vice versa) and being non-linear (particularly in Cp). These are all complicating factor from a control point of view.

The prototype half-cell has been regulated by a PID (Proportional, Integral, Derivative) regulator. PID regulators are not optimal when non-linearities, long dead time and inverse response are present in the process, and it is interesting to assess the advantages of using another control technique.

The MPC approach refers to a class of algorithms that compute a sequence of manipulated variable (MV) adjustments ( $\Delta u$ ) in order to optimize the future behavior of a plant ( $y$ ) over a time interval known as the *prediction horizon*. The algorithm has imbedded a model of the plant, and the optimization is achieved by minimizing a cost function of the form:

$$J = \sum_{j=N_1}^{N_2} [y(t+j) - w(t+j)]^2 + \beta \sum_{j=1}^{NU} [\Delta u(t+j)]^2$$

where  $N_1$  and  $N_2$  bonds the prediction horizons, where the MPC will try to follow an internally calculated reference trajectory  $w(t)$  [4].  $NU$  is the control horizon where different MV adjustments are calculated, and  $\beta$  is the weight factor for the adjustments. The prediction horizon is a basic tuning parameter, and should be set long enough to capture the steady state effect of all computed MV adjustments. Advantages of the MPC methodology are that it incorporates treatment of constraints, has dead time compensation and permits solution of control problems with unusual dynamics. On the other hand it is computationally complex and requiring a suitable process model able to predict future

outputs. In principle a narrower control band can be obtained with MPC when comparing with PID algorithms.

## 5 FIRST RESULTS AND FURTHER WORK

A first principle model of the LHC test String facility has been developed and tested. It is capable of simulating the plant behavior over a prolonged period, and is useful for developing and testing control aspects. An MPC control algorithm has been implemented on the prototype half-cell. This algorithm is working with an identified plant model, but it is the goal to develop an implement a suitable first principle model. Figure 3 shows a real response obtained from a step in the reference. Note that the regulator is anticipating the rise in temperature, and starts closing the valve even before the actual temperature-rise starts. Such a response cannot be obtained with a PID-

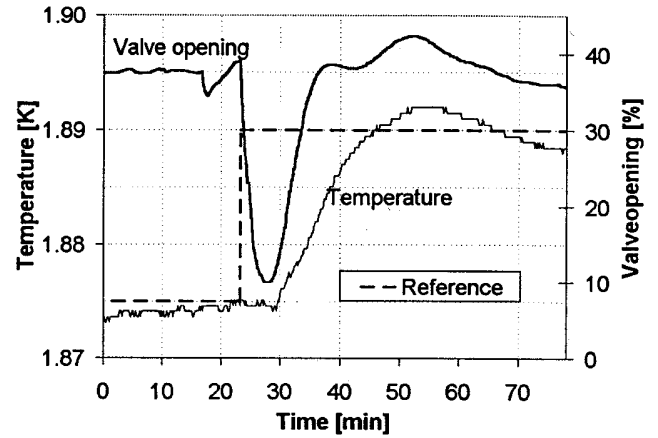


Figure 1 *Measured step response with MPC control*

algorithm. Potential benefits of implementing an advanced controller versus PID are expected to offset the increased initial cost and technical complexity. Considering the plant characteristics and control challenges this represents, also taking into account the future 107-m layout, we believe that the improvements will be noticeable, and it will add to a robust and fault tolerant operation of the system.

## 6 ACKNOWLEDGEMENT

This work has been performed in the framework of the Doctoral Student Programme at CERN (B.F), and the European Training and Mobility of Research (TMR) Programme (E.B.). We would like to thank the String Team for help and cooperation.

## 7 REFERENCES

- 1 Evans, L.R., The LHC in: Proceedings ISEC16ECMC Kitakyushu, Elsevier Science, Oxford 1997, 45-52
- 2 Lebrun, Ph. et. al., Cooling Strings of Superconducting Devices below 2 K: the Helium II Bayonet Heat Exchanger , LHC-PROJECT-REPORT-0144, 1997
- 3 Casas-Cubillos, J et. al., Operation, Testing and long Term behavior of the LHC Test String Cryogenic System, paper presented on this conference
- 4 Clarke, D.W., et. al., Generalized Predictive Control , Automatica Vol23, 137-160